
INFLUENCE OF CONCRETE NEAR-SURFACE DAMAGE TO ULTRASONIC PULSE VELOCITY TESTING

Master Thesis

Author:

Abdullah Gök

Supervisor:

Mohammad Fotouhi

13 MARCH 2025

TU DELFT

Acknowledgements

I am very grateful to everyone who supported and guided me through this thesis. I especially want to thank my supervisor, Dr. Mohammad Fotouhi, for his knowledge, patience, and valuable feedback, which greatly shaped this research. I also appreciate Ali Ghaderiaram for his willingness to help.

I am particularly thankful to the Department of Geotechnical Engineering for allowing me to conduct essential lab tests within their facilities. I extend my sincere appreciation to Karel Heller, whose assistance and expertise were vital during the experimental phase of my research. His support greatly contributed to the successful completion of the lab work.

A special thanks goes to Ton Blom and Maiko van Leeuwen, whose extensive help in the lab of the Faculty of Civil Engineering was essential for this research. They provided invaluable assistance with ordering materials, creating concrete samples, constructing moulds, and supporting the sawing and testing of the mechanical properties of the samples. Their expertise and dedication were key to ensuring the success of my experimental work.

I am also deeply grateful to the Faculty of Civil Engineering and Geosciences, specifically the Section of Materials and Environment, for providing an engaging and challenging master's thesis subject. Their dedication to offering topics that push the boundaries of knowledge has made this research both stimulating and rewarding.

To conclude, I am deeply appreciative of my family and friends, whose support and belief in me have been the foundation for my motivation throughout this journey. This thesis shows the efforts and support of many, and I am sincerely thankful to all who played a role in this achievement.

Abstract

This thesis investigates using Ultrasonic Pulse Velocity (UPV) to check for near-surface damage in concrete structures without causing any harm to the material. The research started by reviewing past studies on UPV methods, helping to compare results and evaluate how well different techniques worked. The main goal then became testing three specific UPV methods: Indirect Method 1, Indirect Method 2, and the Pulse-Echo Method. The damages are intended from the opposite surface as which is being tested, and the purpose was to see how well these methods could spot these near-surface damages and whether they were able to measure the thicknesses of these damages. The study also looked at how different water-cement (W/C) ratios impacted the strength of concrete, including the compressive and the flexural strength, and how these changes in the end had influence on the UPV measurements.

The research was done in two parts. First, the three UPV methods were tested on concrete samples with different W/C ratios to see whether the pre-intended damages could be found, and the thickness could be estimated. Then, additional mechanical tests, like the compressive and the flexural strength test, were used to check the overall strength and condition of the concrete.

The results showed that Indirect Methods 1 and 2 worked well for detecting surface-level damage, but they struggled to find and map deeper damage of the concrete. In comparison, the Pulse-Echo Method was more reliable, as it could better detect changes in depth and accurately measure the thickness of near-surface or inner damage. This was partly because the wave direction of the Pulse-Echo Method is perpendicular to the surface of the concrete sample, and therefore a better control over the wave direction is achieved. Although the Pulse-Echo method had some limitations, such as not being able to fully map the shape of the damage due to a lack of measurement points, it outperformed the other indirect methods in detecting and estimating the sizes of the pre-intended damages.

Another important finding was that concrete with a lower W/C ratio had more pores in this specific case, which seemed to be caused by issues with compaction and curing. These problems weakened the mechanical strength of the low W/C ratio concrete. Due to this finding, the study suggests that future studies should perform quality checks before testing starts, so this phenomenon could be prevented in future research. Other recommendations of this study include, upgrading UPV testing (especially for the indirect methods) with better sensors and signal processing, and exploring hybrid non-destructive testing methods. Furthermore, future research should also involve real-world testing to better understand how these methods perform in practical situations.

To sum up, while the Pulse-Echo Method was the best at detecting and measuring the intended damages, there is still room to improve the indirect methods by refining the tools and techniques. This would probably allow them to localize and determine the size of deeper damage in concrete structures.

Table Of Contents

1	Introduction	1
1.1	Background.....	1
1.2	Aim of the Study	3
1.3	Outline of the Report	4
2	Literature Review.....	5
2.1	Introduction.....	5
2.1.1	Concrete as a Fundamental Construction Material.....	5
2.1.2	Significance of Assessing Concrete Damage for Safety and Durability	5
2.1.3	Role of Non-Destructive Testing Methods in Evaluating Concrete Condition	7
2.2	Concrete Damage Mechanisms and Types	8
2.2.1	Cracking Mechanisms and Causes.....	8
2.2.2	Delamination Mechanisms and causes	9
2.2.3	Honeycombing	12
2.3	Ultrasonic Pulse Velocity (UPV) Technique	16
2.3.1	Principles of Ultrasonic Wave Propagation	16
2.3.2	Pulse-Echo Method.....	17
2.3.3	Factors Affecting UPV Measurements.....	19
2.4	Relationship Between UPV and Concrete Damage	22
2.4.1	Correlation Between UPV Values and Damage Severity	22
2.4.2	Case Studies Demonstrating UPV's Efficacy in Damage Assessment.....	23
2.4.3	Challenges in Quantifying Damage Depth with UPV	24
2.5	Porosity and W/C Ratio Influence on UPV	25
2.5.1	Understanding Porosity and its Importance	25
2.5.2	Research Exploring Porosity-UPV Relationships.....	28
2.6	Mechanical Properties of Concrete.....	30
2.6.1	Overview of Concrete's Mechanical Properties.....	30
2.6.2	How Mechanical Properties Influence UPV Measurements.....	34
2.7	Standards and Guidelines for UPV testing	35
2.7.1	BS EN 12504-4	35
2.7.2	ASTM C597: Standard Test Method for Pulse Velocity through Concrete.....	39
2.7.3	ACI 228.2R: Non-destructive Test Methods for Evaluation of Concrete in Structures	42
2.8	Other Non-Destructive Testing Techniques	48
2.8.1	Visual Inspection.....	48
2.8.2	Impact Echo.....	49

2.8.3	Ground Penetrating Radar	51
2.8.4	Infrared Thermography	54
2.8.5	Acoustic emission	57
2.8.6	Selection of Ultrasonic Pulse Velocity (UPV) Technique	59
2.9	Summary and Conclusion	61
3	Experimental Setup and Methodology	62
3.1	Materials and Mix Design	62
3.2	Introduction of Damage Levels and Depths	64
3.3	Sample Preparation	67
3.4	Measurement Process and Data Collection	70
3.5	Testing with the Ultrasonic Pulse Velocity technique	83
3.6	Mechanical testing	88
4	Results and Discussion.....	93
4.1	Test results of mechanical testing.....	93
4.1.1	Compression test	93
4.1.2	Flexural bending test	95
4.2	Comparison of the mechanical testing results.....	96
4.3	Test results of UPV testing.....	98
4.3.1	Baseline Measurement.....	98
4.3.2	Indirect Method 1 – Low W/C ratio	102
4.3.3	Indirect Method 1 – High W/C ratio	104
4.3.4	Indirect Method 2 – Low W/C ratio	106
4.3.5	Indirect Method 2 – High W/C ratio	109
4.3.6	Pulse-Echo Method – Low W/C ratio	111
4.3.7	Pulse-Echo Method – High W/C ratio.....	115
4.4	Comparison of the UPV testing results	118
5	Conclusions and Recommendations.....	131
5.1	Conclusion	131
5.2	Recommendations	133
Appendices	136
Appendix A.1:	Python code for Indirect Method 1.....	136
Appendix A.2:	Python code for Indirect Method 2.....	137
Appendix A.3:	Python code for the Pulse-Echo Method	138
Appendix A.4:	Python code for the Pulse-Echo Method (Thickness)	139
Appendix A.5:	Python code for Mechanical testing - Compression test	140
Appendix A.6:	Python code for Mechanical testing – Flexural bending test	141

Appendix A.7: Python code for the comparison of Indirect Method 1	142
Appendix A.8: Python code for the comparison of Indirect Method 2	143
Appendix A.9: Python code for the comparison of the Pulse-Echo Method.....	144
Bibliography	145

1 Introduction

This chapter introduces the background and importance of the research, focusing on the need for assessing damage in concrete structures. It outlines the aim of the study and the main research question, setting the foundation for the experiments and analysis discussed in later chapters.

1.1 Background

Concrete is the second most consumed material globally, surpassed only by water, with an annual consumption rate of three tonnes per person. Its use in construction exceeds that of all other materials combined. This dominance is attributable to its ability to be moulded into any desired shape, its superior compressive strength compared to steel, its higher temperature resistance, and the ease of transportation of its components [1, 2]. Given these attributes, concrete will likely remain indispensable for construction in the foreseeable future. However, its extensive use also brings critical challenges, as defects or failures in concrete or reinforced concrete structures can have serious safety implications and lead to costly repairs.

To ensure the safety and reliability of concrete structures, regular maintenance and quality testing are essential throughout their service life. This is particularly crucial in regions prone to seismic activity. Structural assessments are conducted using either destructive testing (DT) or non-destructive testing (NDT). While DT involves extracting samples from built structures (e.g., drilled cores or cube specimens), potentially affecting their functionality, NDT methods allow for on-site evaluations without causing damage. Among the most common NDT methods are Schmidt surface hardness testing, Ultrasonic Pulse Velocity (UPV) testing, and the Sonic Rebound (SonReb) method, which combines UPV and Schmidt hardness testing [3, 4, 5, 6].

Recent studies demonstrate that NDT methods, especially UPV, are not only effective in estimating the compressive strength of concrete but can also detect structural flaws, including damage caused by environmental exposure or mechanical stresses [7, 8, 9]. This capability is particularly valuable for identifying hidden or internal damage that may not be immediately apparent. Such assessments can guide maintenance efforts more efficiently, ensuring timely repairs and reducing costs.

Concrete structures undergo various forms of damage and degradation during their lifespan due to regular use, environmental influences, or accidents. In some cases, flaws originate during construction and remain undetected until they cause significant issues. One notable example is delamination, which involves the separation of layers within concrete due to poor bonding, freeze-thaw cycles, or other stresses. Delamination often begins internally and may only become visible when the damage worsens, leading to reduced load-bearing capacity, water ingress, and corrosion of reinforcement.

Another structural flaw, honeycombing, involves voids or cavities within the concrete mass caused by inadequate compaction, improper mix proportions, or congested reinforcement. Honeycombing typically compromises structural integrity by reducing cross-sectional area and increasing permeability, which accelerates reinforcement

corrosion. Although delamination and honeycombing differ in their causes and characteristics, they share the challenge of being difficult to detect when internal [10].

Studies have highlighted the critical importance of UPV testing for detecting these flaws. For example, ultrasonic methods, including the Pulse-Echo technique, have proven effective in imaging and quantifying internal defects such as delamination and honeycombing. Research on ultrasonic echo tomography has demonstrated its capability to identify large concrete defects, while advances in pulsed phase thermography further showcase the growing potential of NDT techniques in this area [11, 12, 13].

These findings emphasize the need for robust quality control during construction and the ongoing development of effective NDT methods to monitor concrete structures. With its demonstrated ability to assess structural integrity and detect hidden defects, UPV emerges as a promising tool for structural health monitoring. This study explores the potential of UPV in identifying delamination as a primary focus, with secondary consideration given to honeycombing for its similar implications on concrete durability.

1.2 Aim of the Study

Given the extensive use of concrete as a construction material and the critical need for maintaining the safety and reliability of concrete structures, this study focuses on enhancing damage assessment techniques. While non-destructive testing (NDT) methods such as Ultrasonic Pulse Velocity (UPV) have proven effective in estimating concrete strength, they have also shown potential for detecting internal flaws, including delamination and honeycombing. Both types of damage can compromise the structural integrity of concrete, especially when hidden or inaccessible, necessitating advanced detection techniques.

The primary aim of this study is to evaluate the effectiveness of UPV in assessing damage in concrete structures, with a particular focus on its capability to detect and measure the depth and severity of near-surface delamination. Additionally, the study considers honeycombing as a secondary phenomenon, exploring how UPV techniques might detect these defects given their similar challenges of internal detection. Specifically, this research addresses the following question:

“What is the effectiveness of Ultrasonic Pulse Velocity (UPV) in assessing the damage of concrete structures, and can the UPV technique be used to accurately measure the depth of existing near-surface damage?”

To address this research question, the study begins with a comprehensive literature review, exploring the mechanisms of concrete damage and the role of quality control in construction. This review provides the theoretical framework for analysing UPV testing techniques and includes a detailed examination of relevant standards and guidelines. These insights shape the design of the experimental setup and methodology to ensure the research question is thoroughly investigated.

Moreover, the study investigates factors influencing UPV test outcomes, such as the impact of material properties (e.g., water-to-cement ratio) on the measurement of ultrasonic waves. It also examines the relationship between UPV results and the mechanical properties of concrete, providing a critical foundation for interpreting experimental data.

By evaluating UPV as a tool for detecting and measuring delamination and related damage, this study aims to contribute to the field of structural health monitoring. The findings are intended to improve the efficiency of maintenance practices, reduce long-term costs, and enhance the safety and durability of concrete structures.

1.3 Outline of the Report

The report is divided into 5 chapters, with each containing and providing the following information.

Chapter 1 is the current chapter and is an Introduction, it contains background information about this research and provides the aim of the study.

Chapter 2 contains the Literature Review, which discusses relevant research upon the subject of this master thesis. It starts with the description on why damage assessment of concrete is an important matter. Afterwards it describes the role of UPV as a non-destructive testing method and provides relevant correlations between UPV and concrete characteristics. The purpose of this chapter is to get the reader informed about the current developments within the subject area. The information provided by this chapter is used to determine the terms and conditions of the experimental setup and the methodology.

Chapter 3 Experimental setup and methodology, outlines the experimental setup and methodology used in this research. It begins with a detailed description of the mix designs employed for concrete samples. Following this, the damage levels introduced into the samples are explained, including their depths and configurations. The preparation process for the samples is then described, highlighting the equipment and key steps involved in achieving the desired mix designs. Finally, the chapter concludes with an overview of the planned tests, providing insight into the methods and techniques used to achieve the research objectives.

Chapter 4 presents the results of both mechanical and Ultrasonic Pulse Velocity (UPV) tests. It begins with the findings from compression and flexural bending tests, followed by a comparative analysis of these results. The chapter then delves into the UPV outcomes, categorized by testing methods (Indirect Methods 1 and 2, and Pulse-Echo) and the water-cement (W/C) ratio variations (low and high). Each section examines the performance of these methods under different W/C conditions. The chapter concludes with a comprehensive comparison of all UPV results, evaluating the effectiveness of each method in detecting damage and assessing concrete properties.

Chapter 5 provides a summary of the key conclusions from the study and presents recommendations based on its findings. It outlines the effectiveness of the techniques applied and highlights their main outcomes and limitations. The chapter then offers practical suggestions for future research and potential improvements which are identified throughout the study.

2 Literature Review

In this chapter, a literature review was performed to gain a better understanding of the subject and to get an overview of the achievements which have been accomplished by earlier research. This knowledge is used to plan the experiments which are done and was used as a reference to discuss the obtained results from the experiments in a further phase of the research.

2.1 Introduction

2.1.1 Concrete as a Fundamental Construction Material

Concrete is now the most popular building material in the world. This is mainly due to its low costs its availability in most places and its favourable characteristics, such as high compressive strength, durability, and relatively low maintenance. Furthermore, concrete is a material which can be widely used for different civil infrastructure applications, such as buildings, bridges, power plants, dams, and highways [14]. Although concrete might seem like the ideal material it also has some flaws which are worth to be mentioned. One of these flaws is that concrete is not the strongest material in tensile strength. Due to lack of tensile strength, the need arises to use steel within concrete to enforce the parts of the structures loaded with tension. Concrete which is used in combination with steel is called reinforced concrete.

Another thing which concrete might not be the best at, might be its lack of ductility. This causes in the case of failure, that structures build with purely concrete would not have warning mechanisms, such as showing extreme deflections or making sounds before failure but rather fall apart suddenly. The use of steel in concrete also helps the concrete structures to gain some ductility so it will be able to warn its users to evacuate before it collapses.

As it is known concrete is a composite material which consists of cement, supplementary cementitious materials, aggregates, and water. The properties of the concrete mainly depend on the proportions on which the ingredients mentioned above are used in the mix. For instance, a higher cement/binder percentage within the Mix Design generally leads to concrete with a higher compressive strength. In the same manner, other characteristics of the concrete also can be influenced by changing the proportions and/or the ingredients used in the Mix Design depending on the expected functionality of the structure it is being used for.

2.1.2 Significance of Assessing Concrete Damage for Safety and Durability

Concrete is a widely used building material in civil infrastructure, valued for its strength, durability, and versatility. However, the lifespan of concrete structures is influenced by their functionality and the environment in which they exist. Over time, structures are subject to degradation mechanisms, such as carbonation, acid attack, salt attack, bio-organic attack, alkali-silica reaction, rebar corrosion, and thermal radiation [15]. To ensure safety and durability, codes and standards guide the design and

maintenance of concrete structures. However, external influences can still cause damage over time, compromising the integrity of these structures. Regular inspections and maintenance are critical to mitigate these risks.

The consequences of neglecting damage assessment and maintenance have been illustrated by several historical failures:

- **Willow Island Cooling Tower (1978):** Improper strength development due to low temperatures during construction led to the collapse of the cooling tower, resulting in the deaths of 51 workers. This incident is recognized as the worst construction disaster in U.S. history [1].
- **Fontana Concrete Gravity Dam:** Constructed between 1942 and 1945 to manage the Little Tennessee River, the dam exhibited early signs of cracking by 1949. Petrographic research revealed an alkali-aggregate reaction combined with heat-induced expansion as the primary cause. While temporary measures, such as cooling and post-tensioning with steel wires, were implemented, the dam continues to exhibit slow growth, with the top center moving 114.3 mm upstream since 1976. Regular monitoring by the Tennessee Valley Authority (TVA) has prevented catastrophic failure [1].
- **Malpasset Dam (1959):** Cracks near the downstream base of the dam, identified in 1954, were left uninvestigated. By 1959, these cracks had expanded, and leaks were observed. The lack of intervention led to the dam's collapse on December 2, 1959, unleashing a 40-meter-high wall of water at 70 km/h. Over 500 lives were lost in the disaster [1].
- **Highway Overpass Collapse (2006):** On September 30, 2006, the overpass on Boulevard de la Concorde in Montreal, Canada, collapsed due to improper rebar design, installation, and the use of low-quality concrete. This failure caused five fatalities and six injuries [1].

These cases show the critical importance of damage assessment and adherence to standards. Early detection and maintenance are essential to prevent catastrophic outcomes. Neglecting these practices can result in significant loss of life, economic costs, and damage to infrastructure.

2.1.3 Role of Non-Destructive Testing Methods in Evaluating Concrete Condition

The service life of concrete can be considerably reduced by various harmful environmental conditions. Consequently, it has become essential to develop testing methods that evaluate the in-place properties of concrete for quality control and environmental assessment. These tests should be non-destructive, ensuring that they do not impair the structure's functionality and allowing for repeated testing in the same location to monitor changes over time. Non-destructive tests, as the name implies, are those that do not compromise the integrity or performance of the concrete when conducted. Non-destructive testing (NDT) specifically refers to methods that do not affect the ability of the element, part, or structure to function as intended [16].

Compression testing of cubes, which indicates the possible strength of the concrete utilized, is currently the test that serves as the foundation for quality control. The composition, compaction, and curing of concrete are the primary factors affecting its quality. The composition of the concrete going into the cubes and that going into the structure can at most be guaranteed to be same. The results achieved on cubes, however, may not accurately reflect the quality of concrete in the structure since the procedures of compaction and curing are typically different for the cubes and the structural components. Therefore, non-destructive testing (NDT) is required. The necessity for quality assessment of damaged concrete structures makes NDT of concrete a crucial scientific and practical endeavour. The need for a proposed change in a structure's use or extension, the suitability of a building for purchase or insurance, the evaluation of the quality or integrity of repairs, and the observation of strength development in relation to formwork stripping, curing, pre-stressing, or load application are all examples of how important non-destructive testing is [16].

2.2 Concrete Damage Mechanisms and Types

2.2.1 Cracking Mechanisms and Causes

Concrete structures frequently exhibit cracks as a natural feature of their material composition. These cracks can develop due to shrinkage, thermal stresses, or external loading and are commonly initiated at the interfacial transition zone (ITZ) between the cement paste and aggregates, where material heterogeneity leads to stress concentration. While cracks are not always indicative of structural failure, their progression can compromise structural tightness, reduce load-bearing capacity, and accelerate deterioration [17]. Understanding cracking mechanisms is essential for evaluating their role in facilitating other damage mechanisms, particularly delamination.

Cracks in concrete can be classified based on their location, geometry, scope, and other parameters, as shown in Figure 1. This classification aids in diagnosing damage mechanisms and assessing their potential impact on structural performance. Cracks, particularly microcracks, often act as precursors to more severe damage such as delamination. Microcracks in the ITZ weaken interfacial bonds, reduce cohesion between concrete layers, and create pathways for moisture ingress. These processes accelerate freeze-thaw damage, thermal stresses, and ultimately the initiation of delamination [17].

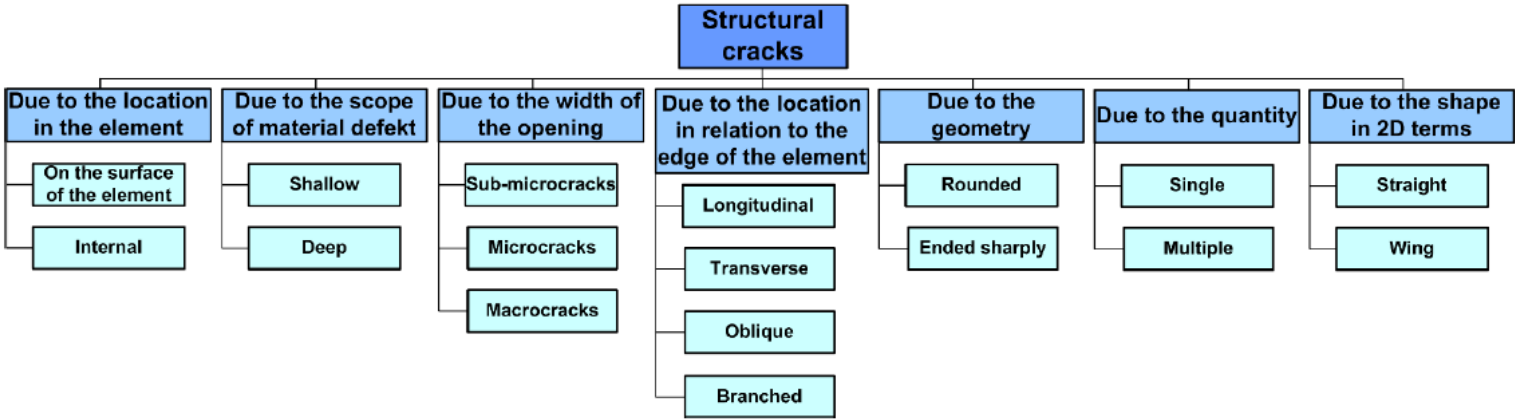


Figure 1: Concrete’s structural fractures and their breakdowns [17]

This figure categorizes structural cracks into various types, including microcracks, macrocracks, and other forms based on their geometry, location, and quantity. Such classifications are essential for understanding how cracks contribute to concrete degradation [17].

Cracks not only serve as initiation points for delamination but also facilitate its progression. As microcracks propagate and connect with other discontinuities, they redistribute stresses in the structure, creating localized weaknesses that can evolve into delamination under cyclic loading or environmental conditions. This interaction shows the importance of understanding cracking as part of the broader degradation process in concrete structures [17, 18].

Although cracking and delamination are distinct damage mechanisms, their interaction is critical to understanding structural deterioration. Cracks are surface or volume-based discontinuities that can sometimes be addressed through surface repairs, whereas delamination represents internal layer separation with more severe implications for structural integrity. Detecting delamination, especially in the presence of complex cracking patterns, requires advanced techniques like Ultrasonic Pulse Velocity (UPV), which is effective at identifying internal separations that are not visible externally.

This research focuses on delamination as the primary damage mechanism of interest, with cracking discussed as a precursor that facilitates its initiation and progression. By exploring the relationship between these mechanisms and employing UPV for non-destructive testing, this study aims to contribute to improved maintenance and monitoring practices for concrete structures.

2.2.2 Delamination Mechanisms and causes

Delamination is a critical form of concrete deterioration that involves the internal separation of layers within the material. This hidden damage poses a significant challenge because it often develops within the material, remaining undetected until it significantly compromises the structural integrity of the affected component. Unlike surface-level damage such as spalling, delamination occurs internally and is influenced by a combination of environmental factors, chemical reactions, and construction deficiencies. Its significance is particularly pronounced in critical infrastructure such as bridges, dams, airport runways, and parking structures, where the consequences of undetected delamination can lead to catastrophic failures or prohibitively costly repairs. Globally, delamination contributes to significant structural failures, with repair costs exceeding \$50 billion annually, highlighting its importance as a critical area of research [19, 20].

One of the primary mechanisms behind delamination is freeze-thaw cycles, which are prevalent in cold climates. Water trapped within the pores of concrete freezes and expands by approximately 9%, generating tensile stresses that can exceed the material's capacity. Over successive freeze-thaw cycles, these stresses propagate microcracks (Figure 2) that coalesce into delaminated layers [21]. The risk is particularly high in concrete that lacks adequate air voids to accommodate the volumetric expansion of freezing water. Freeze-thaw-induced delamination is especially problematic for bridge decks and pavements exposed to de-icing salts, as the ingress of chloride further accelerates the degradation process [22]. Studies indicate that freeze-thaw-related delamination reduces the service life of bridges and pavements by up to 50%, with repair costs exceeding \$5 billion annually in the United States alone [23]. To mitigate these effects, air-entraining admixtures are commonly incorporated into the concrete mix to create microscopic voids that act as pressure-relief zones, preventing tensile stress buildup. Despite these preventive measures, prolonged exposure to freeze-thaw conditions continues to weaken concrete over time, necessitating robust maintenance strategies [24].

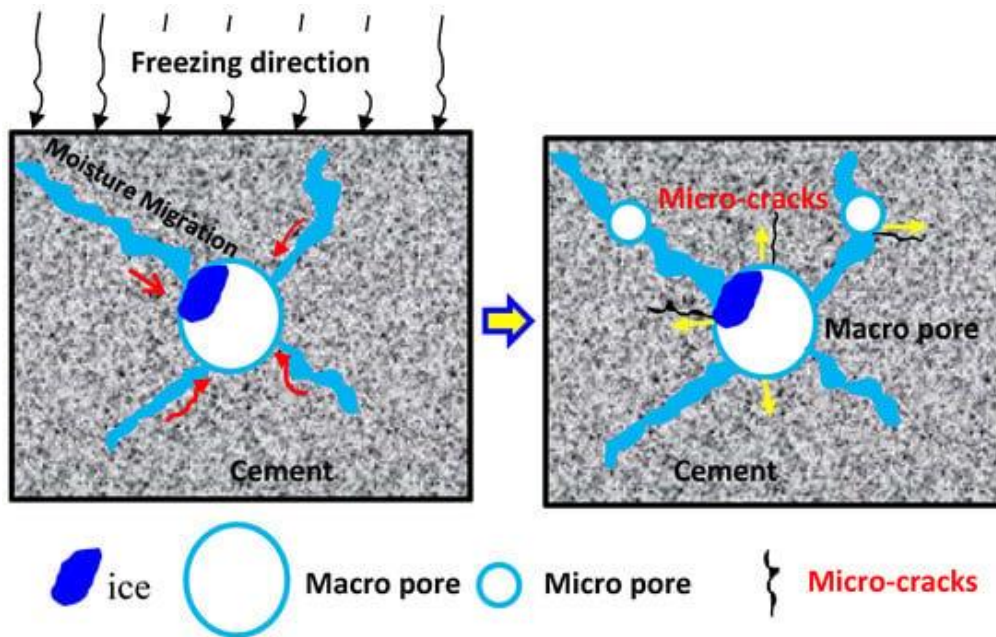


Figure 2: Illustration of a freeze-thaw cycle in concrete [25]

In addition to environmental factors, chemical reactions such as the alkali-aggregate reaction (AAR) (Figure 3) are a significant cause of delamination. AAR occurs when alkalis in Portland cement react with reactive silica or carbonate in aggregates, forming an expansive gel. This gel absorbs water and swells, generating internal stresses that cause microcracking and delamination. AAR is particularly problematic in regions where reactive aggregates are prevalent [26]. There are two primary forms of AAR: alkali-silica reaction (ASR) and alkali-carbonate reaction (ACR). ASR is more common and involves reactive silica aggregates, while ACR occurs with carbonate aggregates, such as dolomitic limestone [27].



Figure 3: Concrete failure due to Alkali Aggregate Reaction [28]

AAR-induced delamination is particularly severe in large infrastructure such as dams and bridges. For instance, the Los Angeles Aqueduct, constructed in 1913, required \$20 million in repairs due to ASR-related delamination [29]. Similarly, approximately 15% of surveyed concrete dams in Canada exhibit signs of AAR-induced delamination, threatening their long-term stability [30]. On a global scale, repair costs for AAR-related damages are estimated to exceed \$10 billion annually. Mitigating AAR risks requires the use of low-alkali cement and non-reactive aggregates, as well as the incorporation of supplementary cementitious materials such as fly ash, which reduce the availability of reactive alkalis [31].

Construction deficiencies also play a major role in the development of delamination, particularly in urban environments where rapid construction schedules and cost-cutting measures often compromise quality. Improper compaction during concrete placement leaves voids and weak interfaces that serve as initiation points for delamination under stress. Air entrapment during finishing further exacerbates the problem by weakening the bond between layers, while inadequate curing practices result in shrinkage stresses that reduce tensile strength. Reinforcement corrosion adds another layer of complexity; as embedded steel corrodes, its volume expands, generating stresses that lead to delamination near the surface (Figure 4) [21].

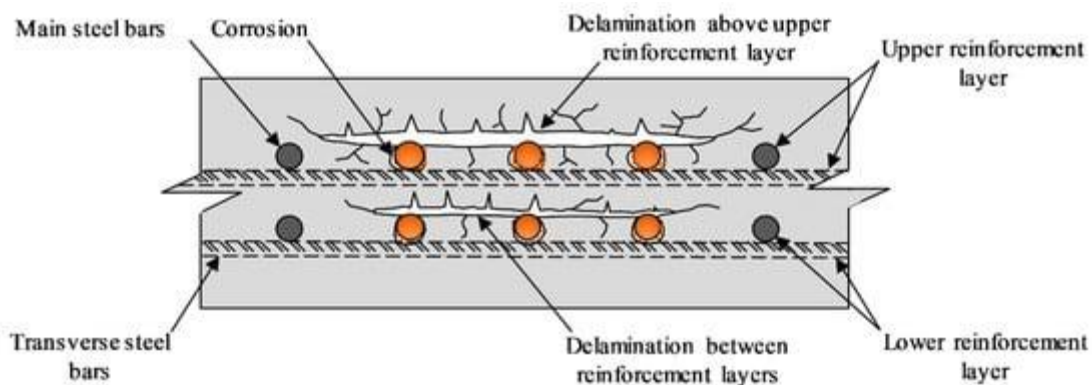


Figure 4: Schematization of delamination occurring due to steel corrosion in concrete [32]

The financial implications of construction-related delamination are substantial. For example, a survey of parking garages in Canada revealed that nearly 30% exhibited delamination due to poor compaction and curing, with repair costs averaging \$50 per square meter [33]. Similarly, a large shopping mall parking structure in the Netherlands required €25 million in repairs after delamination compromised its load-bearing capacity [34]. Preventing such issues necessitates strict adherence to quality control standards during construction, including proper compaction, curing, and the use of high-quality materials. Innovations such as self-compacting concrete and advanced curing techniques have shown promise in reducing construction-related delamination [35].

The implications of delamination extend beyond structural integrity to include economic and safety concerns. Delamination accelerates the ingress of water and chlorides, which in turn promotes reinforcement corrosion and weakens the structure further. Bridge decks, for example, are particularly susceptible, with delamination accounting for 40%–

50% of premature failures in cold climates [36]. In parking structures, exposure to de-icing salts and heavy traffic loads exacerbates delamination, leading to costly repairs and reduced service life. These real-world examples show the importance of understanding delamination mechanisms and their causes as a foundation for developing effective prevention and mitigation strategies. Addressing environmental, chemical, and construction-related factors is critical to extending the service life of concrete infrastructure and ensuring public safety.

2.2.3 Honeycombing

Honeycombing, a structural defect in concrete, manifests as voids or cavities within the material, often resembling the hexagonal pattern of a honeycomb [37]. These voids occur when the mortar fails to fill the spaces between coarse aggregate particles, creating discontinuities that compromise both the uniformity and structural integrity of the concrete. Beyond aesthetic implications, honeycombing poses significant challenges to the performance and durability of concrete elements, as shown in Figure 5.



Figure 5: Honeycombing visible on a concrete element [38]

The formation of honeycombing results from various factors, primarily related to poor construction practices. Inadequate compaction during placement often leaves air pockets trapped within the concrete matrix, while improper mix proportions, such as insufficient fines or an incorrect water-to-cement (W/C) ratio led to reduced workability [39, 40]. These issues hinder the concrete’s ability to flow and encapsulate aggregates effectively, especially in mixes with low slump values [41]. Additionally, congested or poorly spaced reinforcement obstructs proper concrete flow, further contributing to void formation [39]. Deficiencies in formwork design, such as leaky or poorly sealed joints, exacerbate the problem by allowing cement paste to escape during pouring [42]. Combined with improper placement techniques, such as excessive drop heights, these factors increase the likelihood of segregation and honeycombing [37].

Honeycombing defects vary in severity, ranging from small voids measuring a few millimetres to large cavities penetrating deep into the concrete. While small defects may stem from minor compaction issues, large voids are typically caused by severe compaction failures or extreme congestion of reinforcement. Table 1 provides examples of small, medium, and large honeycombing defects, illustrating the variability in severity and their potential impact on the concrete's performance [43].

<p>Small honeycombs (smaller than 10 mm)</p>	
<p>Medium sized honeycombs (between 10 and 30 mm)</p>	

Large sized honeycombs
(Larger than 30 mm)



Table 1: Examples of small, medium, and large honeycombing defects in concrete structures [43]

The presence of honeycombing, regardless of size, adversely affects both the structural integrity and durability of concrete structures. Voids within the concrete reduce the effective cross-sectional area available to bear loads, compromising the strength and load-bearing capacity of structural elements [44]. Increased permeability due to these voids accelerates the ingress of aggressive agents, leading to reinforcement corrosion and further degradation [45].

Detecting honeycombing is essential for assessing the condition of concrete structures, as it often serves as a precursor to more severe damage mechanisms like delamination. The interconnected voids and weakened bonds resulting from honeycombing provide pathways for moisture ingress, which can initiate freeze-thaw cycles or accelerate reinforcement corrosion [37]. These processes create internal stresses that contribute to the separation of concrete layers, particularly under cyclic environmental or mechanical loading. Thus, honeycombing not only weakens the immediate structural integrity but also amplifies the risk and progression of delamination over time.

Non-destructive testing (NDT) methods, such as Ultrasonic Pulse Velocity (UPV) testing, play a crucial role in identifying honeycombing and assessing its implications for delamination. UPV detects changes in wave propagation caused by voids, offering insights into the presence and severity of internal defects [46]. Advanced methods like the Pulse-Echo technique enhance this capability by mapping subsurface voids and identifying delaminated layers [47]. These techniques bridge the gap between detecting surface-level issues and evaluating internal damage, enabling a more comprehensive understanding of structural health. Other NDT techniques, such as impact-echo further contribute to detecting and mapping honeycombing and delamination [48, 49].

Preventing honeycombing remains the most effective approach. Proper mix design, including the use of admixtures to improve workability, and adherence to best practices for compaction, formwork design, and placement techniques, can significantly reduce the risk of honeycombing [40]. However, where defects occur, early detection and remediation are critical to mitigating their impact on structural durability and reducing the risk of delamination.

In summary, honeycombing is not only a defect but also a facilitator of more complex damage mechanisms, including delamination. Its detection and prevention are integral to maintaining the structural integrity and service life of concrete infrastructure. By leveraging advanced NDT methods like UPV, engineers can better understand the interplay between honeycombing and delamination, contributing to improved maintenance strategies and enhanced safety.

2.3 Ultrasonic Pulse Velocity (UPV) Technique

2.3.1 Principles of Ultrasonic Wave Propagation

The ultrasonic pulse velocity (UPV) is a stress wave propagation method which is based on the phenomenon of ultrasonic wave propagation with a variable frequency in the 20–120 Hz range. The test equipment consists of two probes: a mechanical pulse emitter and an equivalent receptor. With the distance between the probes known and the time between the signal's emission and reception observed, the wave velocity is determined [3]. Around the 1940s and 1950s, the first ultrasonic pulse velocity measurements in laboratory specimens were published [50], and it is since the 1960s that actual data from construction sites have begun to be documented [24]. The two most often used NDT techniques are the rebound hammer and ultrasonic pulse velocity (UPV). This is because these tools have the benefits of being portable, inexpensive, and simple to use. Using a spring to measure the hardness of the concrete surface and calculating the rebound number (RN) is the basic idea behind hammer rebound. Additionally, the value of the RN relates to the compressive strength of concrete and shows the characteristics of surface hardness. In the meanwhile, as is told above the UPV's basic operation is to send ultrasonic waves through concrete and track how long it takes for those waves to travel through the concrete and reach the sensor on the other end [51]. In 1951, Whitehurst conducted some research with the use of UPV and created a guideline which allows to get an estimation of the general condition/quality of the concrete with only the pulse velocity as an input, the table below (Table 2) shows these ranges [52].

General condition	Pulse velocity (m/s)
Excellent	Above 4750
Good	3660 – 4570
Questionable	3050 – 3660
Poor	2130 – 3050
Very poor	Below 2130

Table 2: Concrete quality and pulse velocity [16]

There are three ways of making measurements with the use of UPV. The first way is direct transmission through the concrete. In this case the transducers are held on opposite faces of the concrete and the waves go straight from one probe to another. The second method is indirect transmission which is used when access to the opposite face of the test specimen cannot be achieved. The third method is semi-direct which describes the case where the probes are placed on top of two adjacent faces. The three ways of how the probes can be placed are shown in Figure 6.

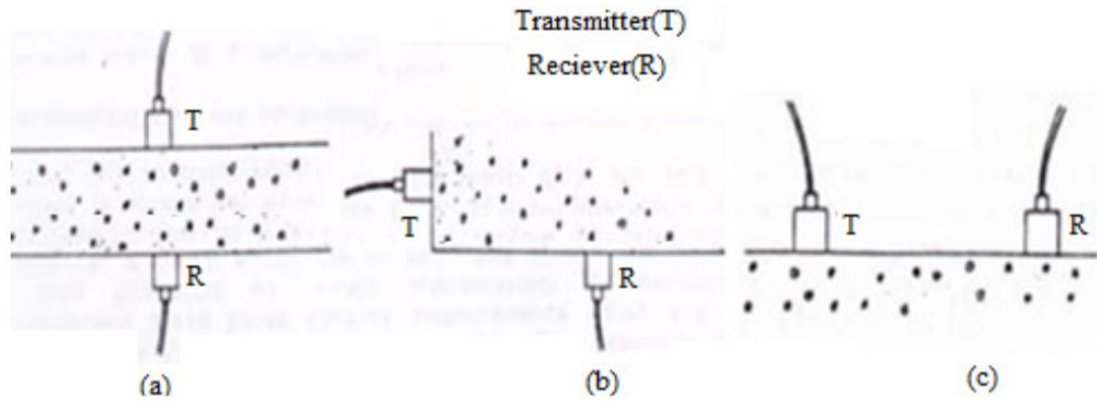


Figure 6: Direct (a), Semi-direct (b), Indirect transmission [53]

2.3.2 Pulse-Echo Method

Building upon the principles of ultrasonic wave propagation and the ultrasonic pulse velocity (UPV) method discussed earlier, the Pulse-Echo technique addresses some limitations of the through-transmission technique, such as the need for access to both sides of the test member and the inability to determine the depth of detected anomalies. The Pulse-Echo method operates entirely from one surface, making it particularly useful for situations where only one side of the structure is accessible. By identifying the arrival time of stress waves that reflect off internal defects or interfaces, this method allows for flaw detection and thickness measurement.

Initially developed for metal testing, the Pulse-Echo method was adapted for concrete testing in the 1960s. Since then, various experimental ultrasonic-echo systems have been developed, primarily for assessing the thickness of thin slabs, pavements, and walls, as well as for locating internal flaws [54, 55, 56, 57]. The principle of the method involves introducing a stress pulse into the material through an accessible surface using a transmitter. The pulse propagates through the material and reflects upon encountering discontinuities such as cracks or voids. These reflected waves, or echoes, are then detected by the same transducer acting as a receiver, as shown in Figure 7 (a). A more common variation involves using a separate receiver transducer placed near the transmitter, known as the "pitch-catch" system (Figure 7 (b)).

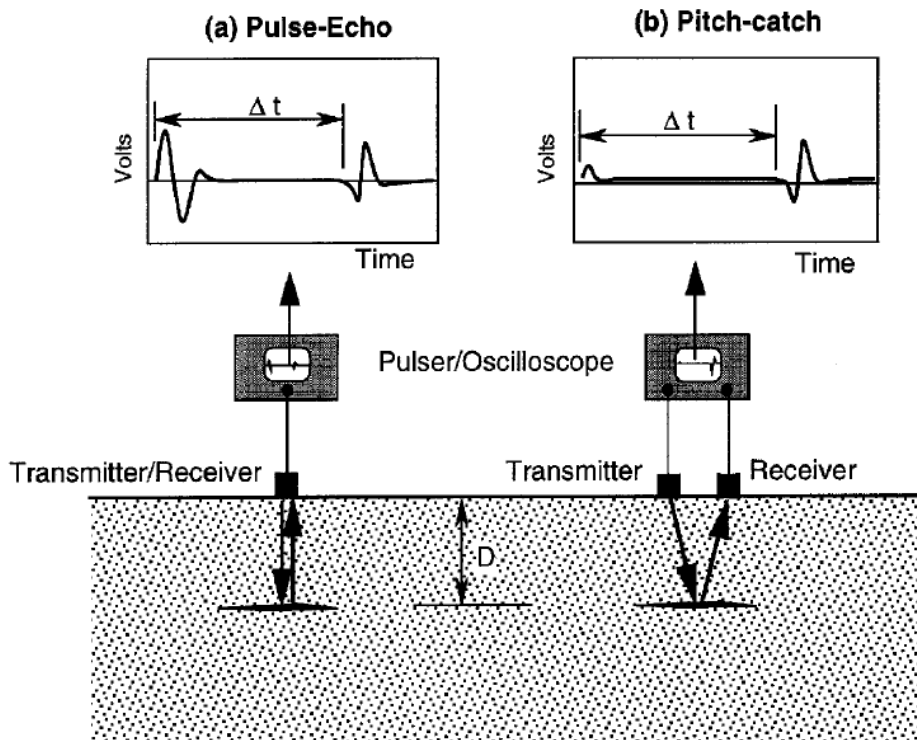


Figure 7: Schematic view of the Pulse-Echo Method and the Pitch-Catch method [58]

The output from the receiver is displayed as a time-domain waveform on an oscilloscope, and the travel time of the pulse determines the depth of the reflecting interface, assuming the wave velocity in the material is known. However, developing transducers suitable for concrete testing has proven challenging due to the heterogeneous nature of concrete and the presence of aggregates [56, 57].

Recent advancements have led to the development of true Pulse-Echo systems, which utilize a single heavily damped 500-kHz transducer. These systems incorporate micro-computers to process data and present results, often in the form of a B-scan image. A B-scan provides a cross-sectional view of the material by compiling time-domain traces gathered as the transducer moves across the surface. For instance, Figure 8 shows a concrete specimen with an artificial defect and the corresponding B-scan that clearly reveals the defect's position [59].

While high-frequency pulses improve defect detection, they limit the penetration depth and reduce the effectiveness of the Pulse-Echo method in concrete containing large aggregates. This limitation, coupled with limited field experience, means that further research is required to fully optimize and extend the applicability of the Pulse-Echo method in diverse concrete structures.

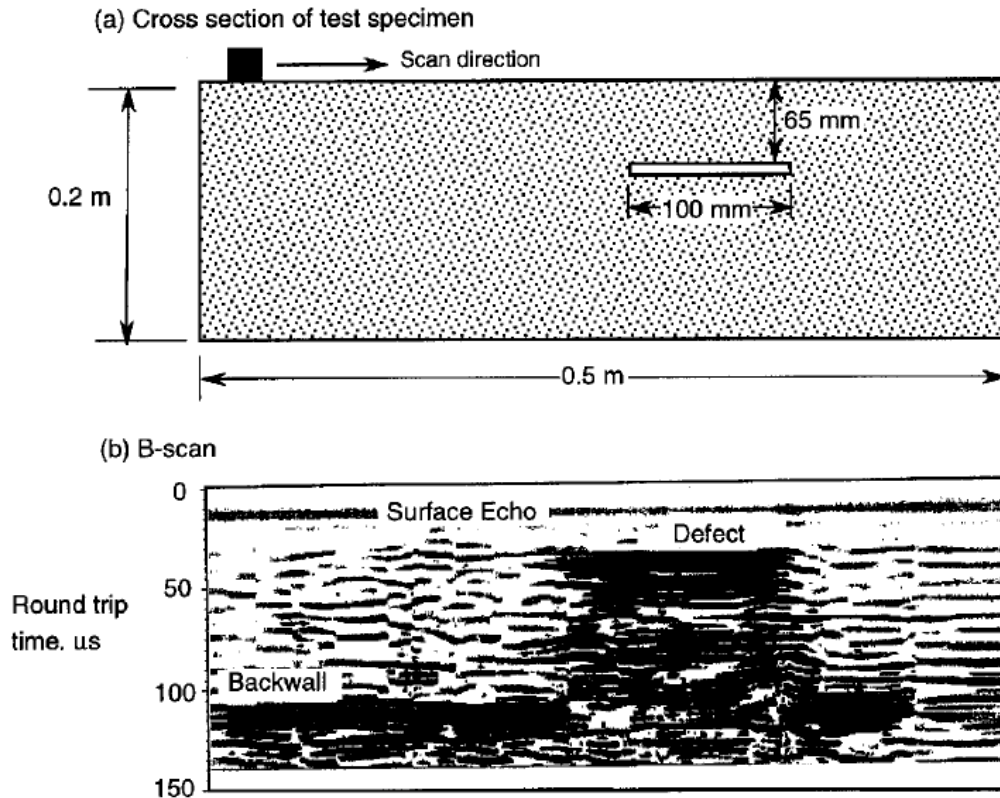


Figure 8: An example of an ultrasonic Pulse-Echo test on concrete: (a) a test sample containing an artificial defect, and (b) a B-scan displaying the defect's position [58, 59]

2.3.3 Factors Affecting UPV Measurements

To ensure a repeatable measurement of pulse velocity that accurately reflects the physical properties of the concrete being tested, it is essential to account for various factors that can influence pulse velocity. According to the European standard EN 12504-4, the factors that affect pulse velocity measurements include the concrete's moisture content, temperature, the path length of the waves, the shape and size of the specimen, the presence of reinforcing bars, as well as the existence of cracks and voids.

The moisture content has a chemical and a physical impact on the pulse velocity. The creation of correlations for the assessment of concrete strength relies heavily on these effects. There can be a sizable pulse velocity difference between a structural element composed of the same concrete and a properly cured standard cubical or cylindrical specimen. While some of the variance can be attributed to the existence of free water in the voids, most of the variation is explained by the impact of various curing conditions on the cement's hydration. When assessing strength, it's critical to properly take these impacts into account.

Tests have shown that to see no change in the pulse velocity measurements, the temperature of concrete should be in between 10 °C and 30 °C. without significant changes in the strength and/or elastic properties. If the samples are beyond this range, corrections based on existing literature must be made to the measured pulse velocity.

The path length over which the pulse velocity is measured needs to be long enough to be unaffected by the concrete's heterogeneity. It is advised that the minimum path length for concrete with a nominal aggregate size of 20 mm or less should be 100 mm and for concrete with a nominal aggregate size between 20 mm and 40 mm should be 150 mm. Changes in path length generally have no effect on pulse velocity, though the electronic timing apparatus may show a trend for velocity to slightly decrease with increasing path length. This is because the pulse's higher frequency components are attenuated more than its lower frequency components, and the pulse's onset form gets more rounded as it travels farther. As a result, the apparent decrease in pulse velocity results from the difficulty in precisely defining the pulse's beginning, which varies on the method employed. Although this apparent decrease in velocity is typically negligible and generally does not influence the measured values more than 2%, extra caution must be used when transmitting over lengthy paths.

Unless the specimen's least lateral dimension is less than a certain value, the speed of short vibration pulses is independent of the size and shape of the specimen under the condition that the lateral dimension is not less than a minimum value. The pulse velocity may be measured significantly lower below this value. The magnitude of this reduction is mostly determined by the ratio between the wavelength of the pulse vibrations to the specimen's smallest lateral dimension. The link between the transducer frequency and the pulse velocity in concrete is given in EN 12504-4 and is shown in the table below (Table 3). In this table also suggestions for the specimen's minimum allowable lateral dimension are provided.

Transducer frequency kHz	Pulse velocity in concrete (km/s)		
	$V_c = 3,5$	$V_c = 4,0$	$V_c = 4,5$
	Minimum recommended lateral specimen dimension (mm)		
24	146	167	188
54	65	74	83
82	43	49	55
150	23	27	30

Table 3: Effect of specimen dimensions on pulse transmission [60]

Furthermore, it also seems that reinforcing bars influence the pulse velocity, therefore EN 12504-4 recommends avoiding close measurements to reinforcing steel bars, in which both the reinforcing bars and the pulse propagation waves are parallel.

In addition, it should be mentioned that cracks and voids also influence the pulse velocity in concrete. This is being caused because there is very little energy transmission across a concrete-air interface when an ultrasonic pulse traveling through concrete encounters it. When the projected length of the void is longer than the width of the transducers and the wavelength of sound being employed, any air-filled crack or void that is directly between two transducers would obstruct the direct ultrasonic beam. When this occurs, the transit time is greater than in concrete of a similar type without a flaw, because the first pulse that arrives at the transducer has to go around the edges of the defect. Depending on the distance between the transducers, it may be feasible to use

this effect to find flaws, voids, or other defects that are deeper or larger than 100 mm. The reason behind this is because they do not have a large influence on the transit times. Thankfully, these defects are in general also less important in terms of safety than the larger ones. Plotting contours with the same velocity generally reveals important details about the quality of a concrete unit. Information may also be usefully obtained by looking at the signal attenuation.

In the same manner, when transducers are positioned so that a cavity is in the direct path between them, a survey of measurements at grid sites on the concrete structure allows for the investigation of a cavity by measuring the transit periods of pulses passing between them. If the pulses follow the path with the shortest transit durations between the transducers and around the cavity, the size of such cavities can be estimated. These estimates are only reliable if the concrete around the cavity is uniformly dense.

In contrast, there are also cases where the pulse energy can pass unhindered through cracked members. This is the case when compressive forces are holding the cracked faces of the members in close contact. This can be seen at cracked vertical bearing piles, for instance. Digital reading technology cannot identify cracks that are partially filled with solid particles or filled with liquid that transmits ultrasonic radiation, such as in maritime constructions. Also in these situations, attenuation measurements can provide useful information.

2.4 Relationship Between UPV and Concrete Damage

2.4.1 Correlation Between UPV Values and Damage Severity

The correlation between Ultrasonic Pulse Velocity (UPV) and concrete damage severity has been a subject of extensive research, yielding insightful findings [61]. The study by Ofuyatan et al. (2021) is a cornerstone in this area, demonstrating a clear linear relationship between the compressive strength of cubic concrete specimens and their UPV readings. This study is not just about establishing a correlation but also about understanding the underlying mechanics of how concrete's structural properties, such as density, elasticity, and internal flaws, affect the velocity of ultrasonic pulses. The linear relationship found is critical because it provides a straightforward, quantifiable link between an easily measurable property (UPV) and a key indicator of concrete's structural integrity (compressive strength). This correlation is a valuable tool for engineers and inspectors, allowing them to quickly assess the quality of concrete structures non-destructively.

Adding depth to this correlation, another research introduced a probability-based method to interpret UPV measurements [62]. This innovative approach addresses the common challenge of data variability in UPV readings, an obstacle that often complicates the interpretation of results. By incorporating probability interpretations, the method allows for a more nuanced understanding of concrete strength, providing a more reliable estimate even when faced with data dispersion. This approach represents a significant advancement in UPV methodology, enhancing the tool's accuracy and applicability in varying field conditions.

Complementing these studies, further research has validated the correlation between concrete strength and UPV by analysing data from various reinforced concrete structures [63]. This extensive analysis confirms that the relationship between UPV and concrete strength is not just a theoretical concept but a consistent, observable phenomenon in various concrete applications. This consistency across different types of concrete structures and conditions validates the reliability and versatility of UPV as a standard tool in structural health monitoring.

An innovative approach for evaluating concrete conditions also integrates UPV readings with other concrete properties, such as compressive strength, concrete cover, surface hardness, and the mix frequency [64]. The application of UPV is expanded by this multi-dimensional analysis, making it a more complete diagnostic tool. By correlating UPV with a range of concrete properties, this approach provides a more holistic view of concrete health, enhancing the potential applications of UPV in both routine assessments and specialized investigations.

Furthermore, it has been observed that concrete mixes with a lower water-to-cement ratio, which typically yield higher compressive strength, also tend to have higher UPV values [65]. This observation links the material composition of concrete directly to its ultrasonic properties, offering valuable insights into how different concrete formulations can be optimized for both strength and UPV performance. This finding is particularly relevant for the development of high-performance concrete mixes where both strength and durability are critical.

2.4.2 Case Studies Demonstrating UPV's Efficacy in Damage Assessment

The application of UPV in real-world scenarios is illustrated through various case studies, providing concrete proof of its effectiveness in assessing concrete damage. The Concrete Quality Designation (CQD) method demonstrates this application, offering a quantifiable measure of concrete degradation by comparing UPV measurements from intact and heavily damaged concrete specimens [66]. This method's strength lies in its ability to provide a normalized assessment scale, applicable across a wide range of structures and conditions. The normalization process is crucial, as it accounts for the inherent variability in concrete properties and environmental conditions, ensuring that the assessment is both accurate and consistent. The CQD method is a significant advancement in concrete diagnostics, providing a standardized, objective measure of concrete health that is invaluable for maintenance and safety evaluations.

In another experimental study, researchers explored the correlation between UPV residual data and the compressive strength of concrete with various mixture proportions [67]. This investigation highlights UPV's adaptability and sensitivity to different concrete conditions, ranging from standard mixtures to those with unique compositions. The study's findings are significant, as they demonstrate UPV's ability to provide reliable data across a wide spectrum of concrete types, making it an indispensable tool in both routine and specialized concrete assessments. The adaptability of UPV to different concrete conditions is a testament to its versatility as a diagnostic tool, capable of providing valuable insights in a variety of construction and repair scenarios.

When several case studies are combined, a strong body of evidence is produced that UPV analysis is a suitable method for assessing concrete damage [68]. These studies, focusing on UPV variations, offer a comprehensive view of how UPV readings can be interpreted to measure the extent of damage in concrete structures. The consistency in findings across various studies not only validates the effectiveness of UPV but also enhances its credibility as a standard tool in structural health monitoring. These case studies demonstrate the practical application of UPV in real-world scenarios, underscoring its role as a reliable, non-destructive evaluation method for assessing the health and integrity of concrete structures.

A specific case study presented an in-depth comparison between traditional methods and a new approach for identifying compressive concrete strength, utilizing a combination of destructive and non-destructive tests, including UPV [62]. This comparative analysis is crucial, as it highlights the evolution in concrete testing methodologies, showcasing the growing significance and reliability of UPV in the context of modern engineering practices. The study provides valuable insights into the advancements in concrete testing, illustrating how UPV, when used in combination with other testing methods, can offer a more comprehensive understanding of concrete's structural health. This comparative approach is indicative of the dynamic nature of the field, where traditional methods are continually being refined and augmented by newer, more sophisticated techniques.

2.4.3 Challenges in Quantifying Damage Depth with UPV

The use of ultrasonic pulse velocity (UPV) to measure the depth of surface cracks in concrete reveals a complicated relationship between the technology and the properties of the concrete material [69]. While UPV can provide general assessments of concrete quality and uniformity, its precision in quantifying the depth of surface cracks or notches remains a challenge. This complexity arises from the heterogeneous nature of concrete, where variations in material composition, crack orientation, and environmental factors can significantly influence UPV wave propagation. Advanced simulations aimed at ascertaining the feasibility of UPV in accurately quantifying crack depth have shown promising results, especially for cracks that develop in the thickness direction on a concrete surface. These simulations are crucial in refining the methodologies for UPV application, ensuring that the assessments are accurate and reliable even in the presence of complex crack geometries.

One of the key challenges in using UPV for damage depth quantification is the sensitivity of the method to various factors that can affect the propagation of ultrasonic waves in concrete [70]. These factors include the moisture content, the presence of microcracks, and the heterogeneous composition of the concrete itself. The studies on this subject highlight the need for careful calibration and interpretation of UPV data, especially when dealing with complex or unusual concrete conditions. For instance, in assessing fire-damaged concrete structures, it has been suggested that UPV tests should be conducted on water-saturated specimens. This recommendation is based on the observation that saturation reduces the impact of microcracking on UPV readings, thereby enhancing the accuracy of the assessment. However, the presence of moisture can introduce its own set of challenges, as it may lead to variations in UPV readings due to changes in the concrete's density and elastic properties. Due to this complexity, UPV testing requires a sophisticated methodology in which the unique circumstances and properties of the concrete under evaluation are carefully considered. The importance of accounting for such variables is shown in research that suggests modifications to testing procedures to ensure the reliability of UPV results. This ongoing research into the complexities of UPV testing reflects the dynamic nature of the field, where new challenges are continually being identified and addressed through innovative methodologies and technologies.

2.5 Porosity and W/C Ratio Influence on UPV

2.5.1 Understanding Porosity and its Importance

The durability and integrity of concrete can be significantly impacted by multiple factors leading to material degradation [71]. A key factor in this is the level of porosity and permeability found within the concrete's internal structure. Typically, concrete with high porosity or poor compactness is more vulnerable to penetration by various liquids and gases, which can deeply infiltrate the material. This infiltration often accelerates issues like freeze-thaw damage, formation of a carbonation layer, chemical corrosion of the concrete, and rusting of reinforcing materials. It also facilitates easier passage of liquids through the structure. Therefore, comprehending the nature and characteristics of the internal porous texture in concrete is crucial when addressing its durability challenges.

Concrete is an inherently complex material, comprising a mix of solid particles (such as coarse and fine aggregates and cement), dissociated and crystalized water, and air trapped in holes and cracks. The formation of these holes and cracks, a natural consequence of the mixing and hardening processes, significantly influences the material's permeability. The size, number, distribution, and configuration (whether open or closed) of these voids vary greatly, depending on their cause and conditions (Table 4). The internal porosity of concrete can be categorized into three distinct types based on the cause and size of these voids. The three categories of holes which are relevant for the porosity are: gelation holes, capillary holes, and non-capillary holes [71, 72].

When concrete is freshly mixed and subsequently sets, a reaction occurs where the cement interacts with water, leading to the formation of cement stone through a process called hydration. Initially, the outermost layer of the cement particles dissolves, leading to the gradual development of gel-like and crystalline structures that encompass the core of the cement that has yet to hydrate. As hydration progresses from the exterior towards the interior, the dehydrated core of the cement particles diminishes. Consequently, the gel layer surrounding each cement particle becomes thicker and begins to interlink with the gel layers of neighbouring particles. In the early stages of hydration, tiny, closed pores known as gelation holes appear within the cement gel. Although their overall volume is relatively small, the porosity within the cement increases over time, primarily due to the evaporation of water. Despite this increase in porosity, these gelation holes exhibit low permeability, rendering them generally harmless to the overall structure of the concrete.

As water evaporates and the gelation process intensifies and solidifies during the hydration of cement, fine capillary holes emerge within the cement stone. Initially, these capillary holes appear at the interfaces where the cement stone meets the coarse and fine aggregates. The size of these holes is influenced by the water-cement ratio in the concrete, with larger ratios leading to bigger holes. As hydration progressively moves deeper into the cement particle, the outer layer transforms into a gel, expanding in volume by approximately 1.2 times, which in turn reduces the porosity of these capillary holes. These capillary holes within the cement stone vary in shape, with most being open, and their collective volume is significant. Particularly, the capillary holes that form at the boundary between the cement stone and the aggregate due to water evaporation are larger and more numerous, resulting in an even greater volume.

Consequently, these capillary holes make up about 10-15% of the total volume of the concrete, significantly impacting its permeability.

Besides the two types of holes which are mentioned above and that inevitably form during the hydration of cement, various non-capillary holes of differing shapes and sizes also emerge irregularly in concrete structures during construction. These include air holes that occur naturally during the processes of mixing, casting, and compacting fresh concrete. Additionally, air holes are sometimes intentionally generated to enhance the concrete's resistance to freeze-thaw cycles. Cracks can also form when the concrete mix or cement mortar separates beneath coarse aggregate and reinforcement, particularly as water evaporates. After the hydration of cement, any excess water that evaporates can leave behind voids. Micro-cracks may develop under the internal stress caused by temperature or humidity differences between the interior and exterior of the concrete. Furthermore, large holes and cracks may appear in both the surface layer and interior of the concrete due to operational mistakes during construction.

Type of porosity	Main Causing Reason	Typical Size (μm)	Total Volume in Concrete (%)	Shape
Gelation hole	Chemical contraction of cement hydration	0.03-3	0.5-10	Closed (most parts)
Capillary hole	Remained after water evaporation	1-50	10-15	Opened (most parts)
Hole due to internal dissociation	Dissociation at boundaries of reinforcement and aggregate	10-100	0.1-1	Opened (most parts)
Horizontal crack	Dissociation by layers	100-1000	1-2	Opened (most parts)
Air hole	Introduced specially by air entraining agent	5-25	3-10	Closed (most parts)
	Introduced occasionally during mixing, casting, and compacting	$(0.1-5) \times 10^3$	1-3	Closed (most parts)
Micro crack	Shrinkage	$(1-5) \times 10^3$	0-0.1	Opened
	Changing temperature	$(1-20) \times 10^3$	0-1	Opened
Large hole and defect	Compacting inadequately or missed	$(1-500) \times 10^3$	0-5	Opened

Table 4: Type and Features of Concrete Porosity Texture [71]

Other factors which influence the texture, and the porosity of concrete are the water-cement ratio, type and fineness of cement, type of aggregate, quality of production, and curing conditions.

In concrete with a higher water-to-cement (W/C) ratio, the water layer around each cement particle is significantly thicker [71]. This excess water is responsible for the formation of a capillary network with larger channels after evaporation, consequently increasing the concrete's total porosity. Generally, the water mixed into fresh concrete is more than what is needed for the complete hydration of the cement. Therefore, the more excess water there is, or the higher the water-cement ratio, the greater the remaining porosity in the concrete after the water has evaporated. A study on the effect of the W/C ratio on the porosity in cement mortar with a constant cement amount found after various durability tests that an increase of the W/C ratio from 0.45 to 0.60 causes an increase of 150% for the porosity. Other factors, such as compressive strength, chloride diffusion coefficient, water loss and air permeability, sorptivity, and moisture diffusion coefficient are also being influenced by the change of porosity. With the increase of the W/C ratio from 0.45 to 0.60 these properties showed the following changes: the compressive strength decreased 24.4%, the water loss increased with 39%, the chloride diffusion increased with 57%, the air permeability increased with 92%, the moisture sorptivity increased with 159%, and the moisture diffusion coefficient increased with 166% [73].

Another factor influencing concrete's porosity is the type and fineness of the cement [71]. Concrete's porosity levels gradually rise when it is mixed separately under the same conditions with other cement kinds, such as alumina, Portland cement, volcanic ash, and slag. Larger gelation and capillary holes, which indicate increased porosity, are especially noticeable in cement that has a higher percentage of coarse particles. On the other hand, if the concrete is properly mixed with fine fly ash or silicon powder particles, the porosity decreases.

When using coarse aggregate made of dense natural rock in concrete, the internal porosity of the aggregate is typically low and most of the holes are closed. However, the porosity varies among different types of rocks, with granite generally having a lower porosity compared to limestone. In the case of various lightweight aggregates, whether they are natural or synthetic, there is a significant presence of porosity, and most of these holes are open. Since the internal porosity can vary among different types of rocks it is also worth to mention that the type of aggregate used within concrete influences its total porosity.

Two other things which also influence the porosity of concrete are the production quality, and the curing conditions. For instance, if concrete is improperly mixed, transported, poured, or compacted during the construction process, it may lead to the formation of significant holes or other flaws. Conversely, when construction is executed with care, the porosity of the concrete tends to decrease. The curing conditions also play a crucial role concerning the porosity of concrete. If the concrete is timely cured and the cement achieves complete hydration, the dimensions and porosity of the capillary holes are likely to diminish. However, curing concrete with heat can significantly impact the structure of these capillary holes due to changes in temperature and humidity. Within certain temperature and humidity conditions, internal cracks can form in the concrete, potentially leading to an increased porosity.

2.5.2 Research Exploring Porosity-UPV Relationships

The correlation between ultrasonic pulse velocity (UPV) and porosity in cementitious materials has been a focal point in recent research, aiming to enhance the quality assessment of building materials. Two notable studies have contributed significantly to this field, each exploring different aspects of the porosity-UPV relationship in mortar with unique additives - limestone and silica fume.

The study titled “Correlation of Ultrasonic Pulse Velocity with Porosity and Compressive Strength of Mortar with Limestone for Building Quality Assessment” [74] delves into the use of UPV tests for predicting mortar quality. This research is crucial in understanding how variations in lime powder addition (20%, 30%, 40%, and 55%) to the mortar mix affect its quality, based on ASTM standards. The key finding of the research is the establishment of a direct proportional relationship between UPV and compressive strength of the mortar, fitting the equation $y = 0.0542e^{0.0015x}$ (Figure 9 (a)). Conversely, it found an inverse relationship between UPV and porosity, indicated by the equation $y = 108.57e^{-6E-04x}$ (Figure 9 (b)). This study shows the effectiveness of non-destructive testing methods in assessing building quality, emphasizing the importance of mortar quality in construction.

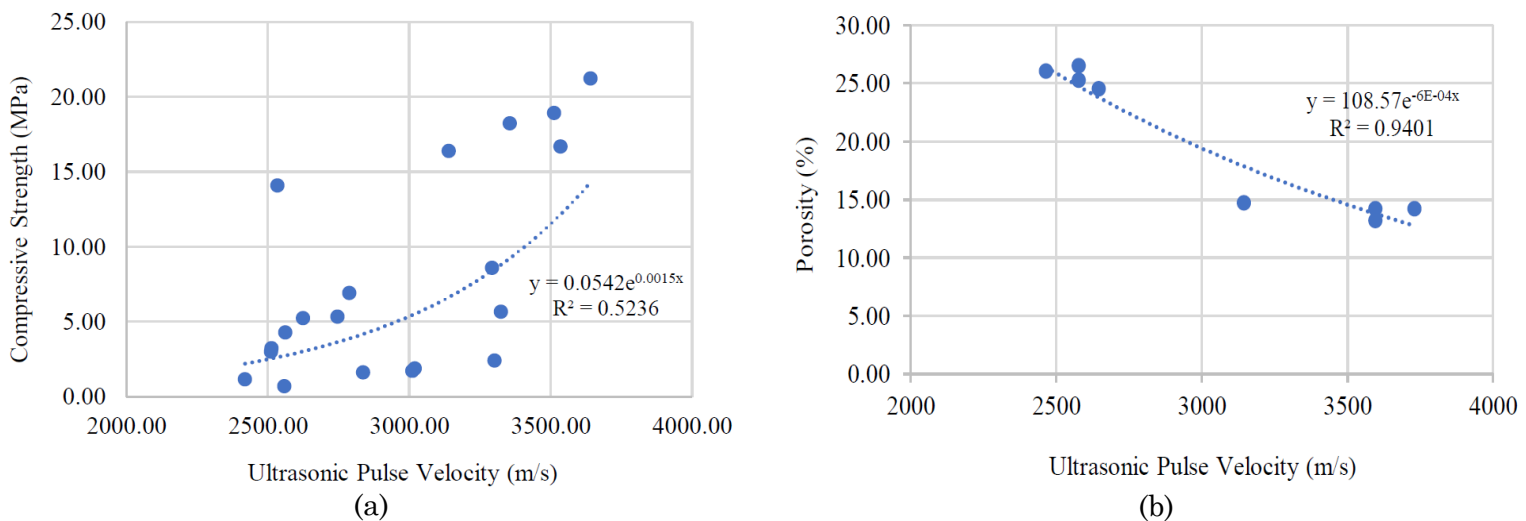


Figure 9: (a) Correlation between Ultrasonic Pulse Velocity and Compressive Strength, (b) Correlation between Ultrasonic Pulse Velocity and Mortar Porosity [74]

Another pivotal research, “Correlation between the Compressive Strength and Ultrasonic Pulse Velocity of Cement Mortars Blended with Silica Fume,” examines how silica fume (SF) replacement rates in cement mortar influence UPV and porosity. This study highlights the role of SF in altering the hydration kinetics and microstructures of cement mortar, thereby impacting its strength and UPV. A notable discovery from this research is that the compressive strength of cement mortar increases with the SF replacement rate, largely at later ages due to a denser microstructure from the pozzolanic reaction of SF. It also established an inverse correlation between compressive strength and porosity, showing that strength increases as porosity decreases. The UPV analysis indicated a gradual increase with age in all specimens, aligning with the

densification of the cement matrix due to hydration and pozzolanic reactions. Furthermore, the study revealed a complex exponential relationship between compressive strength and UPV, influenced by factors like the filling effect and the change in microstructure caused by SF. The conclusions drawn from this study provide a method to estimate the strength of cementitious materials blended with SF, enhancing the understanding of the porosity-UPV relationship in cement mortar.

These two research studies tried to provide a better understanding of the porosity-UPV relationships in mortars with limestone and silica fume additives and offer vital insights into non-destructive testing methods for assessing building materials. They contribute significantly to the field of construction material testing, providing reliable and efficient ways to predict material quality and strength, crucial for the durability and safety of constructions. In general, what could be said about the relationship of the porosity and the UPV measurements is that a larger porosity causes the measured UPV to become smaller.

2.6 Mechanical Properties of Concrete

2.6.1 Overview of Concrete's Mechanical Properties

Concrete's mechanical properties, including compressive strength, tensile strength, and shear resistance, are fundamental for understanding its behaviour under load and evaluating its structural integrity. These properties are crucial for interpreting results from destructive and non-destructive testing methods, such as compressive strength tests, three-point bending tests, and Ultrasonic Pulse Velocity (UPV) measurements.

The compressive strength of concrete is one of its most important mechanical properties. According to Zhenhai Guo in *Principles of Reinforced Concrete* [71] and the Chinese National Standard GB/T 50081-2002 [75], the standard test for compressive strength involves a 150 mm cubic specimen. The specimen is cured in a controlled environment ($20 \pm 3^\circ\text{C}$, relative humidity $> 90\%$) and tested at 28 days by applying a compressive load perpendicular to the casting direction. The maximum load is divided by the cross-sectional area to determine the compressive strength (f_{cu}) in N/mm^2 . The test setup induces complex stress fields within the specimen due to interactions between the concrete and the steel plates transmitting the load. Vertical and horizontal forces combine to create a triaxial stress state near the centre, while uniaxial and biaxial states dominate the edges (Figure 10). This results in a failure pattern typically characterized by cracks extending from the mid-height surface towards the corners, culminating in the formation of pyramidal fragments.

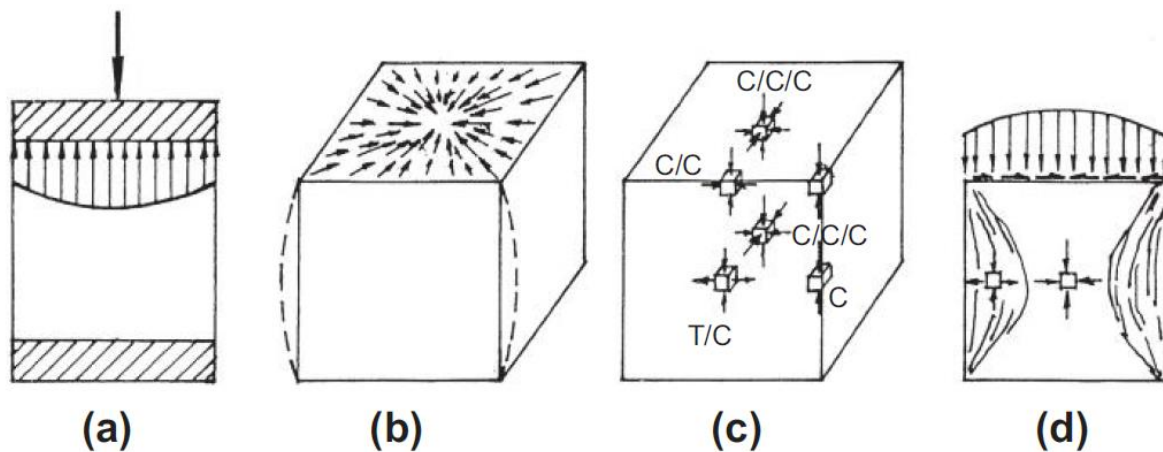


Figure 10: Stress and deformation of cubic specimen under compression. (a) Stress distribution on compressed surface, (b) transverse deformation and restraint on end surface, (c) stress states at several points, (d) failure pattern [71]

Prism specimens are sometimes preferred over cubic specimens for compressive testing, as they provide a more uniform uniaxial stress state in the central section, minimizing the effects of stress concentration at the ends (Figure 11). The prism compressive strength (f_c) is determined by dividing the load at failure by the specimen's cross-sectional area.

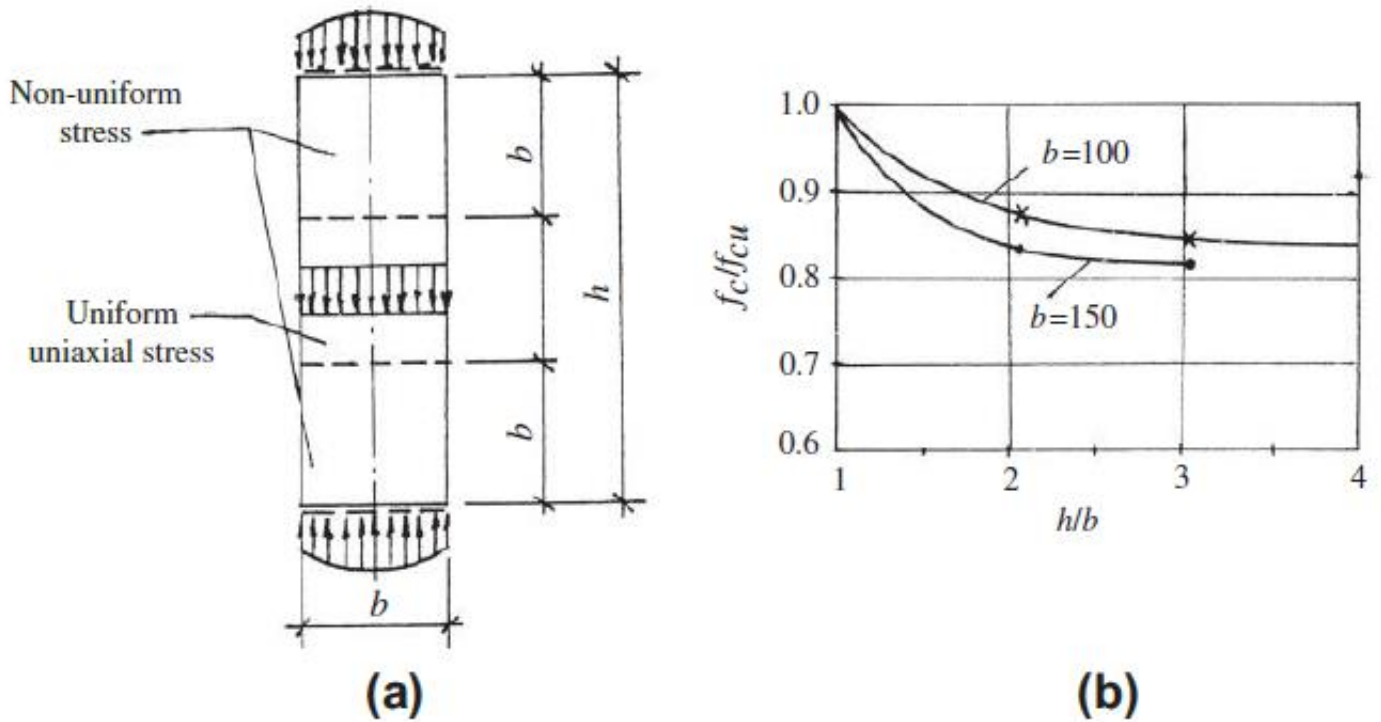


Figure 11: Compression test of prism specimen: (a) distribution of stresses, (b) influence of height-width ratio [71]

Concrete's tensile strength significantly affects its cracking behaviour and deformation under load. Traditionally considered brittle, concrete exhibits limited tensile strength compared to its compressive strength. However, advancements in testing methods have allowed for the measurement of complete tensile stress-strain curves, aiding in understanding its failure mechanisms [76, 77, 71]. Tensile strength is evaluated using three main methods (Figure 12): direct tension tests, splitting tests, and flexural tests. Direct tension tests calculate the central tensile strength (f_t) as $f_t = P/A$, where P is the applied load and A is the fracture surface area. Splitting tests determine the splitting tensile strength ($f_{t,s}$) of concrete, using $f_{t,s} = \frac{2P}{\pi A}$. Flexural tests measure the flexural tensile strength ($f_{t,f}$) using $f_{t,f} = \frac{6M}{(bh^2)}$, or $\frac{Pl}{bh^2}$, where M is the moment and b and h represent the specimen's cross-sectional dimensions. Flexural tests can be performed using both three-point or four-point bending setups. In this study, the three-point bending test is employed, where the load is applied at a single central point to evaluate flexural behaviour. The use of three-point bending is distinct from four-point bending, which applies loads at two points, creating a uniform stress region [78, 77]. Experimental studies reveal a correlation between tensile strength and compressive strength, modelled by regression equations such as $f_t = 0.26f_{cu}^{2/3}$, aligning closely with the CEB-FIP Model Code [79, 80, 81].

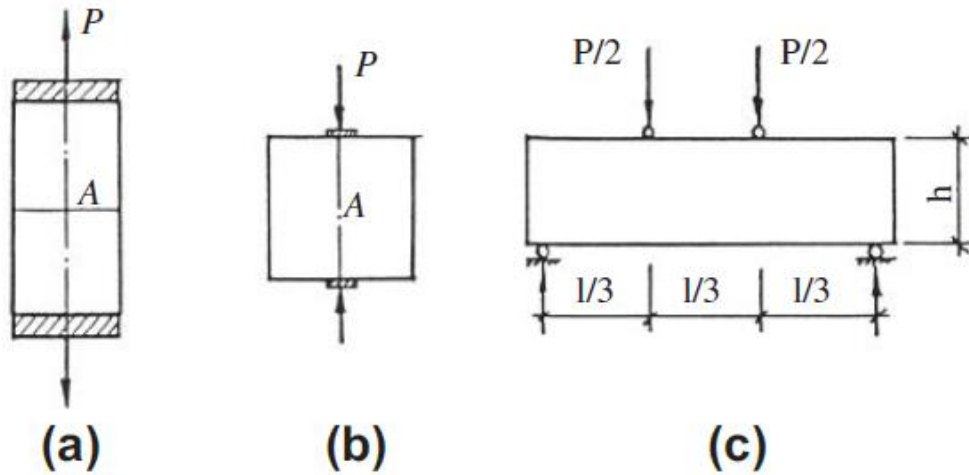


Figure 12: Testing methods for tensile strength: (a) central tension, (b) splitting, (c) bending [71]

Shear strength is critical in analysing concrete's behaviour under complex loading conditions. Various methods are used to evaluate this property, including direct shear, Z-shaped specimens, and torsional tests. These methods yield differing values due to variations in stress distributions (Figure 13). Direct shear tests result in higher shear strength values due to stress concentrations at critical sections. Z-shaped specimens provide consistent shear strength values. Notched beams and tubes simulate near-pure shear stress states, producing results more representative of real-world conditions [82]. Ideal pure shear tests require specialized equipment, limiting their accessibility in standard labs. However, the methods presented offer insights into the shear failure mechanisms and stress distributions critical to structural analysis.

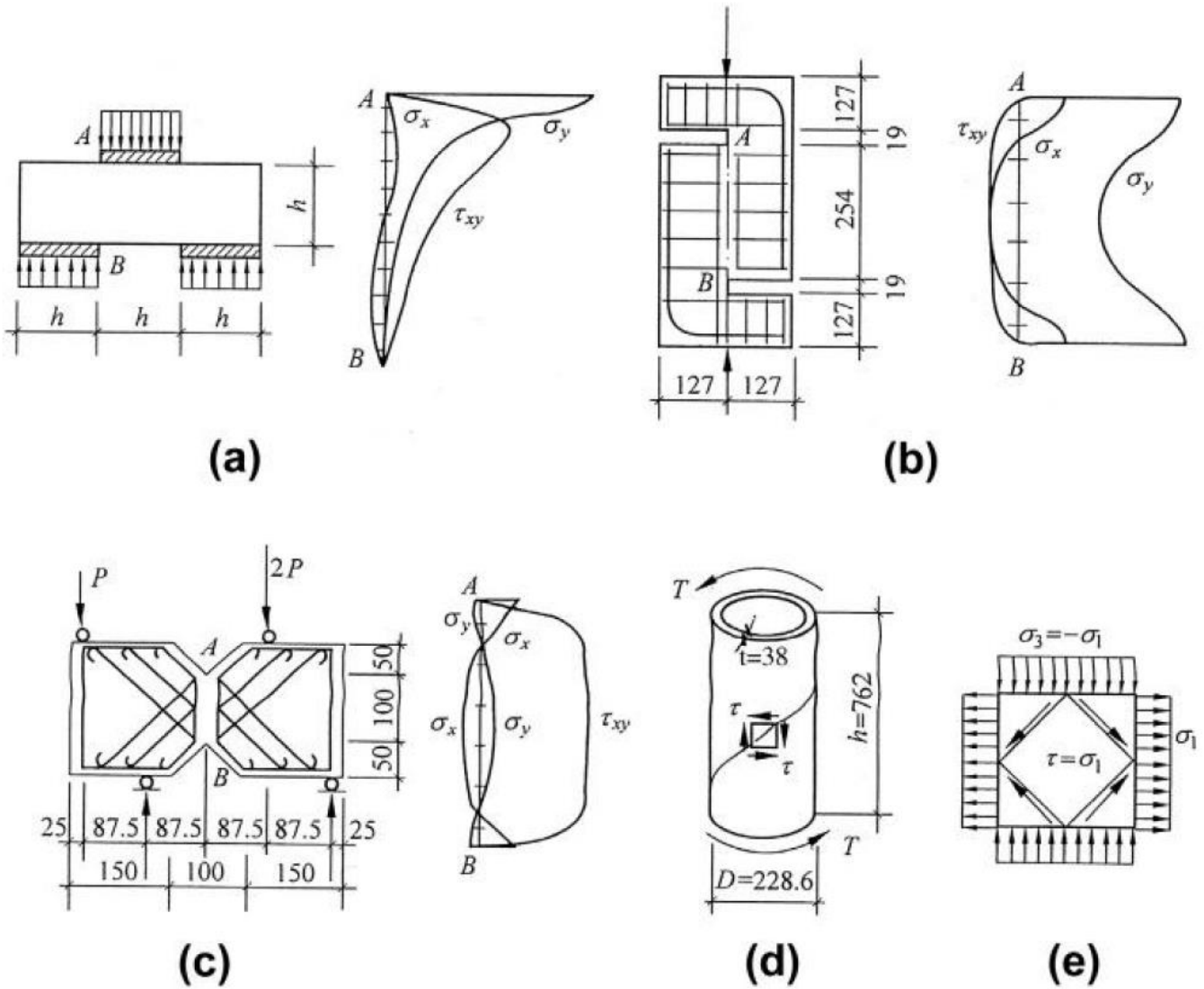


Figure 13: Methods for testing the shear resistance of concrete and the patterns of shear stress distribution on crucial sections, including tension [71, 83]: (a) using a short rectangular beam, (b) employing a Z-shaped specimen, (c) testing a beam equipped with notches, (d) utilizing a circular tube and (e) applying biaxial compression-tension

The mechanical properties of concrete, including compressive, tensile, and shear strength, are fundamental to evaluating its structural performance. While standard testing methods provide essential comparative measures, understanding the limitations and influences of these properties is crucial for interpreting results, particularly in non-destructive testing contexts.

2.6.2 How Mechanical Properties Influence UPV Measurements

Ultrasonic Pulse Velocity (UPV) has emerged as a critical tool in the non-destructive evaluation of concrete structures, allowing for an in-depth assessment of their integrity and mechanical properties. One of the key factors influencing UPV is the concrete's compressive strength. Research shows a strong correlation between compressive strength and UPV readings. The UPV values climb in proportion to the increase in compressive strength, which suggests a denser and more cohesive concrete structure. This relationship is fundamental in non-destructive testing methodologies, as it enables the estimation of concrete strength based on UPV readings, an essential parameter in evaluating structural capacity and stability. Studies have demonstrated that there is a proportionate increase in UPV values as compressive strength increases from moderate to high levels [62, 84, 64, 85].

Additionally, the elasticity and density of the concrete have a significant effect on UPV values. The composition of the concrete, including the types and quantities of cement, aggregates, and water, as well as the curing procedure, determine the influences. Studies have shown that higher density and dynamic modulus of elasticity concrete produces higher UPV readings, indicating a strong internal structure and bonding quality. Furthermore, different aggregate types and cement-to-water ratios in the concrete mix have an impact on UPV. This Phenomena is proven by research where various Mix Designs revealed variable UPV values. For instance, certain mixtures allow faster ultrasonic wave propagation than others [84, 86, 87].

The internal condition of concrete, particularly its moisture content and the presence of flaws like voids or cracks, also significantly impacts UPV readings. Higher moisture levels within the concrete enable the transmission of ultrasonic waves, resulting in increased UPV values. Conversely, the presence of voids or cracks, which can impede wave propagation, is often indicated by reduced UPV values. This sensitivity of UPV to internal concrete conditions has been confirmed in studies, making it a reliable tool for detecting deterioration or internal damage within concrete structures [86].

Predictive models for UPV have been developed because of advances made in the field. These models, which consider the complex relationships between the mechanical characteristics of concrete, allow precise estimations of UPV readings, which helps the adjustment of UPV apparatus and the analysis of outcomes. By accurately predicting UPV values based on known concrete qualities, these models have demonstrated their effectiveness in real-world applications, proving their accuracy and use in real-world situations [88].

Incorporating UPV assessments into the routine evaluation of concrete structures offers a proactive approach to maintenance, significantly contributing to the safety, longevity, and sustainability of these concrete structures. Regular UPV evaluations can facilitate early detection of potential issues, allowing for timely interventions and extending the service life of concrete structures. This application of UPV shows its importance not just as a diagnostic tool, but also as a key component in the preventative maintenance and management of concrete structures [89].

2.7 Standards and Guidelines for UPV testing

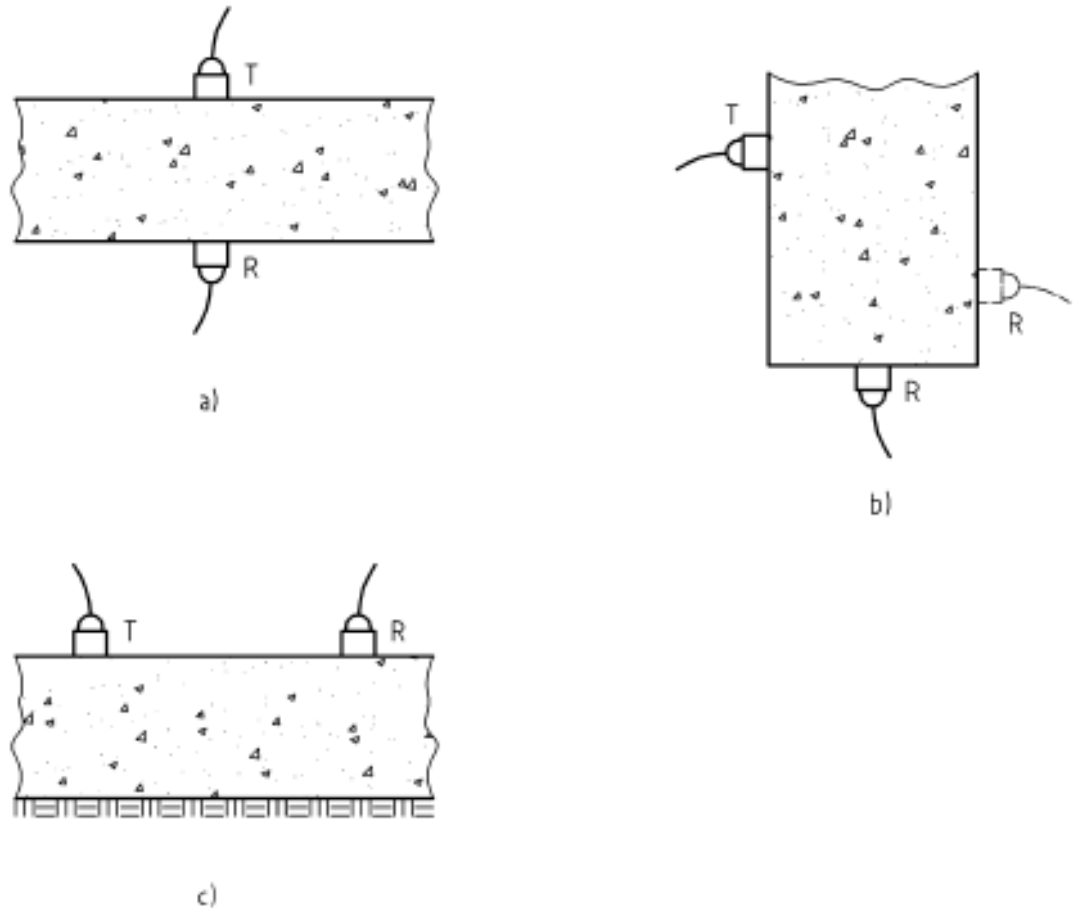
2.7.1 BS EN 12504-4

The BS EN 12504-4:2004 standard provides a comprehensive framework for determining the velocity of ultrasonic longitudinal waves in hardened concrete. This non-destructive testing method is commonly used to evaluate the uniformity of concrete, detect cracks or voids, and assess specific physical properties of the material. The standard outlines the required apparatus, testing procedures, and considerations to ensure accurate and reliable results.

The apparatus specified in the standard includes an electrical pulse generator, a pair of transducers, an electronic timing device, and a calibration bar. The pulse generator produces ultrasonic pulses transmitted through the concrete. Transducers, which typically operate in the frequency range of 20 kHz to 150 kHz, are used to convert these pulses to and from electrical signals. The selection of transducer frequency depends on the path length: higher frequencies (60 kHz to 200 kHz) are preferred for short paths, while lower frequencies (10 kHz to 40 kHz) are suitable for longer paths. For most applications, frequencies between 40 kHz and 60 kHz are commonly used. The timing device measures the transit time of the pulse, either using an oscilloscope to monitor the waveform or an interval timer with a digital display. A calibration bar is used to validate the apparatus, with a required limit deviation of $\pm 0.1 \mu\text{s}$.

The standard describes three main transducer arrangements, as illustrated in Figure 14:

- **Direct Transmission:** Transducers are placed on opposite faces of the concrete, ensuring the shortest and most sensitive path for the ultrasonic pulse.
- **Semi-Direct Transmission:** Transducers are positioned on adjacent faces, typically used at corners or when direct transmission is not feasible.
- **Indirect Transmission:** Both transducers are placed on the same face, often used to assess surface quality or when only one face is accessible. The sensitivity of this arrangement is lower than that of direct or semi-direct transmission.



Key

- R is the receiver transducer
- T is the transmitter transducer

Figure 14: Transducer Arrangements (a) Direct Transmission, (b) Semi-Direct Transmission, (c) Indirect Transmission [60]

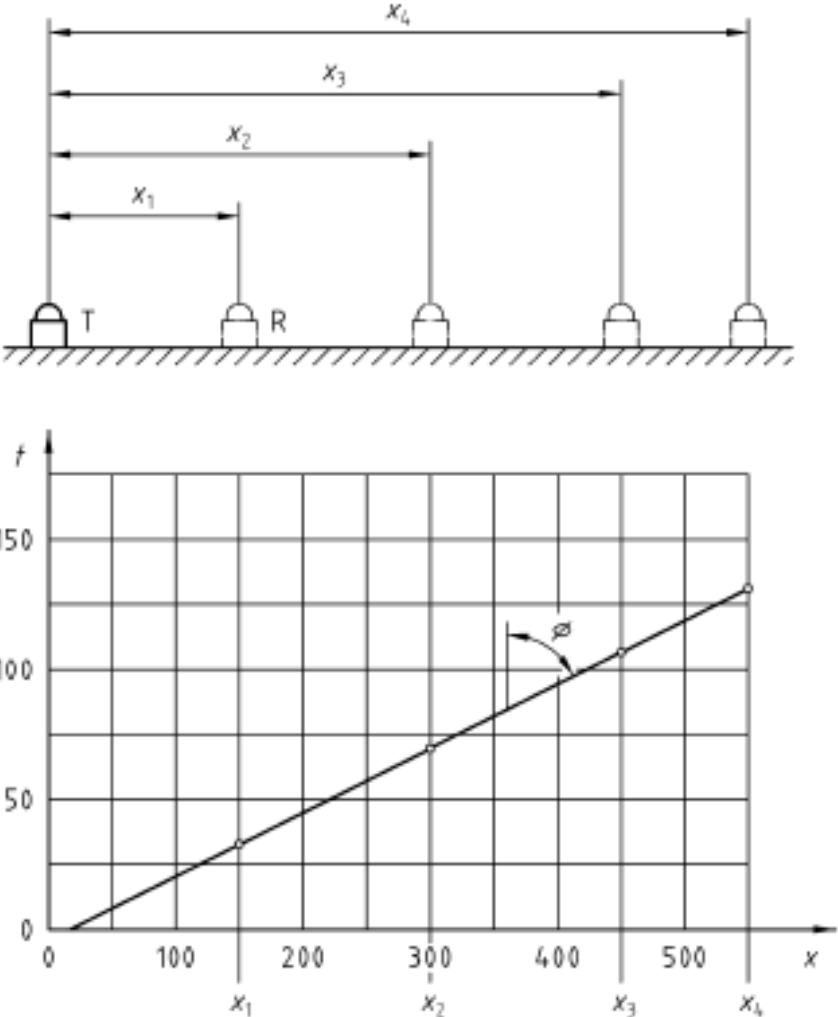
Adequate coupling between the transducer face and the concrete surface is essential for effective ultrasonic energy transmission. The standard recommends the use of coupling media such as petroleum jelly, grease, soft soap, or kaolin/glycerol paste. For rough or uneven surfaces, grinding or applying a quick-setting epoxy resin may be necessary. Repeated measurements are performed to minimize the coupling layer thickness, ensuring consistent transit times.

Pulse velocity (V) is calculated using the formula:

$$V = \frac{L}{T}$$

where L is the path length (m), and T is the transit time (s). For direct and semi-direct arrangements, the path length is measured directly. In the case of indirect transmission,

a series of measurements is taken at varying transducer distances. The slope of the best-fit line plotted from these measurements determines the pulse velocity, as shown in Figure 15.



Key

- R is the receiver transducer
- T is the transmitter transducer

Figure 15: Determination of Pulse Velocity Using Indirect Transmission [60]

As was mentioned earlier in Paragraph 2.2.2, several factors affect pulse velocity measurements, including moisture content, temperature, path length, specimen dimensions, reinforcing bars, and the presence of cracks or voids. The standard recommends a minimum path length of 100 mm for concrete with a maximum aggregate size of 20 mm or less and 150 mm for larger aggregates. Additionally, the smallest lateral dimension of the specimen should exceed the wavelength of the pulse to avoid velocity reduction, as indicated in Table 5.

Transducer frequency kHz	Pulse velocity in concrete (km/s)		
	$V_c = 3,5$	$V_c = 4,0$	$V_c = 4,5$
	Minimum recommended lateral specimen dimension (mm)		
24	146	167	188
54	65	74	83
82	43	49	55
150	23	27	30

Table 5: Minimum Recommended Lateral Dimensions for Specimens Based on Pulse Velocity and Transducer Frequency [60]

The test report, as outlined by the standard, must include details such as the identification of the tested structure or specimen, test setup, transducer arrangement, coupling method, specifications of the equipment, measured path lengths, and calculated pulse velocity values. Any deviations from the standard procedure must also be documented. Results should be expressed to the nearest 0.01 km/s.

In summary, the BS EN 12504-4:2004 standard provides detailed guidelines for conducting ultrasonic pulse velocity tests on concrete. Its structured approach ensures consistency and reliability, making it an essential reference for non-destructive testing of concrete structures. Figures 14 and 15 and Table 5 provide visual and tabular references to support the implementation of the described procedures.

2.7.2 ASTM C597: Standard Test Method for Pulse Velocity through Concrete

ASTM-C-597 outlines the standard test method for measuring pulse velocity through concrete. This method involves generating longitudinal stress wave pulses in concrete and measuring their transit time. It details the significance of these measurements in assessing concrete quality, detecting voids and cracks, and evaluating repair effectiveness. The standard includes guidelines on apparatus setup, procedure, calculations, and reporting. It emphasizes the importance of factors like test location selection, transducer placement, and the influence of concrete conditions on test results. The standard aims to ensure reliable, uniform testing practices for concrete assessment. According to the standard the pulse velocity is related to the elastic properties and the density of concrete and can be determined by using the formula shown below.

$$V = \sqrt{\frac{E(1 - \mu)}{\rho(1 + \mu)(1 - 2\mu)}}$$

Where:

E = dynamic modulus of elasticity

μ = dynamic Poisson's ratio, and

ρ = density

When determining the pulse velocity, the degree of saturation and the dimension of the test object should be taken into consideration. It has been noticed that the pulse velocity in saturated concrete can lead to measured pulse velocities which are 5% higher than in dry concrete. As it comes to the dimensions of the test object, it should at least exceed the wavelength of the ultrasonic waves. The wavelength is equal to the pulse velocity divided by the frequency of vibrations.

To ensure stable transit times and a proper signal strength, sufficient coupling agent and pressure must be applied to the transducers. The strength of the signal is also being affected by the presence of cracking and deterioration, and by the travel path length in the concrete tested. To ensure proper coupling, a verification should be performed by viewing the shape and the magnitude of the received waveform. The shape of the wave can be checked by making use of either an oscilloscope, or digitized display coupled to the device.

Path lengths are approximately 50 mm minimum and 15 m maximum, with the presently available test equipment. The measurable path length is highly dependant upon the frequency and intensity of the produced signal, the surface conditions, the presence of reinforcement, and the interior of the concrete. To perform accurate measurements, it is important to first consider the path length, and based upon this information select the transducers with a proper resonant frequency. Measurements in close to the maximum path length are preferably determined with transducers which have low resonant frequencies (20 to 30 kHz). For shorter path lengths, it is advised to use transducers with a resonant frequency of 50 kHz or higher.

A pulse generator, two transducers (transmitter and receiver), an amplifier, a time measurement circuit, a time display unit, and connecting cables make up the testing apparatus, which is schematically shown in Figure 16.

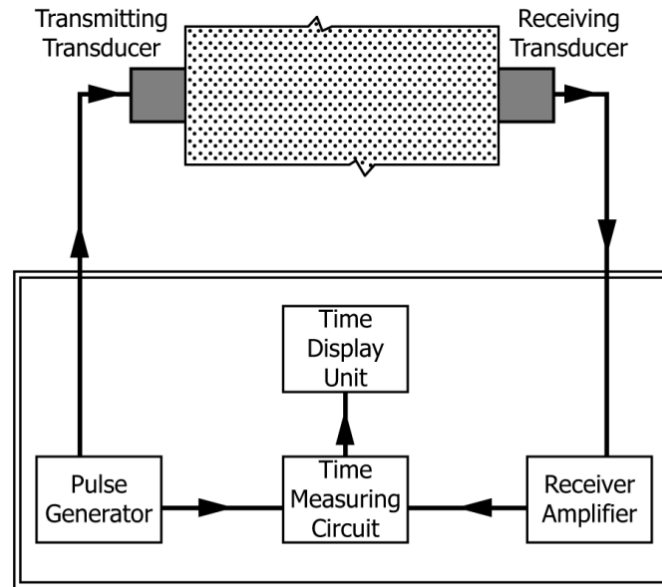


Figure 16: Schematic view of the Ultrasonic pulse velocity device [81]

The following factors should be considered to obtain accurate results. The transducers of the apparatus are being used to transfer the pulses into wave bursts of mechanical energy and should have a resonant frequency in the range from 20 to 100 kHz. The pulse generator should produce repetitive pulses at a rate of not less than 3 pulses per second. The used transducer should be made of piezoelectric, magnetostrictive, or other voltage-sensitive material (Rochelle salt, quartz, barium titanate, lead zirconate-titanate (PZT), etc), housed for protection. The device should be programmed to produce a triggering pulse which starts the time measuring circuit. Both the transmitting and the receiving transducer should be identical. The amplifier should have a flat response which is between one half and three times the resonant frequency of the receiving transducer. The measuring setup should be able to provide an overall time-measurement resolution of at least 1 μ s, and insensitive to operating temperatures in the range from 0 to 40 °C and voltage changes in the power source of $\pm 15\%$.

For the testing two types of display units are available, the first one is a modern unit which makes use of an interval timer and a direct-reading digital display of the interval time, the other one uses a cathode ray tube which presents the deflections of the traces in relation to an established time scale.

Furthermore, the standard also states to make use of a reference bar. This reference bar is made of metal or other durable material for which the transit time of longitudinal waves is known. This reference bar is used to perform a zero-time adjustment, this reduces the delay time of the equipment significantly. For some instruments the zero adjustment can also be performed without the use of a reference bar. In these cases, after applying a coupling agent the faces of the transducers are pressed together and by

doing so, the microprocessor of the device can record the delay time. The measured delay time is automatically subtracted from the subsequent transit time. As a verification the advice is given to also make use of a reference bar to check whether a proper zero-time correction is performed.

It is important that during testing an appropriate coupling agent is being used such as water, oil, petroleum jelly, grease, mouldable rubber, or other viscous materials. This coupling agent should be applied to either the transducer faces or the test surface, or both. After doing so the faces of the transducers should be tightly pressed against the surfaces of the concrete until a stable transit time is displayed and measure this transit time. Afterwards the distance between the centres of the transducers should be measured in a straight line.

The pulse velocity can be calculated with the following formula:

$$V = \frac{L}{T}$$

Where:

V = pulse velocity, m/s,

L = distance between centres of transducer faces, m, and

T = transit time, s

The documentation of the results should at least consist of the location of the test or the identification of the specimen, the location of the transducers, the distance between the transducer faces and the transit time to a precision of at least 0.5%, and the pulse velocity reported to the nearest 10 m/s.

2.7.3 ACI 228:2R: Non-destructive Test Methods for Evaluation of Concrete in Structures

Several techniques utilizing stress-wave propagation are applicable for the non-destructive examination of concrete structures. The ultrasonic pulse velocity approach is effective for identifying irregular areas within a structure. Echo methods are suitable for measuring thickness and identifying defects. The Spectral Analysis of Surface Waves (SASW) technique is utilized for assessing pavement thickness and the elastic properties of layered pavement systems. Stress waves are generated when a sudden force or deformation, such as an impact, is applied to a solid's surface. This disturbance moves through the solid similarly to how sound waves travel through air. The velocity of stress-wave movement in an elastic solid depends on its modulus of elasticity, Poisson's ratio, density, and shape. This relationship between a solid's properties and its stress-wave behaviour enables deductions about the solid's characteristics by observing stress wave movement. When a sudden pressure is exerted at a point on a solid half-space's surface, the disturbance moves through the solid as three distinct waves. The P-wave and S-wave move into the solid in hemispherical wavefronts. The P-wave, or dilatational/compression wave, is linked with the movement of normal stress and has particle motion parallel to its direction. The S-wave, or shear/transverse wave, relates to shear stress and has particle motion perpendicular to its direction. Additionally, an R-wave spreads along the surface away from the disturbance. In an isotropic, elastic solid, the P-wave speed C_p correlates with the Young's modulus of elasticity E , Poisson's ratio ν , and density ρ as described by Krautkrämer and Krautkrämer in 1990.

$$C_p = \sqrt{\frac{E(1-\nu)}{\rho(1+\nu)(1-2\nu)}}$$

According to the following formula (Krautkrämer and Krautkrämer, 1990), the S-wave propagates at a slower speed C_s .

$$C_s = \sqrt{\frac{G}{\rho}}$$

Where:

G = the shear modulus of elasticity

The ratio of S-wave speed to P-wave speed is a useful quantity and is shown below.

$$\frac{C_s}{C_p} = \sqrt{\frac{1-2\nu}{2(1-\nu)}}$$

This ratio is equal to 0.61 for a Poisson's ratio of 0.2, which is common for concrete. The following formula can be used to approximate the ratio of the R-wave speed C_r to the S-wave speed (Krautkrämer & Krautkrämer, 1990).

$$\frac{C_r}{C_s} = \frac{0.87 + 1.12\nu}{1 + \nu}$$

The R-wave travels at a speed between 90% and 92% of the S-wave speed for a Poisson's ratio between 0.15 and 0.25. In an infinite solid, the P-wave speed is represented by C_p . For bounded solids, the solid's geometry also has an impact on the wave speed. The wave speed for wave propagation down the axis of a thin bar is determined by the following formula, which is independent of the Poisson's ratio.

$$C_b = \sqrt{\frac{E}{\rho}}$$

Where C_b is the speed of the bar wave, the wave speed in a thin bar is 3–9% slower than the P-wave speed in a big solid for a Poisson's ratio between 0.15 and 0.25. Only a part of the incident wave is reflected when a stress wave passes through Material 1 and through the interface is being transferred to Material 2. When the angle of incidence is 90 degrees (normal incidence), the amplitude of the reflected wave reaches its maximum. The following formula provides the reflection coefficient R for normal incidence.

$$R = \frac{Z_2 - Z_1}{Z_2 + Z_1}$$

Where:

R = ratio between the sound pressure of the incident and the reflected wave,

Z_2 = specific acoustic impedance of Material 2, and

Z_1 = specific acoustic impedance of Material 1

The specific acoustic impedance is a factor, which is being determined by the wave speed and the density of the material. The estimated Z-values for several materials according to Sansalone and Carino, 1991 are shown in Table 6.

Material	Specific acoustic impedance, kg/(m²s)
Air	0.4
Water	1.5 x 10 ⁶
Soil	0.3 to 4 x 10 ⁶
Concrete	7 to 10 x 10 ⁶
Limestone	7 to 19 x 10 ⁶
Granite	15 to 17 x 10 ⁶
Steel	47 x 10 ⁶

Table 6: Approximate Z-Values for some materials [90]

With this being known, it can be derived that a stress wave which passes through concrete and meets an air interface leads to a reflection coefficient of almost 1.0. In other words, there is almost no reflection at the interface. For this reason, non-destructive testing (NDT) techniques which make use of stress waves have shown promising results in identifying flaws in concrete.

One of the earliest non-destructive testing (NDT) techniques for concrete measures the pulse of ultrasonic compressional waves transit time along a predetermined path length. Ultrasonic via transmission, or more widely, the ultrasonic pulse velocity method, is the name of the methodology. Tomsett (1980) examined the method's numerous uses, while Naik and Malhotra (1991) summarised the test procedure. In the late 1940s, field equipment to measure pulse velocity were developed almost simultaneously in England and Canada (Whitehurst, 1967). An instrument to evaluate the degree of dam cracking was desired in Canada (Leslie and Cheesman, 1949). The focus in England was on creating a tool to evaluate the quality of concrete pavements (Jones, 1949).

The underlying idea of this method is that, as was previously mentioned, the density and elastic constants of the solid determine how quickly stress waves propagate. Changes in materials, mix proportions, or curing can result in changes in elastic characteristics in a concrete member. Non-uniform consolidation in the other hand can cause variations in density. As a result, conclusions regarding the uniformity of the concrete can be drawn by measuring the wave speed at various points across a structure. The stress pulse's travel time over a certain distance is measured to find the compressional wave speed.

Figure 17 demonstrates the testing principle, showing the paths of ultrasonic pulses as they cross from one side of a concrete element to the other. The first scenario depicts the quickest and shortest path through intact concrete, also known as the through-transmission method, leading to the shortest duration or highest apparent wave speed. The second scenario illustrates a path crossing a segment of lower-quality concrete, while the third scenario displays a path deflecting around a large void or crack. In these latter scenarios, the duration is longer than in the first case. The final scenario presents a path obstructed by a void, causing a complete reflection of the stress waves, preventing them from reaching the opposite side. The apparent wave speeds are calculated by dividing the thickness of the member by the recorded travel time. Comparing wave speeds at various testing points helps identify irregularities within the member. Additionally, signal attenuation might serve as a measure of concrete quality, but this demands careful attention to maintain consistent transducer coupling at all test locations, as noted by Teodoru in 1994.

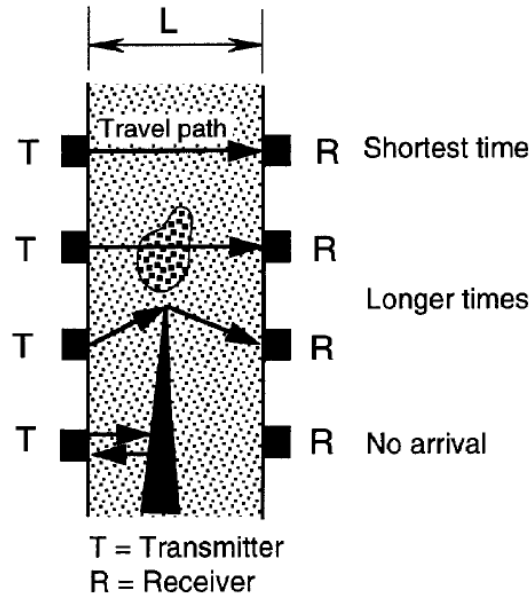
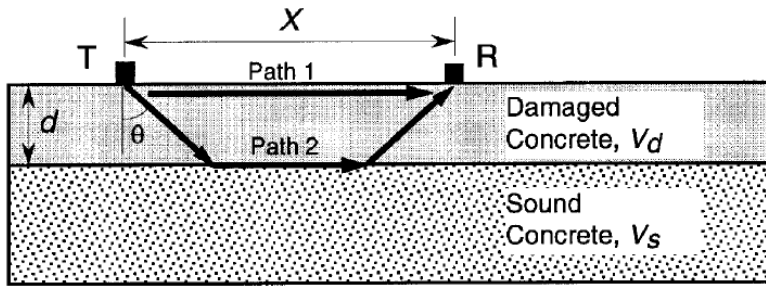
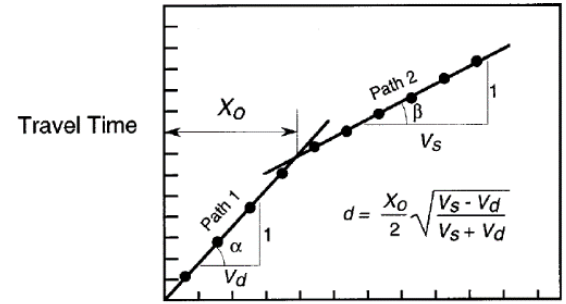


Figure 17: Effects of defects on travel time of the ultrasonic pulse velocity [58]

Equipment for through-transmission tests, as depicted in Figure 18 (a), has been utilized on the same surface. This method is recommended for assessing the depth of a fire-damaged surface layer with a lower wave speed compared to the intact concrete beneath (Chung and Law, 1985), and for determining the depth of concrete affected by freezing (Teodoru and Herf, 1996). The procedure involves measuring the travel time as it relates to the distance X between the transmitter and receiver. It is hypothesized that the stress wave reaches the receiver via two routes: Route 1, directly through the damaged concrete, and Route 2, through both the damaged and the intact concrete. For a smaller separation, the travel time is less for Route 1, while for a greater separation, Route 2 has a shorter travel time. Plotting the travel time against the distance X reveals a damaged surface layer by a shift in the data's slope. The point X_0 , where travel times for both paths equalize, is determined from the intersection of the linear plots as shown in Figure 18 (b). The slopes of these lines inversely represent the wave speeds in the damaged and sound concrete. The depth of the damaged layer is calculated using the method described by Chung and Law in 1985, and the formula which is used by this method is shown below.



(a)



Distance, X

(b)

Figure 18: (a) Wave paths for ultrasonic testing on a concrete surface with a damaged top layer; and (b) transit time as a function of transmitter and receiver distance [58]

$$d = \frac{X_0}{2} \sqrt{\frac{V_s - V_d}{V_s + V_d}}$$

The surface technique depends on recording the arrival time of low amplitude waves. It's essential for the user to comprehend the instrument's ability to accurately measure these arrival times. Additionally, understanding of the fundamental principles of seismic refraction, as outlined by Richart et al. in 1970 is crucial, since this helps to understand the fundamentals of the equation which is used to calculate d. The method to calculate d is only effective when the wave speed in the upper layer is slower than that in the lower layer.

Figure 19 illustrates the key elements of modern tools used for measuring ultrasonic pulse velocity. The setup involves placing a transmitting transducer on one side of the structure and a receiving transducer on the opposite side. These transducers are equipped with piezoelectric ceramic components, which either change size when voltage is applied or experience a voltage change upon deformation. A pulser activates the transmitting transducer (source) with a high voltage, causing it to oscillate at its natural frequency and generate a stress pulse that moves into the structure. Concurrently, a highly precise electronic timer starts as soon as the voltage pulse is initiated. The timer stops when the pulse reaches the receiver and is converted back into a voltage signal, displaying the travel time. The criteria for an appropriate pulse-velocity device are specified in ASTM C 597. To ensure effective contact with the test surfaces, the transducers are bonded using a viscous substance like grease or a non-staining ultrasonic gel couplant, especially if staining of the concrete is a concern. Transducers with various resonant frequencies are employed, with 50 kHz transducers being most used. Lower-frequency transducers (around 20 kHz) are preferred for mass concrete, while higher-frequency transducers (exceeding 100 kHz) are selected for thinner elements where precise measurement of travel times is crucial. However, for most purposes, 50 kHz transducers are adequate.

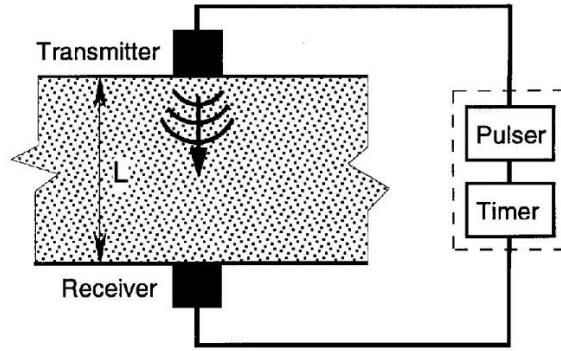


Figure 19: Schematization of the main components to measure the ultrasonic pulse velocity [58]

2.8 Other Non-Destructive Testing Techniques

In addition to the Ultrasonic Pulse Velocity (UPV) and Pulse-Echo methods central to this study, several other Non-Destructive Testing (NDT) techniques have been explored in the literature. While these methods are valuable in assessing concrete integrity, their relevance to delamination and honeycombing detection varies. This section provides a concise overview of these methods, focusing on their principles, applications, and limitations, and their relevance to this research.

2.8.1 Visual Inspection

Visual examination is recognized as a highly adaptable and potent method in the realm of non-destructive testing (NDT) [58]. The utility of this approach is significantly influenced by the skill and knowledge level of the practitioner conducting the inspection. It is important to note that visual inspection primarily allows for the assessment of external surfaces, leaving internal flaws undetected and failing to provide quantitative details about material properties, such as in concrete structures. Consequently, it is common practice to combine visual inspection with other NDT methodologies to achieve a more thorough analysis.

For enhanced effectiveness, inspectors are advised to employ supplementary tools alongside visual inspection. Devices like optical magnifiers, which range from basic hand-held magnifying glasses to sophisticated microscopes, enable detailed examination of specific problem areas. The relationship between magnification power and focal length is inverse; higher magnification necessitates closer proximity to the object being examined. However, this comes with the drawback of a reduced field of view and depth of field, the latter being crucial for keeping textured surfaces in focus. Additionally, greater magnification demands more intense lighting, often necessitating supplemental artificial illumination.

Innovative tools have been developed for more precise inspections, such as hand-held magnifiers with integrated measuring scales for accurate crack assessment. Stereo microscopes which offer a three-dimensional perspective, aiding in evaluating surface elevations. Technologies like fiberscopes and borescopes which are being used for inspecting areas which are not visible to the naked eye. The fiberscope consists of a bundle of optical fibres and a lens system and facilitates the examination of internal cavities through small openings, while a borescope, with its rigid structure and lens system, provides clearer but more limited viewing capabilities.

The introduction of small digital video cameras, equipped with charge-coupled devices (CCDs), represents a significant advancement in visual inspection technology. These cameras come in various sizes and resolutions, and their ability to provide video feeds enhances the inspection process, especially in challenging environments.

To summarize, the efficacy of visual inspection in NDT is dependent upon the inspector's expertise and background knowledge. Typically, visual inspection forms just one component of a comprehensive evaluation strategy, often being combined by a variety of other NDT techniques or more invasive procedures, to provide a holistic understanding of the structure under examination.

2.8.2 Impact Echo

The Impact-Echo method is a well-established non-destructive testing technique that generates a stress pulse through a mechanical impact on a structure's surface. Unlike ultrasonic transducers, which produce focused pulses, the impact-induced stress pulse spreads in multiple directions within the material, leading to reflections from internal and external boundaries. This diffusion allows for the detection of internal defects such as delamination and honeycombing, as well as the measurement of thickness in concrete elements [58].

The fundamental concept of the Impact-Echo method is illustrated in Figure 20. A mechanical impact initiates P-waves and S-waves within the test specimen, which propagate hemispherically through the material. Additionally, surface waves travel along the specimen's surface away from the impact point. When these waves encounter boundaries, such as the bottom of the structure, inclusions, or defects, they are reflected to the surface. These reflections, termed echoes, are detected by a receiving transducer and recorded via a data acquisition system. Analysing these waveforms in the time domain helps identify the location and nature of defects [58].

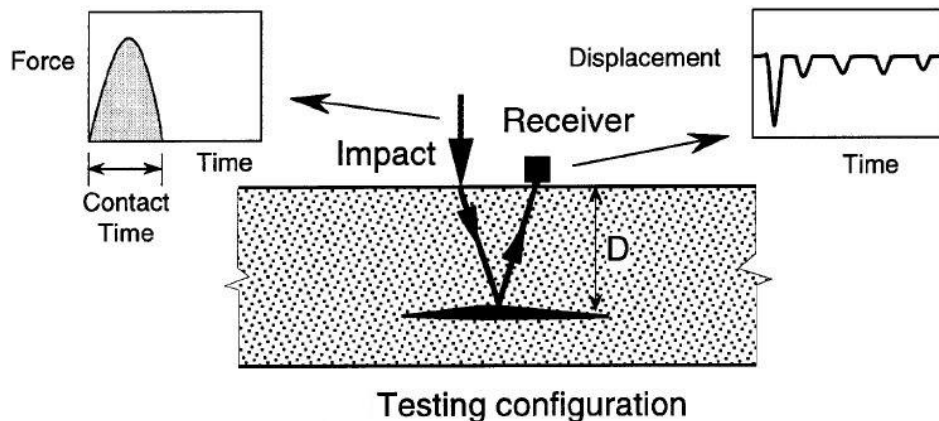


Figure 20: Schematic view of impact-echo method [58]

For plate-like structures, the reflections caused by repeated stress wave interactions between the testing surface and reflective interfaces produce a frequency termed the "thickness frequency," which inversely correlates with the structural thickness. Frequency analysis using the Fast Fourier Transform (FFT) provides an amplitude spectrum to identify this frequency. For example, as shown in Figure 21, a solid slab exhibits a peak corresponding to its intact thickness, whereas a slab with voids displays a shifted peak, indicative of internal defects [58].

The Impact-Echo method has been widely used for measuring the thickness of slabs, bridge decks, and walls, detecting delamination, voids, and other subsurface defects in concrete, and evaluating overlay bond quality and crack depth in beams, columns, and hollow cylindrical structures. This method is particularly advantageous for structures with overlays, as it can detect subsurface defects without requiring access to the opposite

side. Its application in identifying defects in long, slender structural components, such as piles and drilled shafts, has been validated through extensive research [58].

The standard Impact-Echo system comprises three main components. First, the impact source generates stress pulses with varying durations depending on the test structure. Shorter impacts, such as 20-80 μs , are suitable for shallow members, while longer impacts exceeding 1 ms are used for deeper structures [58]. Second, the receiving transducer, often a piezoelectric device, detects surface displacements. For pile evaluations, geophones or accelerometers are preferred due to their sensitivity. Finally, the data acquisition system captures and digitizes waveforms for subsequent frequency domain analysis. Modern systems frequently include advanced software for defect localization [58].

Frequency analysis provides a robust framework for interpreting Impact-Echo results. For instance, a concrete slab with a thickness of 0.5 meters exhibits a thickness frequency at 3.42 kHz, corresponding to a P-wave velocity of 3,420 m/s. In contrast, a void within the slab shifts this frequency to 7.32 kHz, indicating a defect at approximately mid-depth (Figure 21).

The Impact-Echo method's ability to detect subsurface anomalies such as delamination and honeycombing makes it integral to this study. Its effectiveness in assessing internal defects and structural integrity complements other techniques like Ultrasonic Pulse Velocity and Ground Penetrating Radar, offering a comprehensive approach to evaluating concrete structures [58].

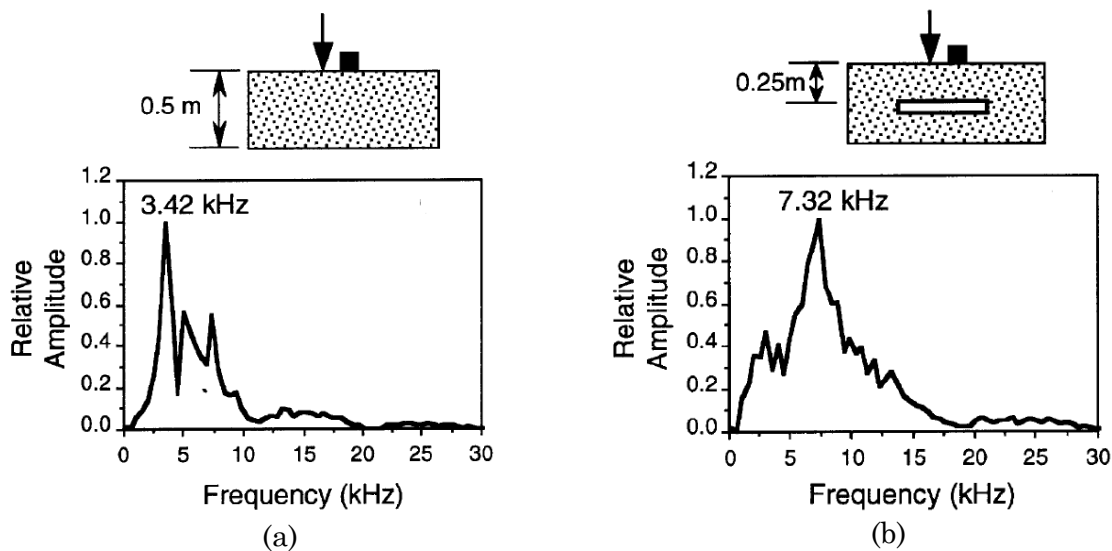


Figure 21: Amplitude spectrum test results: (a) solid slab, (b) slab with void [58]

2.8.3 Ground Penetrating Radar

Ground Penetrating Radar (GPR) is a non-destructive testing method that utilizes electromagnetic waves to evaluate subsurface conditions in concrete structures. Functioning on principles like the Pulse-Echo method, GPR uses electromagnetic waves instead of stress waves. Initially developed for military purposes, the technology has since been adapted for civil engineering applications such as detecting underground voids, locating reinforcing bars, assessing concrete thickness, and identifying material degradation. Its effectiveness in large-scale infrastructure assessments, such as airfield pavements and bridge decks, has been supported by numerous studies, including those by Bungey and Millard (1993) and Halabe et al. (1993, 1995) [58, 91].

The GPR system consists of a transmitter that emits short electromagnetic pulses, typically in the microwave frequency range, into the structure. These pulses travel through the material and reflect when encountering boundaries with differing dielectric properties, such as concrete-air or concrete-reinforcement interfaces. The reflected signals are received by an antenna and analysed to determine the characteristics and location of the interface. For concrete inspections, pulse durations typically range from 1 to 3 nanoseconds, with centre frequencies between 500 MHz and 1 GHz commonly used for structural surveys. The principles of electromagnetic wave propagation and reflection in GPR are illustrated in Figure 22.

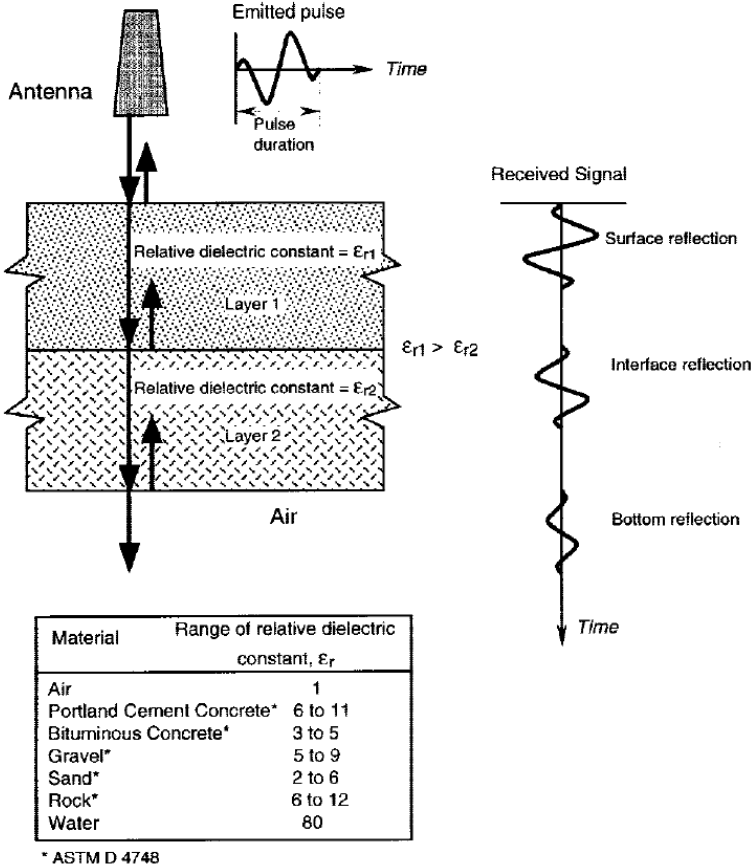


Figure 22: Electromagnetic radiation pulse reflections at the interfaces between materials whose relative dielectric constants differ [91]

Key to the method's accuracy is the dielectric constant of the material, which determines the velocity of electromagnetic waves and affects signal attenuation. The relative dielectric constant (ϵ_r) is the ratio of the material's dielectric constant (ϵ) to the dielectric constant of free space ($\epsilon_0 = 8.85 \times 10^{-12}$ farad/m). This relationship is expressed as:

$$\epsilon_r = \frac{\epsilon}{\epsilon_0}$$

Where:

ϵ = dielectric constant (farad/m), and

ϵ_0 = dielectric constant of free space (air), which is 8.85×10^{-12} farad/m

The relative dielectric constant is a key factor in determining the velocity of electromagnetic waves within a specific material. In the case of low-loss materials, the speed of these electromagnetic waves, denoted as C , can be calculated using the following formula.

$$C = \frac{C_0}{\sqrt{\epsilon_r}}$$

Where:

C_0 = speed of light in air (3×10^8 m/s), and

ϵ_r = relative dielectric constant

By analysing the captured time-domain waveforms, one can ascertain the depth of the reflecting interface, provided the relative dielectric constant is known. This depth is derived from the calculated round trip travel time of the electromagnetic wave and its speed. If the round-trip travel time of the pulse is represented as t , then the depth D can be determined as follows.

$$D = \frac{Ct}{2}$$

The difference in dielectric constant between two distinct materials dictates the quantity of energy reflected at their interface. In the context of low-loss dielectrics, the reflection coefficient, which is the ratio of the amplitudes of the reflected electromagnetic field to those of the incident field at an interface, can be calculated using the following formula, as described in the works of Clemeña (1991) and Bungey and Millard (1993).

$$\rho_{1,2} = \frac{\sqrt{\epsilon_{r1}} - \sqrt{\epsilon_{r2}}}{\sqrt{\epsilon_{r1}} + \sqrt{\epsilon_{r2}}}$$

Where:

$\rho_{1,2}$ = reflection coefficient

ϵ_{r1} = relative dielectric constant of Material 1 (incident wave), and

ϵ_{r2} = relative dielectric constant of Material 2

These relationships enable GPR to detect subsurface defects such as voids, delamination, and honeycombing by identifying variations in dielectric properties. For instance, water has a significantly higher dielectric constant than concrete, making moisture-laden areas highly reflective. However, closely spaced reinforcement bars can overshadow weaker signals from voids, complicating interpretation [91].

The GPR system typically includes an antenna, control unit, data storage, and display devices. Lower-frequency antennas penetrate deeper but provide lower resolution, while higher-frequency antennas offer finer detail at shallower depths. For example, a 1-GHz antenna achieves a penetration depth of approximately 400 mm in concrete. Portable systems are suitable for localized evaluations, while vehicle-mounted systems are preferred for large-scale assessments, such as scanning bridge decks for delamination and corrosion [58].

Compared to stress-wave methods like Impact-Echo, GPR is less sensitive to concrete-air interfaces because only about 50% of the energy reflects at such boundaries. However, its ability to penetrate beyond these interfaces enables detection of features located below surface voids. Research has demonstrated GPR's utility in detecting defects beneath asphalt overlays and evaluating moisture intrusion, further solidifying its role in structural health monitoring [91].

Ground Penetrating Radar complements techniques like Ultrasonic Pulse Velocity and Impact-Echo by offering rapid, non-invasive assessments of concrete structures. Its ability to identify moisture content, voids, and reinforcing bars enhances its relevance for evaluating delamination and honeycombing, making it an integral component of a comprehensive diagnostic approach [58, 91].

2.8.4 Infrared Thermography

Infrared thermography is a non-destructive testing method widely employed to identify subsurface irregularities in concrete structures, such as delamination, cracks, and voids. Its application spans various infrastructure types, including bridge decks, roads, pipelines, and buildings. The method is governed by ASTM D 4788, which outlines procedures for detecting delamination in concrete bridge decks with or without asphalt overlays [58].

Infrared thermography detects and visualizes thermal radiation emitted from surfaces, effectively measuring changes in surface brightness rather than directly recording temperature. These variations in surface radiance provide insights into underlying conditions in the concrete. The method is based on two primary principles: radiation and conduction. Radiation emission follows the Stefan-Boltzmann law:

$$R = e\sigma T^4$$

Where:

R = rate of energy radiation per unit area of surface, W/m^2

e = the emissivity of the surface

σ = the Stefan – Boltzmann constant, $5.67 \times 10^{-8} \frac{W}{m^2} * K^4$, and

T = absolute temperature of the surface K

At room temperature, the emitted radiation has a wavelength of approximately 10 μm , placing it in the infrared spectrum. Specialized sensors capture this radiation, generating electrical signals proportional to the energy received. Calibrating the sensor output allows for accurate temperature measurements, facilitating the detection of surface temperature anomalies caused by subsurface defects [58].

Heat transfer anomalies caused by internal defects such as delamination can lead to localized variations in surface temperature. These irregularities disrupt the natural conduction of heat through the material, making them detectable when thermal gradients are present (Figure 23). Heat flow can be artificially induced using heating lamps or naturally achieved through solar heating during the day and cooling at night. The latter methods are cost-effective and commonly used for large-scale inspections [58].

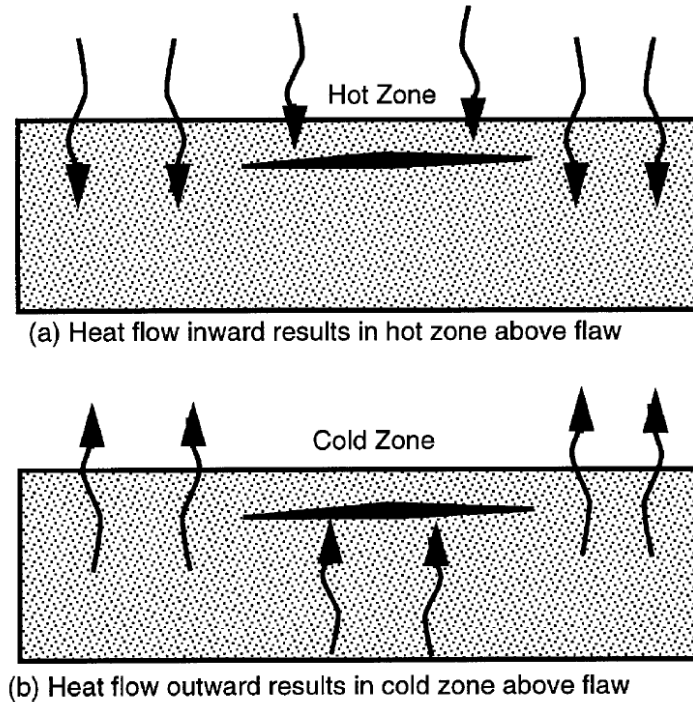


Figure 23: Impact of interior irregularities on surface temperature during heat transfer [58]

Environmental conditions significantly impact the accuracy of thermographic surveys. Factors such as cloud cover, wind, surface moisture, and ambient temperature fluctuations can obscure surface temperature gradients. For optimal results, ASTM D 4788 recommends conducting surveys under clear skies with minimal wind and dry surfaces. Additionally, testing should occur during periods of maximum thermal differential, such as early morning or shortly after sunset. This timing ensures that subsurface anomalies are highlighted by distinct surface temperature variations [92].

Infrared thermography systems typically consist of a scanner/detector unit, data collection and analysis device, and a visual image recording component. The scanner uses lenses to capture infrared radiation in specific wavelength ranges, such as 3 to 5.6 μm (shortwave) or 8 to 12 μm (medium wave). Older systems employ rotating mirrors for two-dimensional scanning, whereas modern devices use two-dimensional arrays of infrared-sensitive materials, eliminating the need for mechanical components. The scanner setup is depicted in Figure 24.

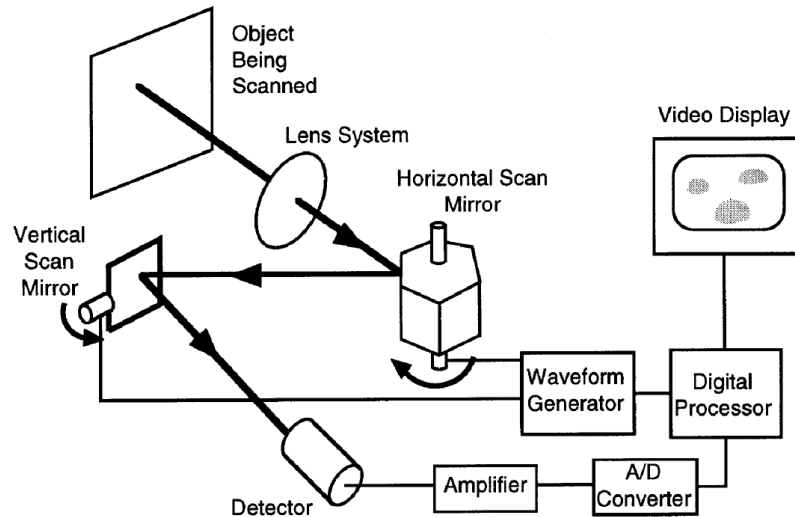


Figure 24: Schematic view of the infrared scanner equipment that produces thermal images [58, 93]

The captured data is processed into grayscale or coloured thermal images, highlighting regions with temperature anomalies. These images are often compared to visual photographs to differentiate true subsurface defects from surface emissivity variations caused by contaminants like oil or rubber residues. Figure 25 illustrates a concrete bridge deck's optical image alongside its corresponding infrared thermogram, where delaminated areas are identified as bright "hot spots." False indications, such as those caused by asphalt patches, are also noted in the thermographic image [58].

Infrared thermography provides a rapid, non-invasive method for assessing large concrete surfaces, making it especially useful for inspecting bridge decks, highways, and airport runways. Although primarily suited for detecting shallow subsurface defects, it offers a broad overview of surface and near-surface conditions. Its ability to visualize thermal anomalies ensures its continued relevance in structural health monitoring [58, 93].

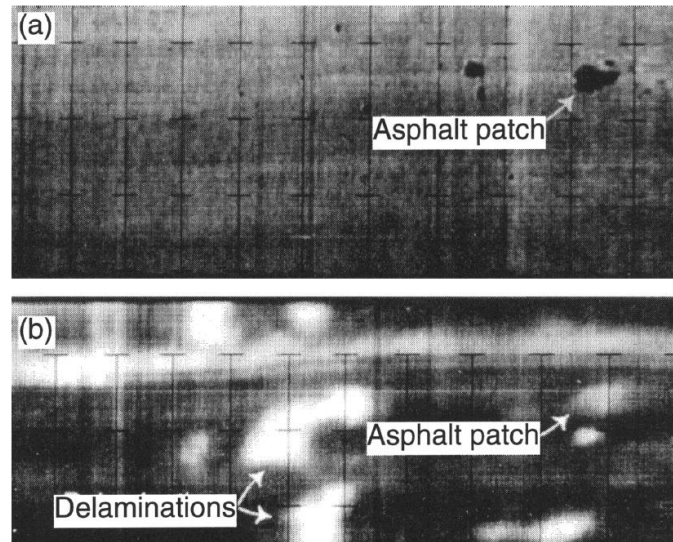


Figure 25: Example of (a) A concrete bridge deck optical image, and (b) an infrared thermogram displaying “hot spots” that correspond to concrete delamination areas and false indications caused by asphalt patches [58]

2.8.5 Acoustic emission

Acoustic emission (AE) refers to the generation of transient elastic waves caused by the sudden release of energy from specific points within a material [94]. These waves are commonly produced during processes such as crack formation and growth, dislocation movements, and phase changes in metals. AE can also originate from natural events like earthquakes or secondary sources such as leaks, cavitation, and the Barkhausen effect. By capturing these waves using sensitive transducers placed on the material’s surface, AE provides valuable insights into energy release points and damage mechanisms, making it widely applicable in material science and structural health monitoring [94].

AE signals are generally categorized into two types: continuous and burst. Continuous emissions are assessed by their root mean square (RMS) voltage, while burst-type signals are analysed using threshold-dependent parameters (Figure 26). The threshold refers to the voltage level set by the instrument to filter out low-amplitude noise, ensuring that only significant events are recorded. AE systems typically consist of signal detection, data acquisition, processing, and analysis units. Piezoelectric sensors are the most used detectors due to their sensitivity and reliability. Coupling agents like silicone grease are applied to ensure optimal acoustic contact between the sensor and the material’s surface. In cases where direct sensor attachment is not feasible, waveguides can be used to transmit signals effectively. Before use, sensors must be calibrated for frequency response and sensitivity to meet standard requirements [94].

The typical AE testing procedure involves several key steps: selecting the appropriate instrument, positioning the sensors, calibrating the system, applying the stimulus to the test component, and recording and analysing the data. Standards and guidelines provided by organizations such as ASTM, EWGAE, and JSNDI govern these procedures. For example, ASTM standards outline requirements for using AE to monitor structures,

detect welding defects, and identify leaks. These standards ensure consistency and reliability in AE measurements across applications [94].

AE has proven to be particularly effective for real-time monitoring of dynamic damage processes, such as crack propagation or delamination in concrete structures. Its ability to detect energy release events as they occur makes it a valuable complement to other non-destructive testing methods, providing a deeper understanding of the structural integrity of materials.

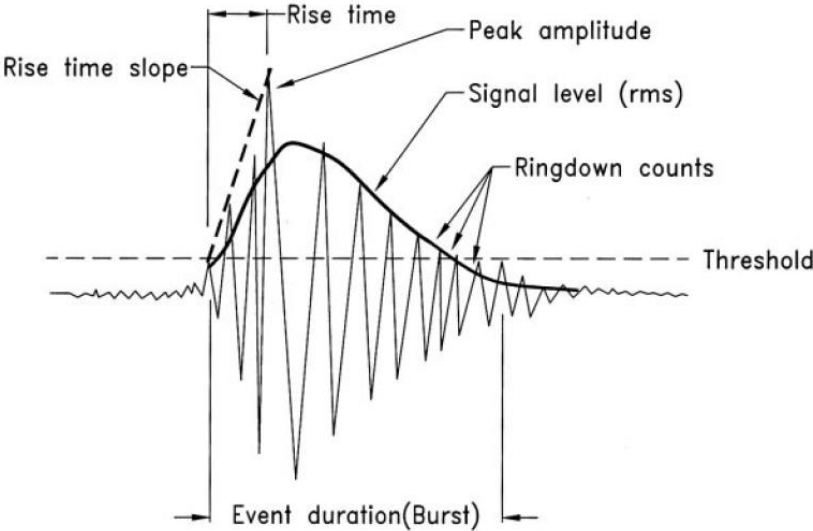


Figure 26: Acoustic emission signal characteristic [94]

2.8.6 Selection of Ultrasonic Pulse Velocity (UPV) Technique

Each non-destructive testing (NDT) technique has distinct advantages and limitations, depending on its suitability for assessing different types of concrete defects. Visual inspection is the simplest and most used approach but is limited to detecting surface-level damage. Impact-Echo and Ground Penetrating Radar (GPR) are valuable for detecting internal voids, delamination, and embedded elements, but these techniques require specialized expertise for data interpretation and can be costly. Infrared Thermography is effective for identifying moisture ingress and thermal variations related to structural defects, but its accuracy depends on environmental conditions, such as surface emissivity and ambient temperature fluctuations. Similarly, Acoustic Emission (AE) techniques enable real-time monitoring of crack propagation but are highly sensitive to background noise, which can affect data reliability in field conditions. A comparative evaluation of these NDT techniques is summarized in Table 7, which highlights their respective advantages and limitations:

NDT Method	Principle	Advantages	Limitations
Visual Inspection	Direct observation of surface defects	Simple, cost-effective, no equipment required	Limited to surface defects, relies on human expertise, no quantitative data
Impact-Echo Method	Uses mechanical impact to generate stress waves and analyse reflections	Effective in detecting delamination, voids, and thickness variations	Requires skilled interpretation, may not detect small cracks, equipment cost
Ground Penetrating Radar (GPR)	Uses electromagnetic waves to detect subsurface features	Can locate voids, moisture, and reinforcement	Expensive, affected by moisture levels, requires trained personnel
Infrared Thermography	Detects temperature variations due to subsurface defects	Non-contact method, useful for moisture ingress and delamination detection	Limited penetration depth, affected by surface conditions and ambient temperature
Acoustic Emission (AE)	Detects stress waves generated by crack propagation	Effective for real-time monitoring of crack activity	Sensitive to background noise, requires continuous monitoring, difficult data interpretation
Ultrasonic Pulse Velocity (UPV)	Measures wave velocity through material to detect internal flaws	Provides quantitative data, detects internal defects, applicable in multiple settings	Requires surface coupling, affected by material heterogeneity

Table 7: Comparison of Non-Destructive Testing Techniques

Among these techniques, Ultrasonic Pulse Velocity (UPV) was chosen as the primary NDT method in this study due to its effectiveness in detecting internal damage, its quantitative assessment capability, and its adaptability in both laboratory and field conditions. Unlike visual inspection, which is limited to detecting external flaws, UPV can identify internal defects such as honeycombing, voids, and delamination. Compared to Impact-Echo and GPR, UPV provides a simpler and more cost-effective approach while still delivering accurate subsurface damage assessment. Additionally, UPV correlates well with mechanical properties, particularly compressive strength and material density, making it a reliable tool for structural health monitoring and quality control.

Furthermore, the Pulse-Echo variation of UPV enhances its application by enabling the detection of defects when only one side of the structure is accessible. This is a significant advantage over other NDT techniques that require access to multiple surfaces for comprehensive analysis. Pulse-Echo not only improves defect localization but also allows for a better estimation of damage depth, which is critical for assessing the severity of internal flaws.

Compared to Impact-Echo, which requires advanced signal processing, UPV offers a more direct and interpretable approach to evaluating structural integrity. Additionally, GPR, while highly effective for reinforcement mapping, is costly and affected by moisture content, making it less practical for routine structural assessments. Infrared Thermography, on the other hand, is useful for detecting moisture-related damage but has limited penetration capabilities, reducing its applicability for deep structural evaluation.

By integrating UPV with the Pulse-Echo method, this study seeks to enhance the accuracy of near-surface damage detection, particularly for delamination and honeycombing, which are critical concerns in concrete structures. Previous research has confirmed UPV's effectiveness in evaluating concrete quality, demonstrating that it is one of the most reliable, cost-effective, and versatile NDT methods available for structural evaluation [24]. Thus, UPV was chosen as the preferred NDT method for this study due to its balance between accuracy, cost-efficiency, and practical applicability. While other techniques remain valuable in specific contexts, UPV in combination with Pulse-Echo offers a robust and reliable approach for assessing concrete integrity in both research and real-world applications.

2.9 Summary and Conclusion

This chapter provided a comprehensive review of the existing literature on damage assessment in concrete structures, focusing on the role of Ultrasonic Pulse Velocity (UPV) as a non-destructive testing (NDT) method. The review covered fundamental aspects of concrete as a construction material, emphasizing its widespread use and inherent durability challenges. It explored the significance of assessing concrete damage, particularly in relation to delamination and honeycombing, which can severely compromise structural integrity if left undetected.

One of the key takeaways from this review was the importance of UPV testing in evaluating the condition of concrete structures. The technique was examined in detail, highlighting its ability to detect internal defects, assess material uniformity, and provide quantitative data on structural health. However, the literature also revealed certain limitations of UPV, including its sensitivity to material properties such as porosity and water-to-cement (W/C) ratio. Studies showed that a higher W/C ratio generally leads to increased porosity, which in turn reduces UPV values, making damage assessment more challenging.

Furthermore, the chapter examined the mechanical properties of concrete and their influence on UPV measurements. It was noted that UPV correlates with compressive strength, but variations in porosity, microcracking, and moisture content can introduce complexities in data interpretation. The review also discussed the relationship between UPV values and damage severity, including the challenges in accurately quantifying the depth of internal flaws.

In addition to UPV, other NDT techniques, such as Impact Echo, Ground Penetrating Radar (GPR), and Infrared Thermography, were reviewed to assess their effectiveness in concrete condition evaluation. Each method has its strengths and weaknesses, but the literature suggests that combining UPV with complementary techniques could enhance damage detection accuracy. While UPV provides reliable velocity-based measurements, methods like Pulse-Echo offer improved depth detection and localization of defects, making them suitable for advanced structural assessments.

The literature review established a strong foundation for the experimental phase of this study by identifying key research gaps and methodological considerations. It confirmed that while UPV is an effective tool for detecting damage in concrete structures, its accuracy is influenced by material properties, measurement techniques, and external conditions. The review also underscored the need for refined testing procedures, improved sensor technology, and hybrid NDT approaches to overcome current limitations.

The findings from this review informed the development of the experimental methodology outlined in the next chapter. By integrating insights from previous studies, this research aims to enhance the reliability of UPV in detecting near-surface delamination and honeycombing defects. Ultimately, the goal is to contribute to the advancement of structural health monitoring techniques, ensuring safer and more durable concrete infrastructure.

3 Experimental Setup and Methodology

In this chapter, the experimental setup and methodology are described in detail. The process of designing and preparing concrete samples, introducing different levels of damage, and performing Ultrasonic Pulse Velocity (UPV) tests is explained. The steps taken to ensure accurate measurements and reliable results are also outlined, providing a clear understanding of how the experiments were conducted.

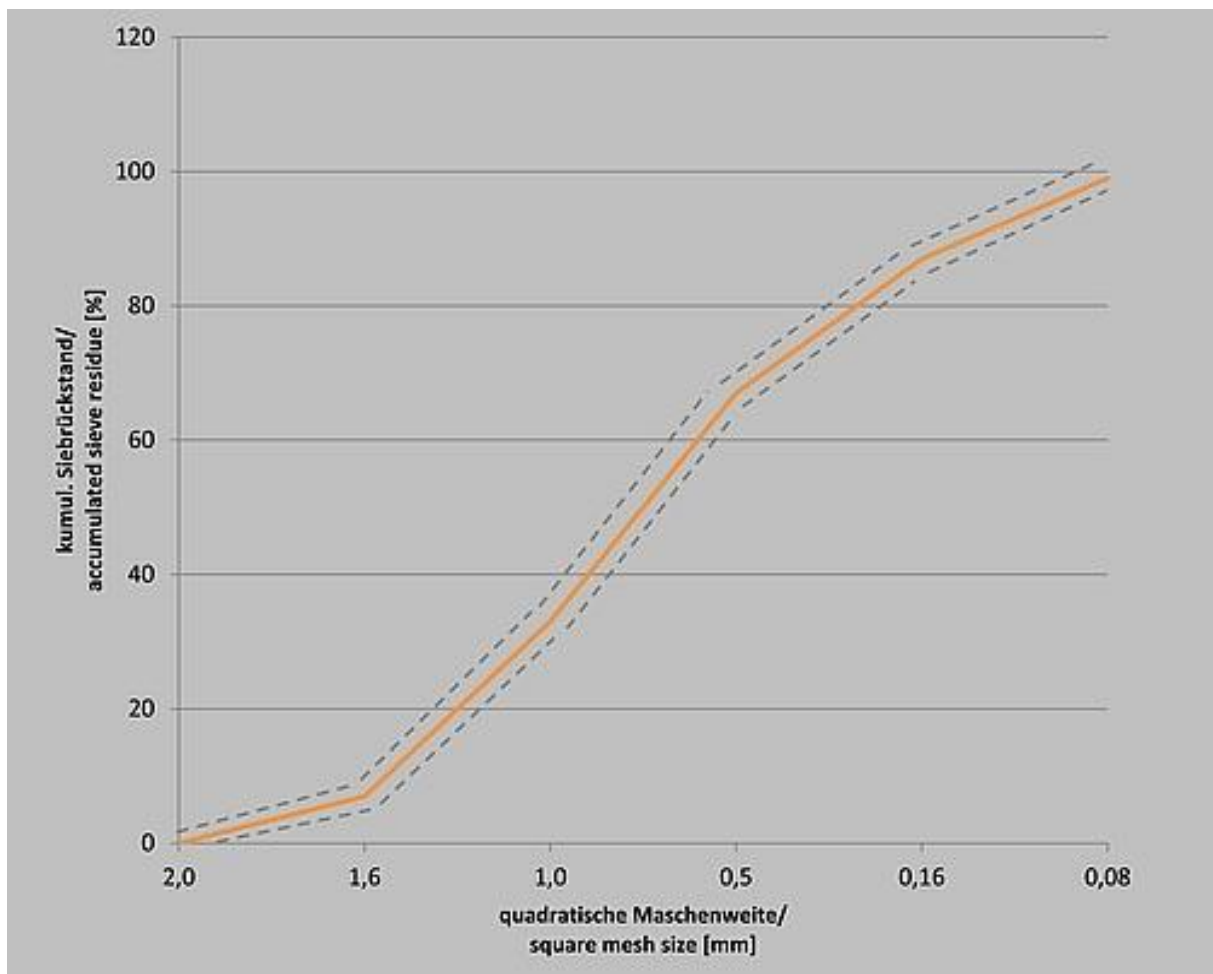
3.1 Materials and Mix Design

To perform tests with the Ultrasonic Pulse Velocity technique, concrete samples needed to be created. These samples consist of several components, like cement, water, aggregate, etc. The ratio and the amount of each component is being described in a Mix Design. To decide the fraction of each component the guidelines in some standards and existing research are considered. From this, the decision is made to make use of two Mix Designs. From some earlier research it has been seen that the porosity of concrete is being significantly affected by the W/C ratio. Since the porosity is an important influence factor on UPV measurements, the decision is made to vary the two Mix Designs on their W/C ratio. Research [39], has shown that a change of W/C ratio from 0.45 to 0.6 causes an increase of 150% for the porosity. The samples vary in their void levels and the applied damage levels (see Section 3.2). To get different void levels it is decided to vary the W/C ratio of the two Mix Designs. The first Mix Design ‘Mix Design 1’ has a W/C ratio of 0.4, while the second Mix Design ‘Mix Design 2’ has a W/C ratio of 0.6. As can be seen in Table 8, both Mix Designs are using the same cement type (Cement I 42.5) and amount. As we come to the water amount used within the Mix Designs, you can notice that both Mix Designs are different in this aspect. With the first Mix Design using less water than the second one. This difference leads to the difference in the W/C ratio which is mentioned above. For the sand, firstly it was planned to make use of CEN Standard Sand according to EN 196-1. This sand can be ordered in portioned bags of approximately 1350 g, which is enough for relatively small samples. Since the dimensions of the samples of this research are quite large and 52.74 kg of sand is needed, the choice is made to not make use of the portioned bags but instead mix the fractions manually with the sand types which can be seen in Table 8, conform the grain size distribution according to EN 196-1 (Figure 27).

Although this study frequently refers to the samples as “Concrete,” the actual mixtures here do not include coarse aggregates. Instead, only fine aggregates (sand) were used (as shown in Table 8), resulting in a mortar-like mix. The principal reason for this choice is related to the dimensions of the test samples. Larger coarse aggregates would pose challenges for compaction and might cause significant wave scattering or inconsistent UPV readings, especially given the relatively modest thickness of the specimens. By relying on a mortar-like composition (cement, water, and sand), the internal structure remains more uniform, which helps reduce variations in ultrasonic measurements. This approach aligns with common practice in non-destructive testing of smaller-scale specimens, where eliminating coarse aggregate can yield more reliable and reproducible wave velocity results.

Component	Mix Design 1	Mix Design 2
Cement I 42.5	17.58 kg	17.58 kg
Water	7.02 kg	10.56 kg
Total Sand	52.74 kg	52.74 kg
0.125-0.25 mm	6.84 kg	6.84 kg
0.25-0.5 mm	10.56 kg	10.56 kg
0.5-1 mm	17.94 kg	17.94 kg
1-2 mm	17.4 kg	17.4 kg

Table 8: Mix proportions of the two Mix Designs



(a)

Mesh size (mm)	Lower limit	Interval average	Upper limit
2.00	0	0	0
1.60	2	7	12
1.00	28	33	38
0.50	62	67	72
0.16	82	87	92
0.08	98	99	100

(b)

Figure 27: Grain size distribution shown by a graph (a), and shown by a table (b), according to EN 196-1 [95, 96]

3.2 Introduction of Damage Levels and Depths

The main goal of this research is to determine whether near-surface damage can be detected using Ultrasonic Pulse Velocity (UPV). Therefore, it is necessary to introduce damage into the samples. In this research, four levels of damage are introduced to each sample, varying in depth at 0 cm, 2 cm, 4 cm, and 6 cm, respectively. These damages are introduced during the casting process by incorporating cylinders within the moulds. Each cylinder has a diameter of $\text{Ø}50$ mm and a height corresponding to the specific damage depth level.

A circular pattern is chosen for the damage shape primarily due to practical reasons. The cylindrical shape facilitates the removal of the cylinders from the hardened concrete without causing additional unintended damage to the samples. This ease of removal is crucial for maintaining the integrity of the test specimens and ensuring that the introduced damage is controlled and consistent across samples.

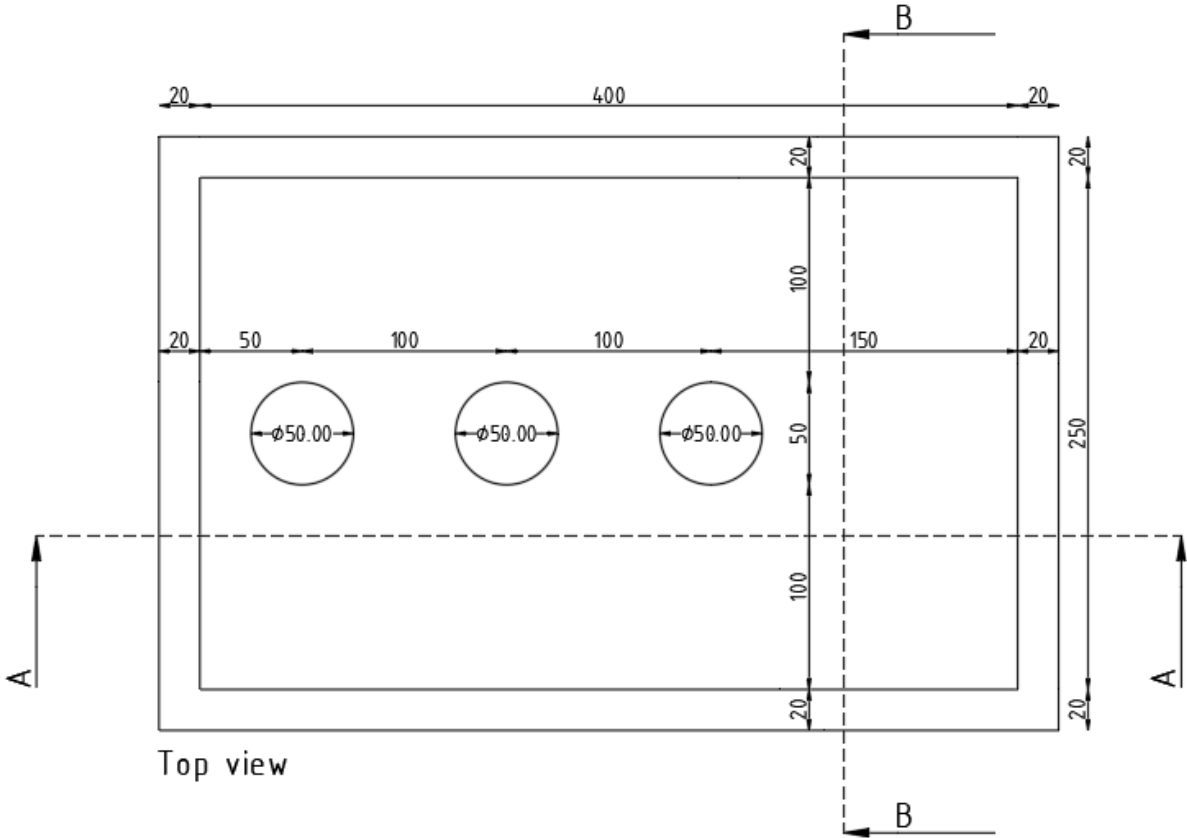
The diameter of 50 mm is based on the study by Lorenzi et al. [97], which demonstrated that non-destructive testing (NDT) methods can be used to locate relatively small defects (around 35 mm) in concrete beams that may cause structural performance problems. By selecting a slightly larger diameter, we aim to enhance the detectability of the defects using UPV while still representing realistic flaw sizes that could impact structural integrity. This approach aligns with the findings of Lorenzi et al. [97], emphasizing the effectiveness of NDT methods in detecting small-scale defects.

The circular damages in the concrete samples are designed primarily to simulate delamination, a defect where layers within the material separate, creating voids or cracks parallel to the surface [98]. Due to their planar profile, these damages effectively replicate delamination in concrete. Additionally, although not the primary focus, the cylindrical voids may also resemble honeycombing when viewed as a whole. Honeycombing, caused by improper compaction, manifests as rounded voids within the

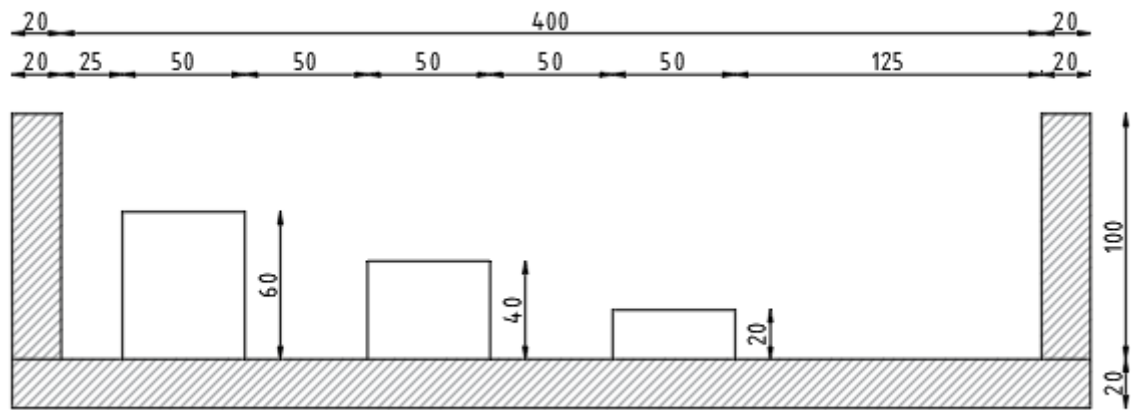
concrete structure [37]. Therefore, the cylindrical shape also makes it a suitable approximation for honeycombing.

Beyond delamination and honeycombing, the cylindrical voids can also represent other common types of concrete defects such as voids, inclusions, cavities, and segregation. Voids and inclusions occur when foreign materials or air pockets are trapped within the concrete, potentially weakening its structure [40]. Cavities can form due to improper vibration or consolidation during casting, leading to large empty spaces within the concrete mass [44]. Segregation is another damage type which refers to the separation of concrete components, and can cause non-uniformity and localized weaknesses, often resulting in irregular voids that can also be approximated by the cylindrical shapes for testing purposes [99].

The dimensions of the damage introduced in the samples are intentionally larger than what is typically observed in real-world scenarios. Defects like delamination, honeycombing, or voids would be smaller relative to the size of the concrete element. However, to effectively test the sensitivity and capability of the UPV technique in detecting near-surface damage, larger dimensions are utilized. This approach ensures that the effects of the damage on the UPV measurements are significant enough to be analysed and interpreted accurately. The figure below (Figure 28) shows a drawing of the wooden mould with the cylinders indicating the damage levels from three perspectives.

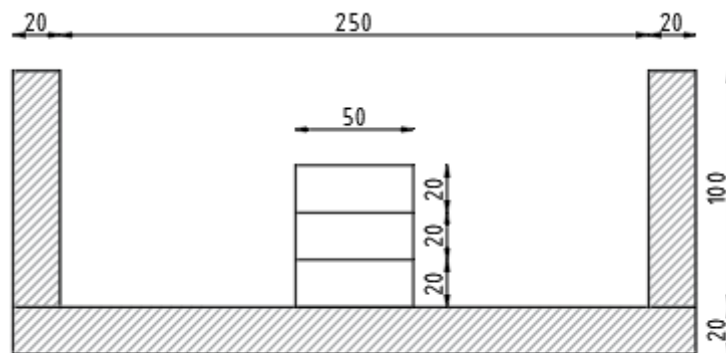


(a)



Cross section A-A

(b)



Cross section B-B

(c)

Figure 28: Drawing of wooden mould for concrete sample casting from three perspectives: (a) top view, (b) cross section A-A, and (c) cross section B-B

Once the concrete is mixed, it is poured into the wooden moulds containing the cylinders. After the concrete hardens, the samples are removed from the moulds. This results in concrete samples with cylindrical voids of varying depths in the middle, representing different levels of damage as previously mentioned. A picture of the wooden mould used is shown in Figure 29.



Figure 29: Wooden mould with cylinders

3.3 Sample Preparation

After deciding on the proportions for each component in the mix designs, the next step was to begin the production of the concrete samples. A total of six samples were made, but since only three wooden moulds were available, the casting process was divided into two batches.

Casting Process:

The first step was to grease the wooden moulds thoroughly. This was done to eliminate or reduce the risk of the samples adhering to the moulds after hardening, which could lead to unwanted damage during demoulding.

Each sample had dimensions of $400 \times 250 \times 100$ mm, equating to a volume of 10 litres per sample. With three samples per mix design, the total volume per batch was approximately 30 litres. Given this substantial volume, a concrete mixer was utilized to ensure efficient and consistent mixing. The concrete mixer used is shown in Figure 30 (a).

Mixing Procedure:

- Adding Sand:
 - All the different grain sizes of sand were combined and added to the mixer simultaneously.

- The sand was mixed for at least one minute to ensure uniform distribution and to break up any clumps.
- Incorporating Cement:
 - After the sand was thoroughly mixed, the required amount of cement was added to the mixer.
 - Mixing continued for another minute to achieve an even distribution of cement throughout the sand.
- Gradual Addition of Water:
 - Water was added to the mixer in decreasing portions to achieve better control over the mix consistency.
 - First Addition: 50% of the total water was added to the dry mix.
 - The mixture was allowed to mix thoroughly.
 - Second Addition: An additional 25 % of the water was added.
 - Mixing continued to ensure the water was fully integrated.
 - Subsequent Additions: The remaining water was added incrementally in smaller portions, approximately 12.5% each time, mixing well after each addition until all the water was incorporated.
 - This gradual addition allowed for precise control over the mix's consistency and prevented the mixture from becoming too fluid too quickly.
 - The readiness of the concrete was determined through visual inspection using a small shovel.

Pouring and Compaction:

Once the concrete was prepared, it was emptied into a wheelbarrow and transported to the moulds. Using a small shovel, the concrete was carefully poured into the moulds.

As the moulds were filled, it was necessary to eliminate air bubbles within the mixture to enhance the quality and strength of the concrete. This was achieved by compacting the mix. The moulds were placed on top of a vibration table (Figure 30 (b)), which vibrated the samples, allowing most of the air bubbles within the mix to rise to the surface and escape, resulting in a denser and more uniform concrete.

Curing Process:

After casting and compaction, a plastic seal was placed over the samples to prevent water evaporation. The samples remained in the moulds for about a week to harden. After demoulding, they were moved to the curing room.

The samples were cured for at least 28 days to develop their full strength. Proper curing is vital in concrete production, as it ensures the hydration process continues, leading to improved durability and mechanical properties. The curing room provided controlled temperature and humidity conditions to facilitate optimal curing.

The above-described process was repeated in the same manner for the second batch. Consistency in the procedure was essential to ensure that any differences observed in the samples could be attributed to the variables being tested rather than inconsistencies in the preparation process.



(a)



(b)

Figure 30: (a) concrete mixer, (b) Vibration table

3.4 Measurement Process and Data Collection

Once the samples have fully cured, the initial test performed is the Ultrasonic Pulse Velocity (UPV) test. For this procedure, the samples are placed on a table with the damaged side facing downward. The experimental setup is illustrated in Figure 31.

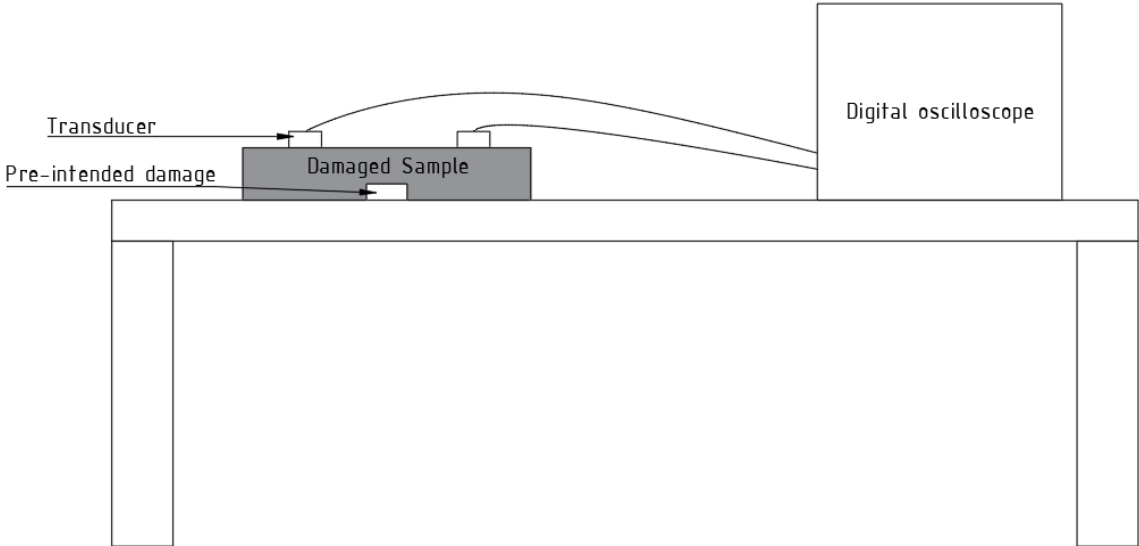


Figure 31: Experimental setup of the Ultrasonic Pulse Velocity Test

As previously mentioned, and shown by Figure 32, the test samples measure $400 \times 250 \times 100$ mm and contain four predefined damage levels: No damage, Damage Level 1, Damage Level 2, and Damage Level 3. The dimensions and damage levels are also presented from a different angle as a cross-sectional view in Figure 33.

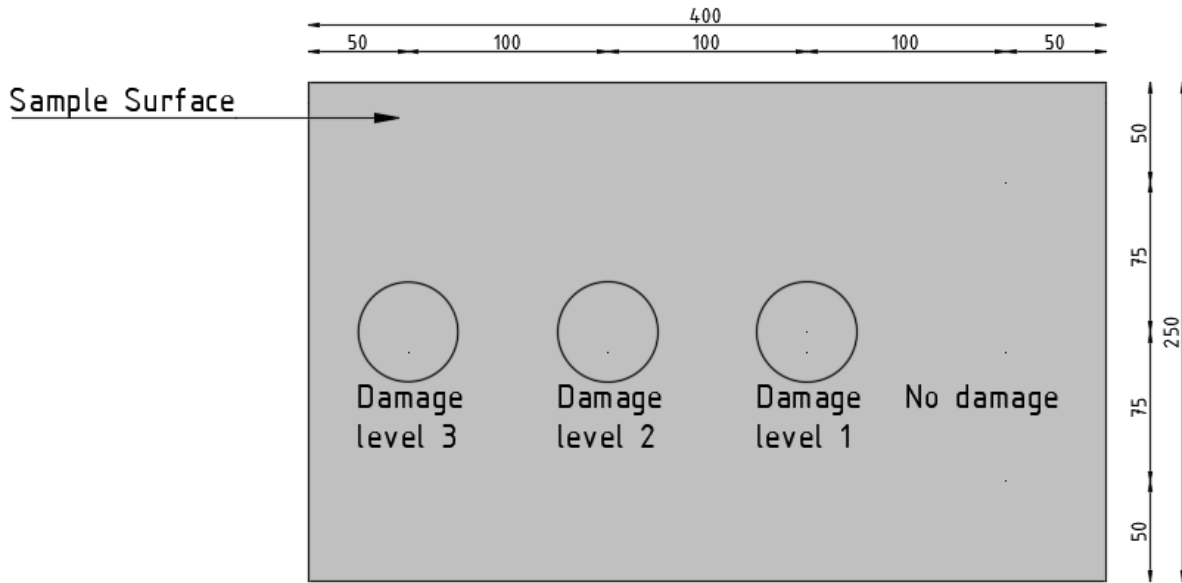


Figure 32: Test sample with the four damage levels

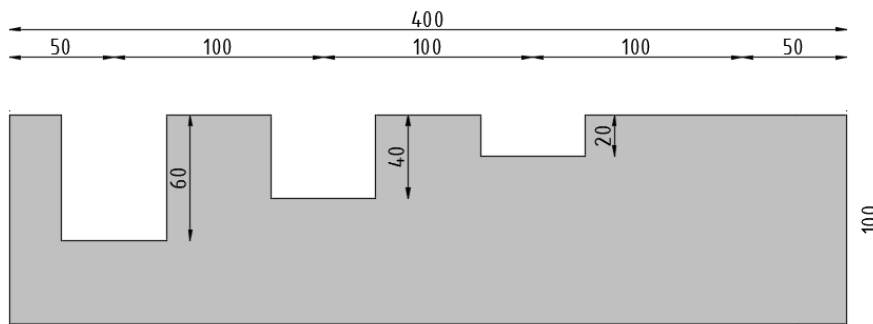


Figure 33: Cross-section of the sample with the four damage levels

While the rebound hammer test initially appeared as a potential option for evaluating the concrete samples, the Ultrasonic Pulse Velocity (UPV) method was selected instead for this research. This decision was driven by several key reasons that align with the objectives of the study.

The primary goal of this study is to detect near-surface damage and internal voids introduced at varying depths within concrete samples. Although both the rebound hammer test and the UPV method are non-destructive testing (NDT) techniques that can be performed with access to only one surface of the concrete [60], the rebound hammer test has limitations in detecting internal defects [7].

The rebound hammer test primarily assesses surface hardness by measuring the rebound of a spring-loaded mass impacting the concrete surface [60], providing an indirect estimate of compressive strength based on surface properties. It is less sensitive to internal flaws such as voids, cracks, and delamination, especially when these defects are located beneath the surface layer [7]. Additionally, surface conditions, such as roughness, moisture, and carbonation can significantly affect the rebound number, potentially leading to inaccurate assessments of internal integrity [24].

In contrast, the UPV method offers several advantages that make it more suitable for the objectives of this research:

Advantages of UPV Method:

- **Detection of Internal Defects:** UPV is highly effective in identifying internal flaws within concrete structures. Ultrasonic pulses transmitted through the material are affected by internal anomalies, causing changes in pulse velocity that can be detected and analysed [24].
- **Sensitivity to Subsurface Anomalies:** The method is capable of detecting variations in material properties below the surface, which is essential for assessing the introduced damage levels at different depths.
- **Quantitative Data:** UPV provides quantitative measurements of pulse velocity, allowing for precise evaluation of material uniformity and the extent of defects.

Supporting Evidence from Previous Studies:

The choice of UPV over the rebound hammer test is further supported by findings from previous research:

- Lorenzi et al. [97] demonstrated that UPV is more effective than the rebound hammer test in detecting internal anomalies within concrete structures. Their study successfully located relatively small defects (around 35 mm in diameter) using UPV measurements, while the rebound hammer test was less sensitive to such internal flaws.
- Malhotra & Carino [24] highlighted that the rebound hammer test is influenced by surface conditions and may not accurately reflect the presence of subsurface defects. They emphasized that UPV offers a more comprehensive evaluation of concrete quality by detecting variations in pulse velocity caused by internal anomalies.

In summary, the Ultrasonic Pulse Velocity (UPV) method was chosen over the rebound hammer test due to its superior ability to detect internal defects and assess near-surface damage within concrete structures. While both methods allow for one-sided access, UPV aligns more closely with the specific objectives of this research by enabling accurate detection and characterization of subsurface flaws introduced at varying depths. This decision was supported by theoretical considerations and empirical findings from previous research [97, 24]. By employing UPV and integrating different testing methods, the study aimed to achieve a more accurate and comprehensive evaluation of the introduced damage levels. Ultimately, this approach contributes to the advancement of non-destructive testing (NDT) techniques in concrete assessment, providing valuable insights into the material's internal integrity.

UPV Test Methods

The aim was to conduct three types of UPV tests and two tests to determine the concrete's mechanical properties. The mechanical properties were assessed using the three-point bending test and the compression test. Regarding the UPV tests, the primary goal was to ascertain whether the proposed damage levels could be located and whether the thickness of these voids could be estimated. To achieve this, three testing methods were proposed:

- Indirect Method 1 (Combination of Pulse-Echo and Indirect Methods on a Grid):
 - This method involves a combination of the Pulse-Echo method at grid points and the indirect method along the grid lines between the grid points.
 - Pulse-Echo at Grid Points:
 - Ultrasonic pulses are sent and received from the same surface at predefined grid points across the sample.
 - This technique is sensitive to reflections from internal defects directly beneath each grid point, enabling the detection of voids and flaws located below the surface.
 - Indirect Method along Grid Lines:
 - Measurements are taken between two transducers placed on the surface, separated by a known distance along the grid lines connecting the grid points.
 - This method assesses the pulse velocity between points, helping to identify anomalies in the material's properties along those lines.
 - The combination allows for comprehensive mapping of the internal structure, enhancing the ability to detect and characterize subsurface defects.

- Indirect Method 2 (Damage Levels Considered Separately):
 - Each damage level is tested individually by placing transducers along the surface area corresponding to that specific damage level.
 - This method focuses on assessing the impact of each damage depth on the pulse velocity, facilitating a comparative analysis between different damage levels.

- Pulse-Echo Method (Focused on Specific Areas):
 - Ultrasonic pulses are sent and received from the same surface, targeting specific areas of interest identified from the previous methods.

- This method provides detailed information about the depth and size of defects by analysing the time it takes for echoes to return from internal features.

All these methods involved measurements taken from only one surface of the concrete sample, intentionally simulating practical scenarios where access is limited to a single side. The parameters on which the experiments are based on are shown below:

– Transducer Spacing:

- During testing, the distance between the transducers was typically 150 mm. This choice was guided by the recommendations of Ashok Kumar and Santhanam [7], who suggest a preferred transducer spacing of 100–200 mm to achieve accurate results with minimal interference.
- A 150 mm spacing provides a balance between resolution and practicality, allowing for effective detection of defects without excessive signal attenuation.

– Grid Configuration:

- The use of a 150 × 150 mm grid for measurements was supported by the findings of Lorenzi et al. [97], who demonstrated that this grid size provides good accuracy for UPV testing.
- The grid approach, combining Pulse-Echo and indirect methods, allows for comprehensive mapping of the internal structure, facilitating the identification of anomalies associated with different damage levels.

– Sample Thickness and Damage Levels:

- The sample thickness was set at 100 mm, consistent with the study by Ashok Kumar and Santhanam [7], who investigated UPV testing on concrete specimens of similar dimensions.
- The sample was divided into four damage levels, each with a strip width of 100 mm, to systematically assess the effect of damage depth on UPV measurements.
- This configuration enables a direct comparison of pulse velocities across regions with different damage levels, enhancing the reliability of the results.

– Repetition of Measurements:

- To ensure the validity and reliability of the results, each measurement was repeated at least three times.

- Repeating measurements reduces the impact of random errors and increases confidence in the observed trends and patterns.

As the parameters of the experiments have been determined the next step will be to explain the three types of tests of UPV which were mentioned earlier in the report. In Indirect Method 1, we employ a comprehensive measurement procedure to detect and characterize internal defects within the concrete samples by combining the indirect method and the Pulse-Echo method on a grid, as was also stated earlier above. For each grid cell, six measurements are performed using the indirect method:

- Four measurements between neighbouring horizontal and vertical grid points.
- Two measurements along the diagonals of the grid cell.

In these indirect measurements, two transducers are placed on the same surface of the concrete sample, with one acting as the transmitter ("T") and the other as the receiver ("R"). The distance between them (the heart-to-heart distance) is used as the path length for calculating the Ultrasonic Pulse Velocity (UPV). Importantly, the first arrival time of the ultrasonic wave is recorded for each measurement, as it represents the quickest path through the material and is essential for accurate UPV calculation.

The UPV for the indirect method is calculated using the formula:

$$UPV_{Indirect} = \frac{\text{Path Length}}{\text{Transit Time}}$$

where:

- Path Length is the heart-to-heart distance between the transducers.
- Transit Time is the first arrival time of the ultrasonic wave measured between the transducers.

The measured UPV values between each pair of grid points are assigned to the midpoints between those points. For the diagonals, the average value of the two measurements is placed at the centre of the grid cell. This approach provides UPV values along each edge of the grid cells, but the grid points at the corners remain without direct measurements. To address this, we employ the pulse-echo method at the grid points. In this method, a single transducer acts as both the transmitter and the receiver. Since one transducer performs both functions in the pulse-echo measurements (sending/receiving). The first arrival time (as in the indirect method) could not be used, since you have to allow the wave to get away from the transducer first and bounce back from internal features (such as an internal defect or the opposite surface), otherwise the send wave would be measured which is not useful.

After determining the arrival time of the wave (Transit Time) in the Pulse-Echo measurements, we had to make an assumption for the path length because the damage (reduction of thickness) is unknown. Therefore, the full thickness of the sample (undamaged) is taken as a reference, for the measurements of Indirect Method 1. We assume the path length is twice the full thickness of the sample to calculate the pulse velocity. The UPV for the Pulse-Echo measurements is calculated using the formula:

$$UPV_{Pulse-Echo} = \frac{Path\ Length}{Transit\ Time}$$

where:

- Path Length is twice the thickness of the sample.
- Transit Time is the first arrival time of the reflected ultrasonic wave from the inner boundary of the sample

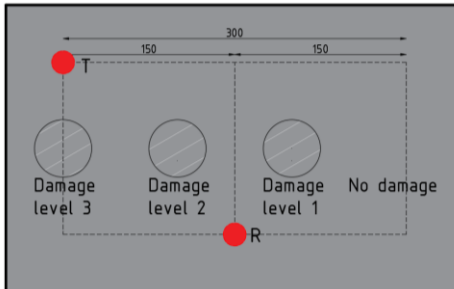
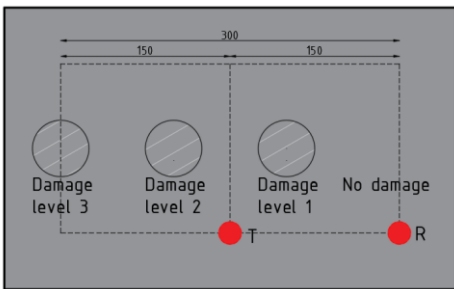
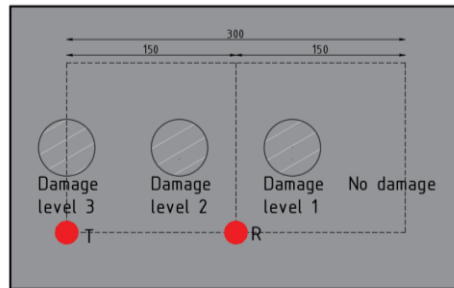
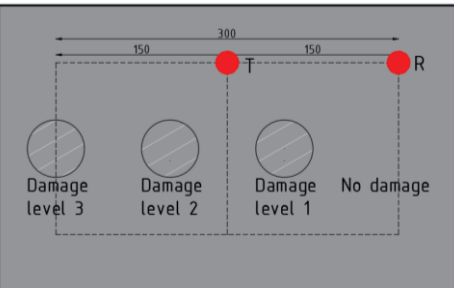
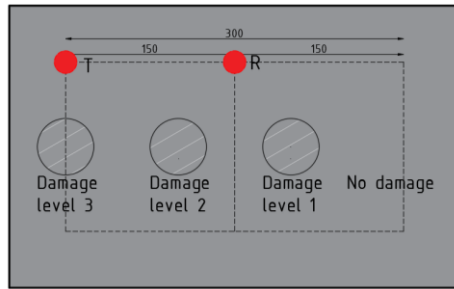
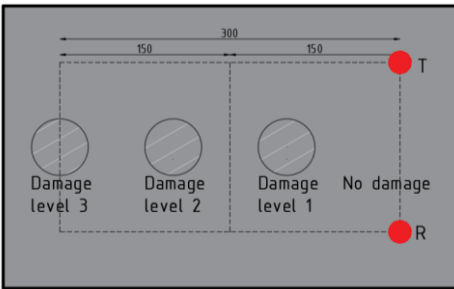
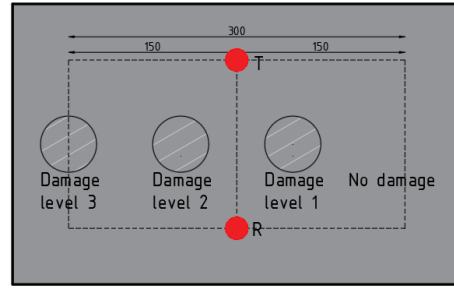
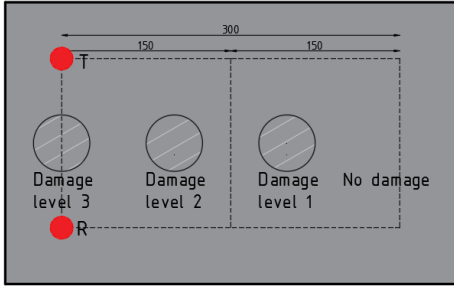
By using the full thickness as the reference, we establish a baseline for expected travel times in defect-free areas. Any deviations in the measured times may indicate the presence of internal defects or changes in material properties.

Moreover, since the pulse-echo measurements are performed in a different direction (depth-wise) compared to the indirect method measurements (surface-wise), there was a need to convert the Time of Flight (TOF) values from the pulse-echo method to UPV values. This conversion ensures that the results from both methods are in the same units and are directly comparable. By converting the TOF values to UPV values, we can present the results of both the indirect measurements and the pulse-echo measurements of Indirect Method 1 in a single contour plot. This unified representation allows for a comprehensive visualization of the internal condition of the concrete samples, facilitating the localization of damaged zones and the estimation of the thickness of the damaged areas.

In Table 9, the measurement setup is illustrated, showing the positions of the transducers for Indirect Method 1. The red solid circles represent the transducer locations. For the indirect method, T and R are shown next to the red solid circles, indicating the transmitter and receiver, respectively. For the pulse-echo measurements within Indirect Method 1, T/R is shown next to a single red solid circle, indicating that one transducer acts as both the transmitter and the receiver. This notation clarifies the roles of the transducers in each measurement configuration and aids in understanding the measurement paths.

Using the Pulse-Echo technique, introduces six additional measurements to Indirect Method 1, which aligns with the total number of grid points as can be also noticed in Table 9. In total, 17 measurements are performed for Indirect Method 1. Each measurement is repeated at least three times to ensure the validity and reliability of the results, reducing the impact of random errors and enhancing data accuracy. The collected measurements are used to create contour plots, which help localize the damaged zones and assess whether the thickness of the damaged areas can be estimated.

Positioning of transducers – Indirect Method 1



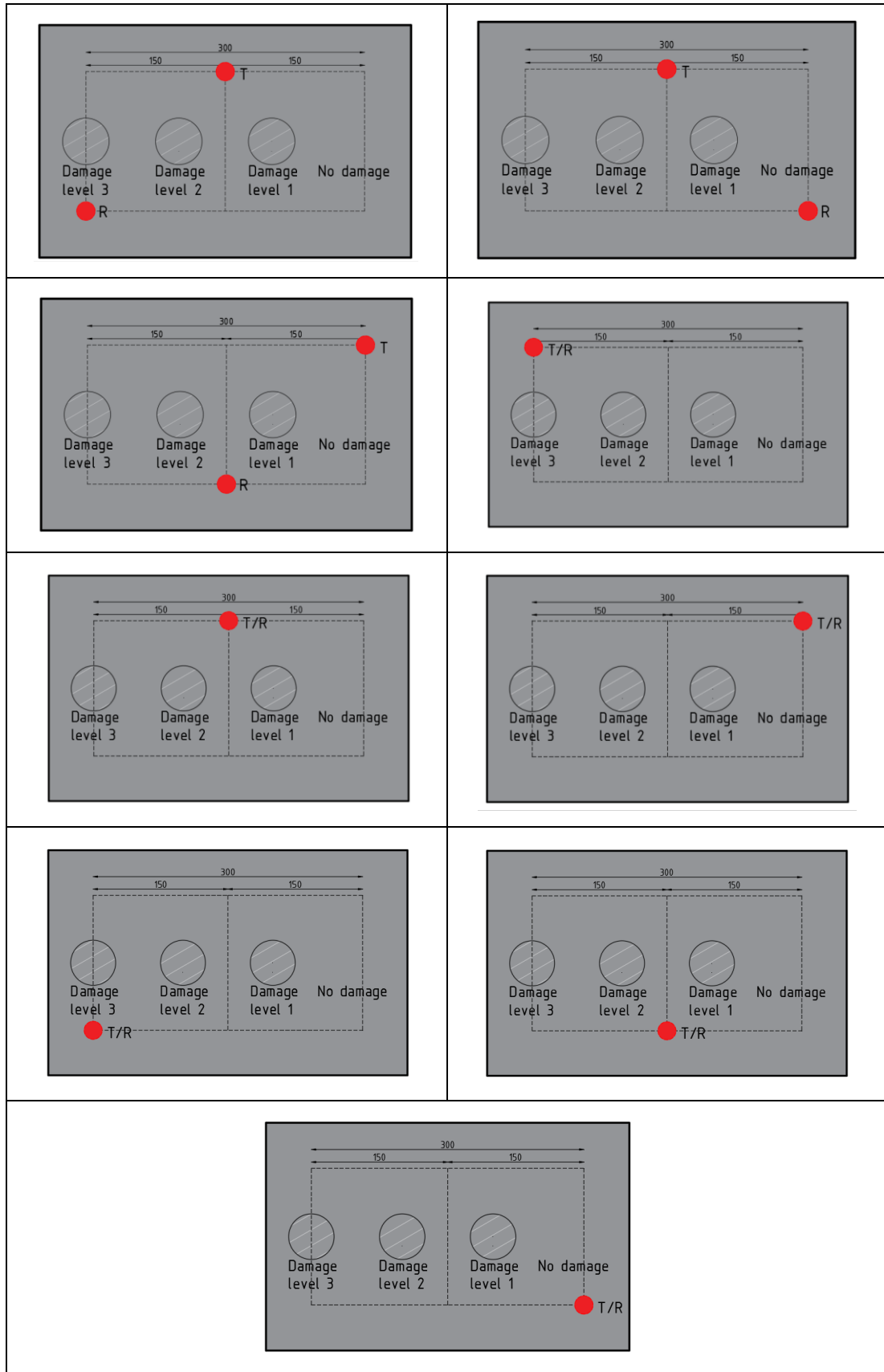


Table 9: Positioning of transducers - Indirect Method 1

In Indirect Method 2, we continue to utilize two transducers placed on the same surface of the concrete sample, like Indirect Method 1. However, the primary distinction lies in the positioning of the transducers relative to predefined damage levels. Indirect Method 2 is designed to assess each pre-intended damage level separately by strategically positioning the two transducers with the pre-intended damage centred between them for each case. This targeted placement ensures that the ultrasonic pulse directly interacts with the damaged zone, providing accurate Ultrasonic Pulse Velocity (UPV) readings reflective of the specific damage severity. Given that there are four damage levels: No Damage, Damage Level 1, Damage Level 2, and Damage Level 3, which makes a total of four measurements for this method. For each damage level, the transducers are symmetrically placed on either side of the designated damage area, maintaining a consistent heart-to-heart distance that serves as the path length for UPV calculations. The first arrival time of the ultrasonic wave is recorded for each measurement, representing the quickest path through the material and essential for accurate UPV calculation. The UPV is calculated with the same formula which is used for the indirect measurements of Indirect Method 1, which is:

$$UPV_{Indirect} = \frac{\text{Path Length}}{\text{Transit Time}}$$

where:

- Path Length is the heart-to-heart distance between the transducers.
- Transit Time is the first arrival time of the ultrasonic wave measured between the transducers.

To ensure the validity and reliability of the results, each of the four measurements is repeated for at least three times, as was also the case for Indirect method 1. This is done to minimize random errors and to enhance the data accuracy. The specific positioning of the transducers for Indirect Method 2 is illustrated in Table 10, where red solid circles labelled T (Transmitter) and R (Receiver) denote the respective transducer positions surrounding each predefined damage level.

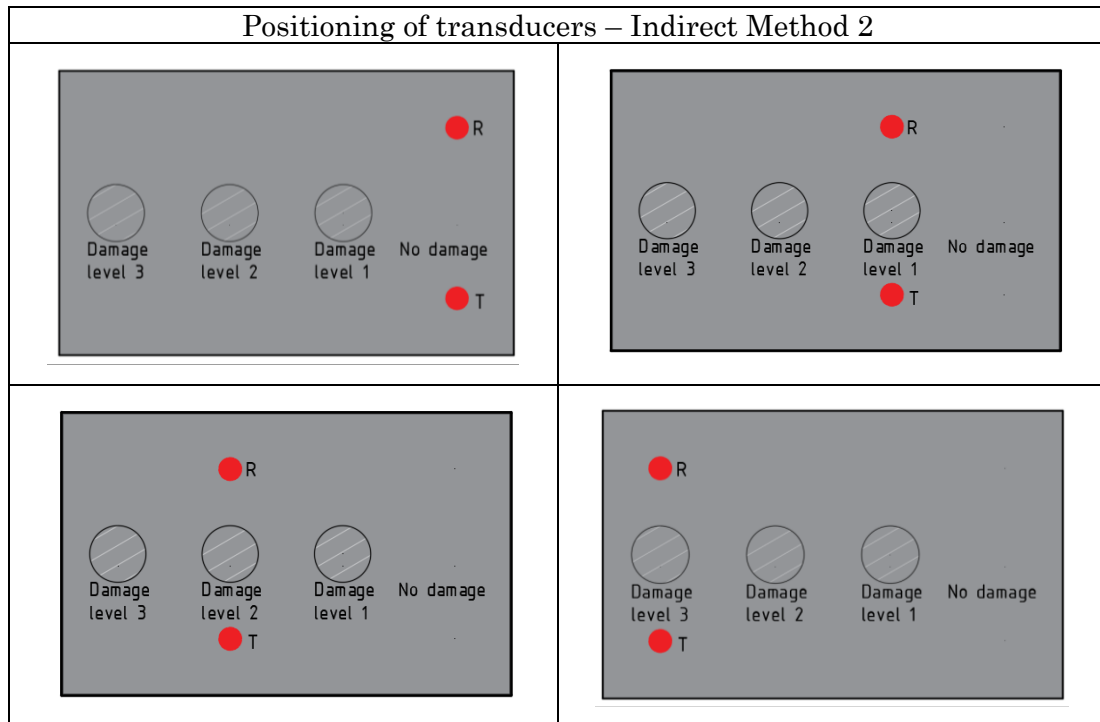


Table 10: Positioning of transducers - Indirect Method 2

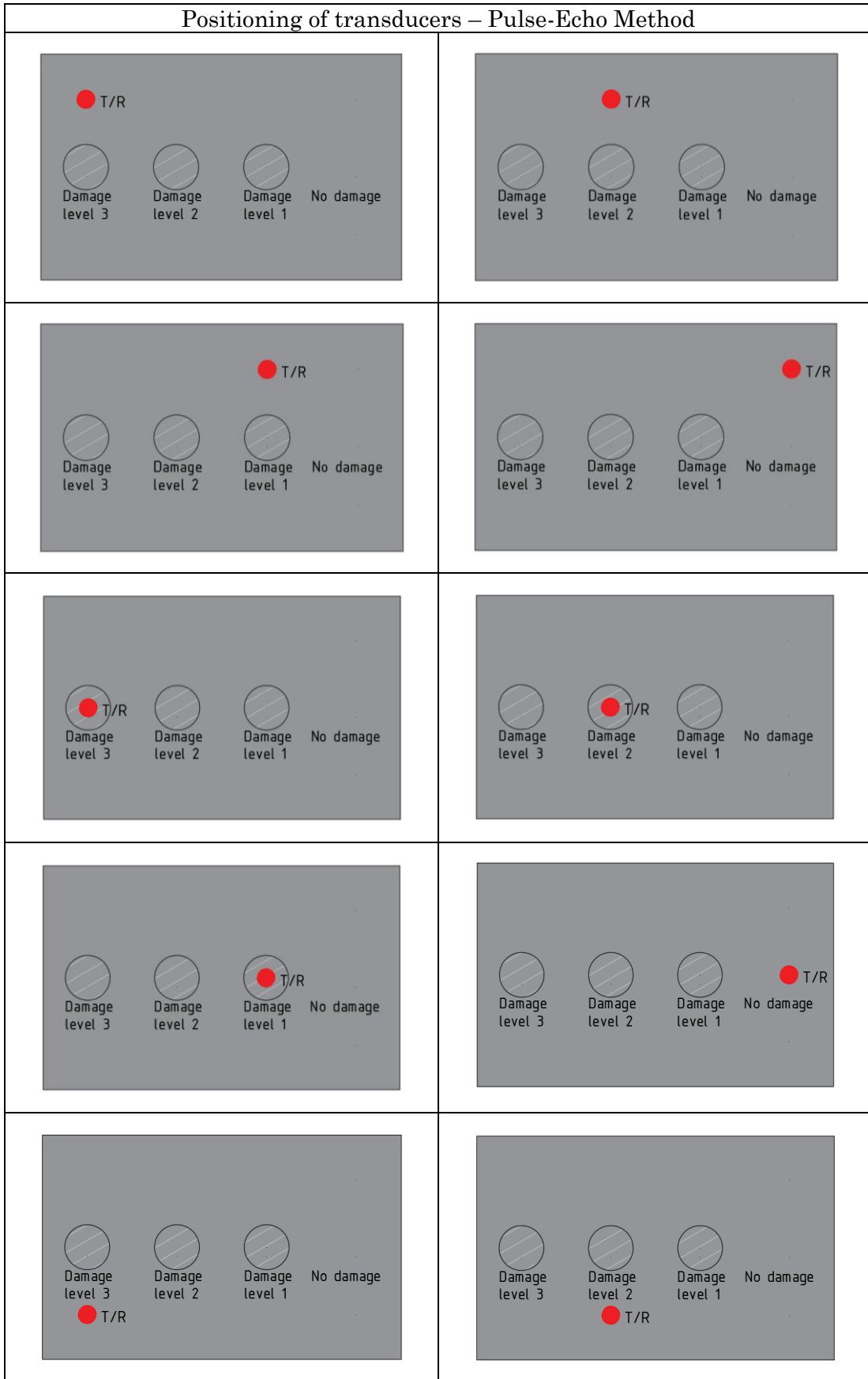
The Pulse-Echo Method is employed to accurately detect and characterize internal defects within concrete samples through the execution of 12 measurements. This method targets four predefined damage levels: No Damage, Damage Level 1, Damage Level 2, and Damage Level 3. For each damage level, measurements are conducted at three distinct positions, one centrally located within the damage zone and two positioned on either side of the damage zone. This configuration results in three measurements per position, ensuring comprehensive coverage of each damage level. Consistent with the other two methods, each measurement in this approach is repeated three times to enhance the validity and reliability of the Time of Flight (TOF) values.

The transducers utilized in the Pulse-Echo Method are configured as single units functioning as both Transmitter and Receiver (T/R), as depicted by red solid circles labelled T/R in Table 11. This dual functionality facilitates efficient measurement of ultrasonic waves as they interact with internal defects. During each measurement, the Time of Flight (TOF) of the ultrasonic pulse is recorded, specifically using the arrival time of the reflected wave from the inner boundary of the sample.

Given that the extent of damage (reduction in thickness) within the concrete samples is unknown, the full thickness of the sample is not assumed as a reference in this method. Instead, thickness measurements are first conducted on undamaged samples to establish a baseline thickness. These baseline measurements enable the accurate estimation of damage thickness based on the TOF data obtained from the Pulse-Echo Method.

The TOF values collected from the Pulse-Echo Method are utilized to create contour plots. These plots provide a unified and comprehensive visualization of internal defects, allowing for the localization of damaged zones and the estimation of damage thickness.

Positioning of transducers – Pulse-Echo Method



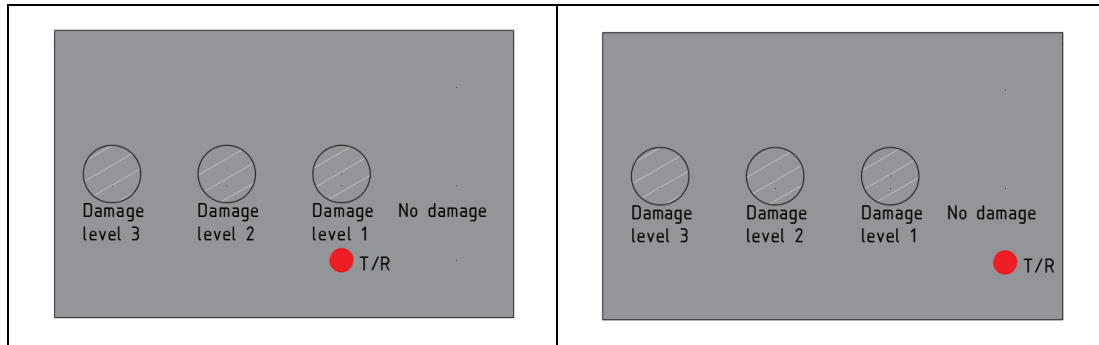


Table 11: Positioning of transducers - Pulse-Echo Method

The results obtained from the three Ultrasonic Pulse Velocity (UPV) testing methods: Indirect Method 1, Indirect Method 2, and the Pulse-Echo Method are utilized to create contour plots and graphs. These visual representations are essential for determining whether near-surface damages are detected and for estimating the thicknesses of these damages. Specifically, Indirect Method 2 involves only four measurements, which limits the amount of data available. To effectively present the findings from this method, graphs are employed to visualize the results despite the smaller dataset. These graphs facilitate the identification and assessment of damage locations and their respective severities.

3.5 Testing with the Ultrasonic Pulse Velocity technique

Before beginning the Ultrasonic Pulse Velocity (UPV) testing, each sample was meticulously labelled to specify the exact locations where sensors would be positioned for the different testing methods. This careful marking process is essential to ensure that the sensors are consistently and accurately placed, which is crucial for obtaining reliable and reproducible measurement data throughout the testing process. Once the samples were properly marked, as shown in Figure 34, the UPV testing could commence without any delays.



Figure 34: Marked Samples Indicating Sensor Positions for UPV Testing

The UPV testing setup includes a variety of specialized equipment, each selected in accordance with the ASTM C 597 guidelines to ensure adherence to industry standards. Although the apparatus selection was guided by ASTM C 597 due to its detailed and specific requirements, the testing process complies with all the criteria set forth in EN 12504-4. For instance, EN 12504-4 was the primary standard used to process the results of the tests, ensuring consistency and reliability. However, the guidelines for indirect measurements (Annex A of EN 12504-4) were not directly applicable, as they require measurements at varying distances, which is a technique incompatible with the grid-based approach used in this research. As a result, a slightly modified approach was adopted for indirect measurements.

For Pulse-Echo measurements, EN 12504-4 was followed. Although this standard does not explicitly address the path length for such measurements, it was assumed to be twice the thickness of the sample, a common practice in ultrasonic testing. This assumption

provided the necessary framework for calculating time-of-flight (TOF) and UPV values with accuracy.

The frequency used in this study was carefully selected following the guidelines in ASTM C 597, which recommends that the wavelength of the ultrasonic waves should not exceed the smallest dimension of the sample. The smallest dimension of the samples in this study is 40 mm. Using a transducer with a resonant frequency of 500 kHz and an assumed pulse velocity of 4000 m/s, the calculated wavelength is:

$$\text{Wavelength} = \frac{\text{Pulse Velocity}}{\text{Frequency}} = \frac{4000}{500000} = 0.008 \text{ m (8 mm)}$$

This wavelength is significantly smaller than the smallest dimension of the sample, ensuring the chosen frequency is suitable for the study. Additionally, the 500 kHz transducer was employed for both indirect and Pulse-Echo measurements due to its compatibility with the sample dimensions and its capability to produce clear and precise signals.

An amplifier is utilized to increase the strength of the ultrasonic signals, ensuring that they are powerful enough to travel through the material being tested without significant loss or attenuation. Transducers are integral to the system, functioning both as emitters and receivers by converting electrical signals into ultrasonic waves and then back into electrical signals after the waves have passed through the sample. For indirect measurements, an arbitrary waveform generator is employed to create the specific waveform patterns required for the UPV test. This device provides precise control over the signal's frequency, amplitude, and shape, which are critical parameters for accurate measurement and analysis. In contrast, for the Pulse-Echo method, a pulser/receiver is used instead of the arbitrary waveform generator. The pulser/receiver is responsible for generating the necessary ultrasonic pulses and receiving the echoes reflected from the material, enabling accurate Pulse-Echo measurements that are essential for assessing the material's properties.

A digital oscilloscope is connected to the setup to capture and display the ultrasonic waveforms, allowing for real-time visualization of the signals as they propagate through the material. This real-time monitoring is crucial for observing the behaviour of the waves and identifying any anomalies or variations that may indicate issues within the material. The computer in the setup is dedicated solely to recording the data transmitted from the digital oscilloscope. It does not control testing parameters or process data beyond simple recording, ensuring that the recorded data is accurately preserved for subsequent analysis.

Additionally, an RF power amplifier is incorporated into the system to further amplify the radio frequency signals. This amplification ensures that the ultrasonic pulses maintain sufficient power for effective transmission through the sample, thereby enhancing the overall reliability and accuracy of the measurements. All these instruments are seamlessly integrated into the UPV testing apparatus, as shown in Figure 35, which provides a visual representation of the arrangement of the equipment. By adhering to ASTM C 597 guidelines, the testing methodology meets established

criteria for accuracy, consistency, and reliability, facilitating a thorough and effective evaluation of the material's characteristics.



Figure 35: Testing instruments for the UPV test

Before testing could begin, the transducers to be used needed to be calibrated. This was accomplished by first bringing the sensors into direct contact with each other and subsequently by measuring the wave speed in an aluminium bar for both the indirect and Pulse-Echo measurement techniques. By knowing the length of the aluminium bar and the wave speed within it, the calibration of the transducers/sensors could be accurately performed. As stated in EN 12504-4, the equipment "shall be capable of

measuring transit times in the calibration bar to a limit deviation of $\pm 0.1 \mu\text{s}$ and an accuracy of 2%." This requirement was met during the calibration process, ensuring that the equipment used in this study adhered to the stringent accuracy and precision standards necessary for reliable UPV measurements. After verifying that the results closely matched the expected values, the testing commenced. The calibration of the sensors using the Pulse-Echo method is illustrated in Figure 36.



Figure 36: Calibration of the sensors using the aluminium bar for the Pulse-Echo method

For the indirect measurement methods, sensors with a resonant frequency of 500 kHz are employed. These transducers have a diameter of approximately 2.5 cm and are connected to a function/arbitrary waveform generator. The waveform generator induces a decaying sinusoidal signal with an amplitude of 800 mV peak-to-peak (mVpp) at a frequency of 500 kHz.

In contrast, for Pulse-Echo measurements, the same transducer is used. Instead of utilizing two separate sensors as in the indirect measurements, a single sensor is connected to a Pulser/Receiver instead of the waveform generator. This configuration allows the single transducer to both emit and receive ultrasonic pulses effectively.

For all measurement techniques, the sensors are placed on the undamaged surface of the samples to ensure consistent and accurate data acquisition. An illustration of the transducer used in both measurement methods is provided in Figure 37.



Figure 37: Transducer used for both the Indirect Methods as the Pulse-Echo Method with a resonant frequency of 500 kHz

The results of the Ultrasonic Pulse Velocity (UPV) tests are collected and analysed using both contour plots and graphs. Contour plots are utilized to delineate the boundaries of the sample's dimensions, except for the second test method, which comprises only four measurements. For this method, a graph is employed to provide a clearer representation of the data. Both Time-of-Flight (TOF) and UPV are used to present the data, with each measured position detailed in Tables 9, 10, and 11. The TOF is measured directly from the tests and analysed using MATLAB. When the distance between the transducers is known, the UPV is calculated by dividing this distance by the TOF. The contour plots, graphs, and other test results are discussed in the following chapter of this report.

Python is utilized to generate the contour plots and graphs, facilitating clear visualization of the results. The code used for creating these visualizations is included in the appendices of this thesis to ensure transparency and reproducibility.

3.6 Mechanical testing

After completing the Ultrasonic Pulse Velocity (UPV) tests, the concrete samples underwent a meticulous preparation process to facilitate subsequent mechanical evaluations. The initial step involved precisely cutting each concrete sample into smaller specimens with dimensions of $40 \times 40 \times 160$ mm, adhering strictly to the specifications outlined in the European Standard EN 196-1. This cutting was executed using a concrete saw (see Figure 38), ensuring uniformity and consistency across all specimens, which is crucial for reliable test results.



Figure 38: Concrete samples being cut by a saw

Following the cutting process, each $40 \times 40 \times 160$ mm specimen was further divided into three equal portions using the concrete saw. This division resulted in three individual specimens per original sample, each designated for specific mechanical tests. Specifically, three specimens were allocated for the 3-point bending test, and six specimens were reserved for the compressive strength test. The mechanical tests were conducted using the MATEST CYBER-PLUS EVOLUTION machine (Figure 39), which was configured appropriately for each type of test to ensure accurate and consistent results.



Figure 39: MATEST CYBER-PLUS EVOLUTION machine used for mechanical testing

For the flexural strength assessment, the 3-point bending tests were conducted (see Figure 40). In this setup, the machine applies a controlled and uniform load across the center of each specimen to evaluate the concrete's flexural properties.



Figure 40: Setup of the 3-point bending test

A detailed view of a specimen undergoing the 3-point bending test is illustrated in Figure 41, showcasing the application of the controlled load and the specimen's response to the bending force.



Figure 41: Sample undergoing the 3-point bending test

Upon completion of the bending tests, the specimens typically fractured due to the applied load, as depicted in Figure 42. These broken specimens were then repurposed for the compressive strength tests, maximizing the use of available material and ensuring comprehensive mechanical evaluation.



Figure 42: Sample broken into two pieces after the 3-point bending test

For the compressive strength tests, the MATEST CYBER-PLUS EVOLUTION machine was reconfigured to accommodate compressive loading. This reconfiguration involved adjusting the fixture setup and modifying the loading parameters to apply a steadily increasing compressive force until failure (see Figure 43).



Figure 43: Sample undergoing the compressive strength test

The compressive strength tests were performed on the six specimens derived from the broken pieces of the bending tests. Utilizing the same machine for both types of tests ensured consistency in testing conditions, thereby enhancing the reliability of the comparative analysis between flexural and compressive properties.

The mechanical properties obtained from both the compressive strength and 3-point bending tests were systematically analysed to determine the overall structural integrity and performance of the concrete. These analyses provided critical insights into the concrete's behaviour under different loading conditions, highlighting its strengths and potential weaknesses. Additionally, the results from the mechanical tests were instrumental in explaining the variations observed in the UPV test outcomes. By correlating the mechanical properties with the ultrasonic measurements, a comprehensive understanding of the concrete's structural integrity and performance was achieved, thereby reinforcing the validity of the experimental findings.

4 Results and Discussion

In this chapter, the results of the mechanical and Ultrasonic Pulse Velocity (UPV) tests are presented and analysed. The performance of the concrete samples, based on different water-cement ratios, is evaluated through compression and flexural bending tests. Additionally, the effectiveness of UPV methods in detecting near-surface damage and estimating its depth is discussed, with comparisons made between the different testing approaches.

4.1 Test results of mechanical testing

4.1.1 Compression test

As can be seen in Figure 44 below the test results of the compression tests performed on both the Mix Designs is being shown. The box plot for Mix Design 1 shows the compressive strength values for the low water-cement (W/C) ratio concrete samples. The compressive strength values for this Mix Design range from approximately 57 MPa to 67 MPa. The mean compressive strength is indicated by a red dot within the box and is drawn at 62.52 MPa. The interquartile range (IQR), which is represented by the box, displays the middle 50% of the data and is between approximately 60.5 MPa and 65.2 MPa, suggesting moderate spread among the values. The whiskers extend to the minimum and maximum values within 1.5 times the IQR and are between the values of 57 MPa and 67 MPa.

The box plot of Mix Design 2, show the compressive strength values for the High W/C ratio concrete samples. As can be seen in the figure the values of the test for this Mix Design span from approximately 54 MPa to 80 MPa. The mean compressive strength, which is also marked by a red dot within the box, is equal to 67.30 MPa. The interquartile range (IQR) is wider compared to Mix Design 1, indicating greater variability among the compressive strength values. The whiskers stretch to the minimum and maximum values indicated above.

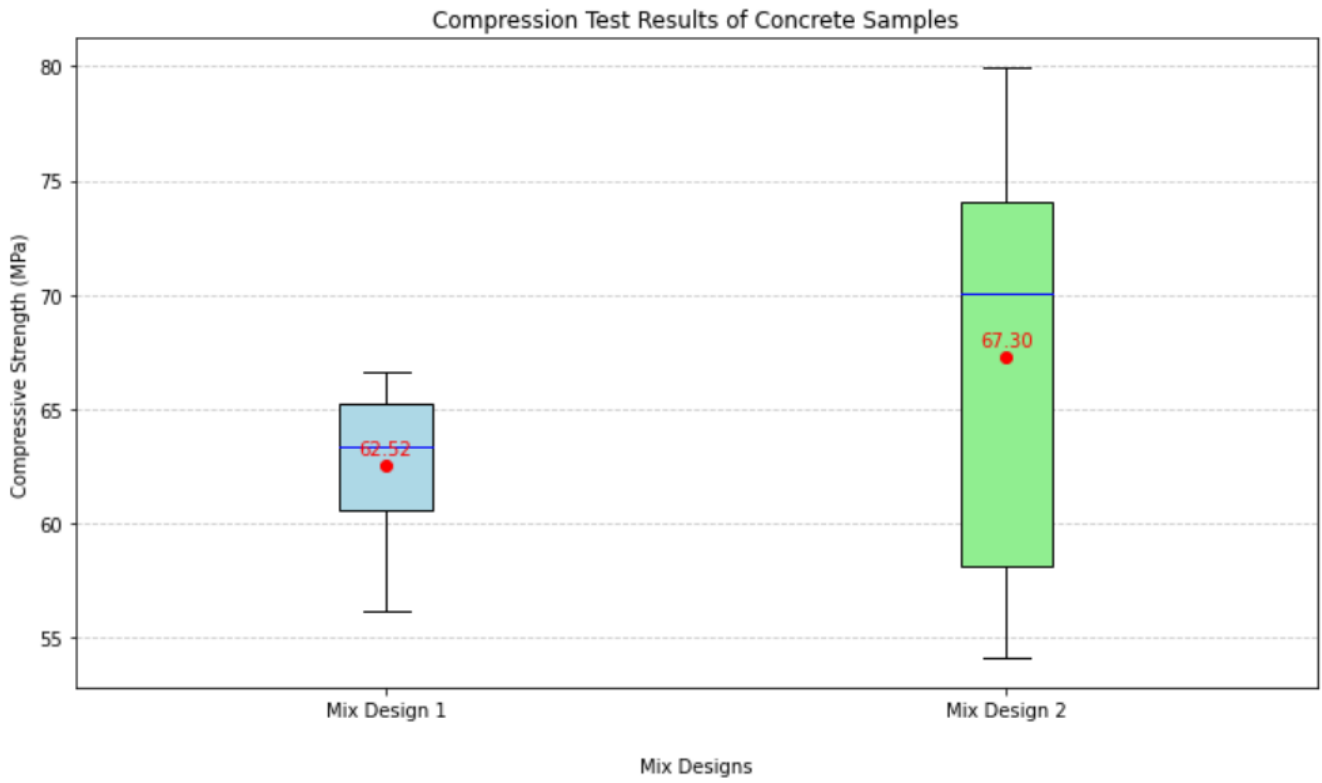


Figure 44: Compression test of both Mix Designs presented by using boxplots

4.1.2 Flexural bending test

The flexural strength test results for the concrete samples with different Mix Designs provide important information about the material's ability to withstand bending forces and are shown in the figure below (Figure 45). The box plot for Mix Design 1 illustrates the flexural strength values for the Low W/C ratio concrete samples. The flexural strength values range from approximately 9.2 MPa to 11.8 MPa. The mean flexural strength is shown by a red dot within the box, placed at 10.84 MPa. The interquartile range (IQR) represented by the box signifies a moderate spread of the values, suggesting consistency in the sample set. The whiskers extend to the minimum and maximum values within 1.5 times the IQR and go from 9.2 MPa to approximately 11.8 MPa. The Median is shown by a blue line in both the boxplots.

For the High W/C ratio samples, the box plot for Mix Design 2 is shown. As can be seen, the values of this boxplot range from approximately 8.7 MPa to 11.5 MPa. The mean flexural strength is in this case also indicated by a red dot within the box and is positioned at 10.38 MPa. The interquartile range (IQR) is slightly wider compared to Mix Design 1, indicating more variability in the flexural strength values. The whiskers extend to the minimum and maximum values and are equal to 8.7 MPa and 11.5 MPa respectively.

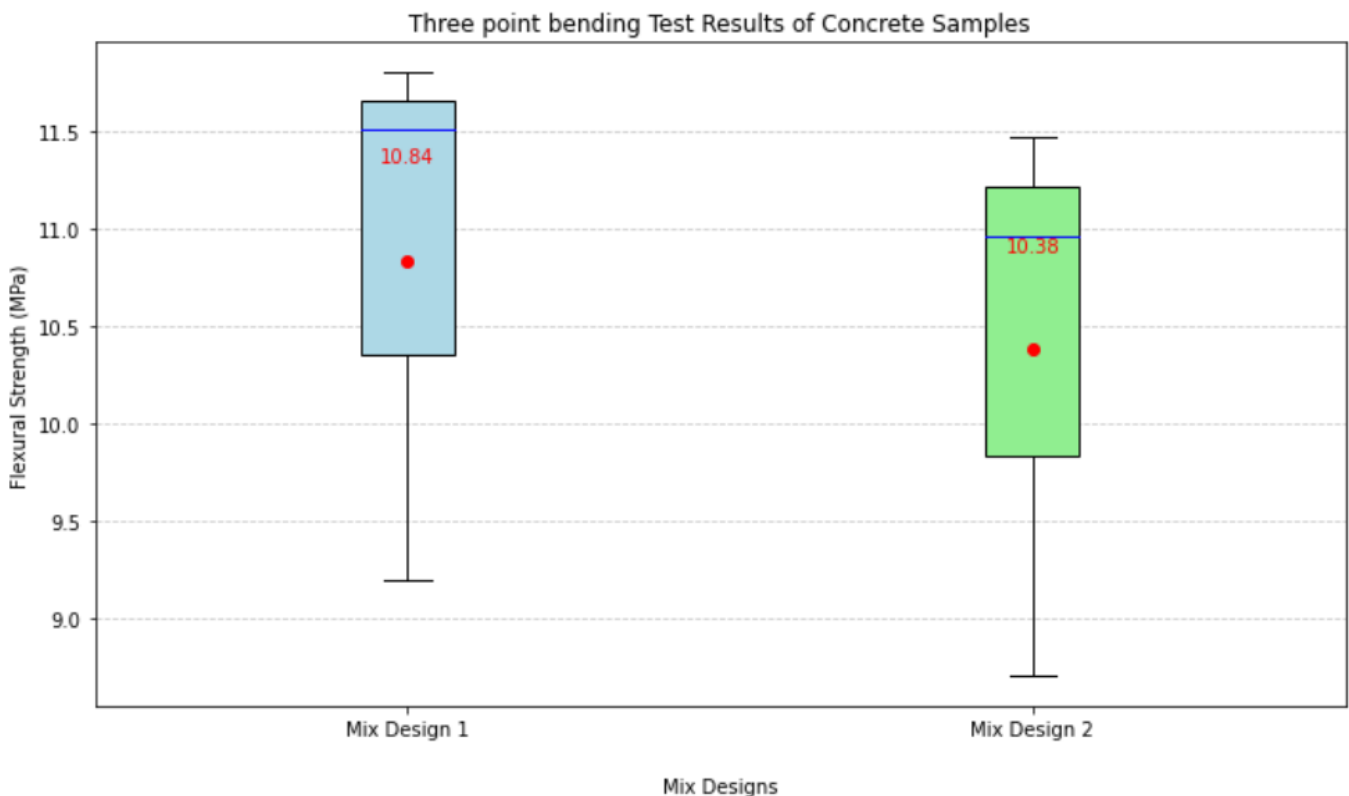


Figure 45: Flexural bending test of both Mix Designs presented by using boxplots

4.2 Comparison of the mechanical testing results

The mechanical testing results from the compression and flexural strength tests provide critical insights into the performance characteristics of concrete samples with varying water-cement (W/C) ratios, which are essential for determining their suitability for structural applications. The comparison between the Low W/C ratio mix (Mix Design 1) and the High W/C ratio mix (Mix Design 2) reveals significant differences in how these mixes respond to mechanical stresses.

For the Low W/C ratio mix (Mix Design 1), the compression test results indicated a relatively narrow range of compressive strength values, with the mean strength recorded at 62.52 MPa. This narrow range suggests a level of consistency in the internal structure of the concrete, although based on the visual inspection of Mix Design 1, more and larger visible pores can be seen (Figure 46 (a)), compared to Mix Design 2 (Figure 46 (b)). This increased porosity, despite the Low W/C ratio, may suggest potential issues during compaction or curing. The larger pores likely reduce the overall density of the mix, creating weak points that could explain why the compressive strength, though consistent, is not significantly higher. The presence of these voids can affect load distribution, making the material more susceptible to stress concentrations, limiting its overall strength under compressive loads.

In contrast, the High W/C ratio mix (Mix Design 2) exhibited a broader range of compressive strength values, with a mean strength of 67.30 MPa. The visual inspection of Mix Design 2 (Figure 46 (b)) sample shows fewer and smaller pores compared to Mix Design 1, suggesting that despite the higher water content, the mix achieved better compaction with fewer voids. This reduced porosity could explain the higher mean compressive strength, as fewer voids contribute to a denser, more uniform structure, which allows for better stress distribution. However, the wider range of compressive strength values still indicates variability, likely due to issues such as bleeding or uneven curing, which can still create weak spots even in a denser concrete matrix.

The flexural strength tests further showed the differences between the two Mix Designs. The Low W/C ratio mix (Mix Design 1) showed a mean flexural strength of 10.84 MPa. While this result suggests the mix can maintain its integrity under bending forces, the larger pores visible in the sample of Mix Design 1 (Figure 46 (a)) could have contributed to internal weak points, affecting its ability to resist bending stresses over time. Larger voids may increase the likelihood of stress concentrations under flexural loading, potentially leading to failure if the concrete is subjected to significant bending forces.

On the other hand, the High W/C ratio mix (Mix Design 2), although achieving a slightly lower mean flexural strength of 10.38 MPa, displayed more uniform material behaviour, as seen from the smaller pores observed in Figure 46 (b). The denser structure observed in Mix Design 2 likely allowed it to resist bending forces more effectively, with fewer stress concentrations compared to the more porous Mix Design 1. While Mix Design 2 showed more variability in compressive strength, the smaller voids observed visually may contribute to better overall performance under bending forces, reducing the risk of sudden failure under flexural stress.

These findings highlight the complex relationship between concrete strength, porosity, and water content. Despite having a lower W/C ratio, Mix Design 1 exhibited more and

larger pores, as seen in Figure 46 (a), which likely compromised its mechanical properties. Conversely, Mix Design 2, with fewer and smaller pores, performed better in the compressive strength test and showed reasonable performance in the flexural bending tests, despite its higher water content. This suggests that factors beyond the water-cement ratio, such as compaction quality and curing conditions, played a significant role in determining the mechanical properties of the concrete.

In conclusion, this comparative analysis of the mechanical testing results, supported by the visual inspection of the samples Figure 46 (a), and Figure 46 (b) highlights the importance of not only optimizing the water-cement ratio, but also ensuring proper compaction and curing techniques to minimize porosity and voids. While Mix Design 1 demonstrated consistency in performance, its larger pores potentially limited its strength. On the other hand, Mix Design 2 achieved better mechanical performance due to its denser structure, as indicated by the fewer and smaller voids, despite the higher water content. Achieving the desired concrete performance requires careful control of both the water content and the physical processing of the concrete to ensure strength, durability, and uniformity. The mechanical testing results revealed significant differences in compressive and flexural strength between Mix Designs 1 and 2. This prompted further investigation through ultrasonic pulse velocity (UPV) testing to examine internal defects such as voids or cracks, which were likely contributors to the observed mechanical weaknesses.

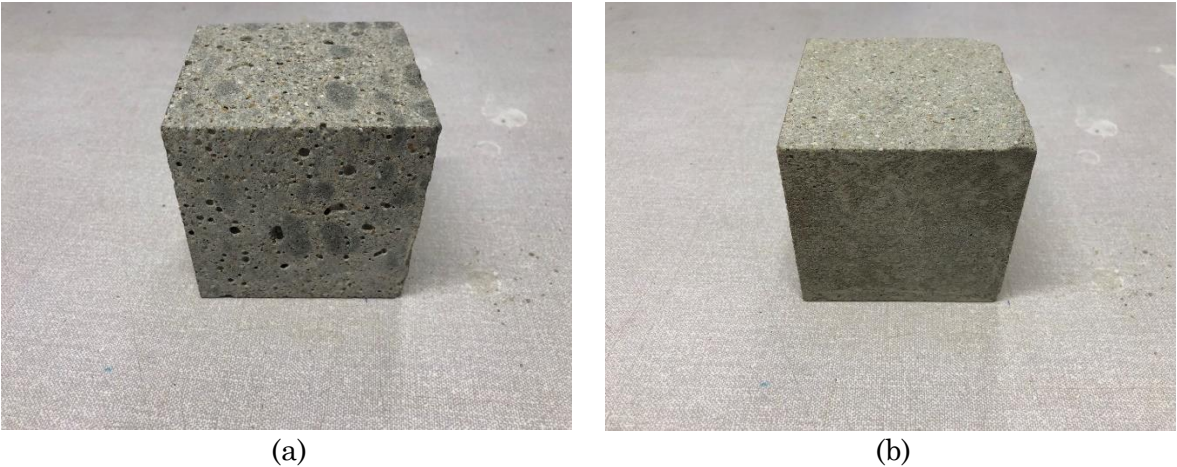


Figure 46: Concrete samples of both Mix Designs: (a) Mix Design 1, and (b) Mix Design 2

4.3 Test results of UPV testing

4.3.1 Baseline Measurement

To establish reliable baseline Ultrasonic Pulse Velocity (UPV) values for undamaged concrete specimens, the two distinct concrete mix designs were utilized: one with a low water-to-cement (W/C) ratio and another with a high W/C ratio. Each mix design was employed to produce cubic concrete specimens with dimensions of $8 \times 8 \times 8$ cm, ensuring uniformity across all measurements. These baseline measurements provide essential reference data for evaluating the impact of induced damage in subsequent experimental phases.

Direct transmission was employed to determine the baseline UPV value. This complementary approach offers a comprehensive characterization of ultrasonic wave propagation through the concrete matrix.

Figure 47 shows the cubic specimens representing the low and high W/C ratio mix designs alongside measuring tools. These images confirm that both sets adhere to the same dimensional specifications of $8 \times 8 \times 8$ cm, ensuring consistency in subsequent measurements.

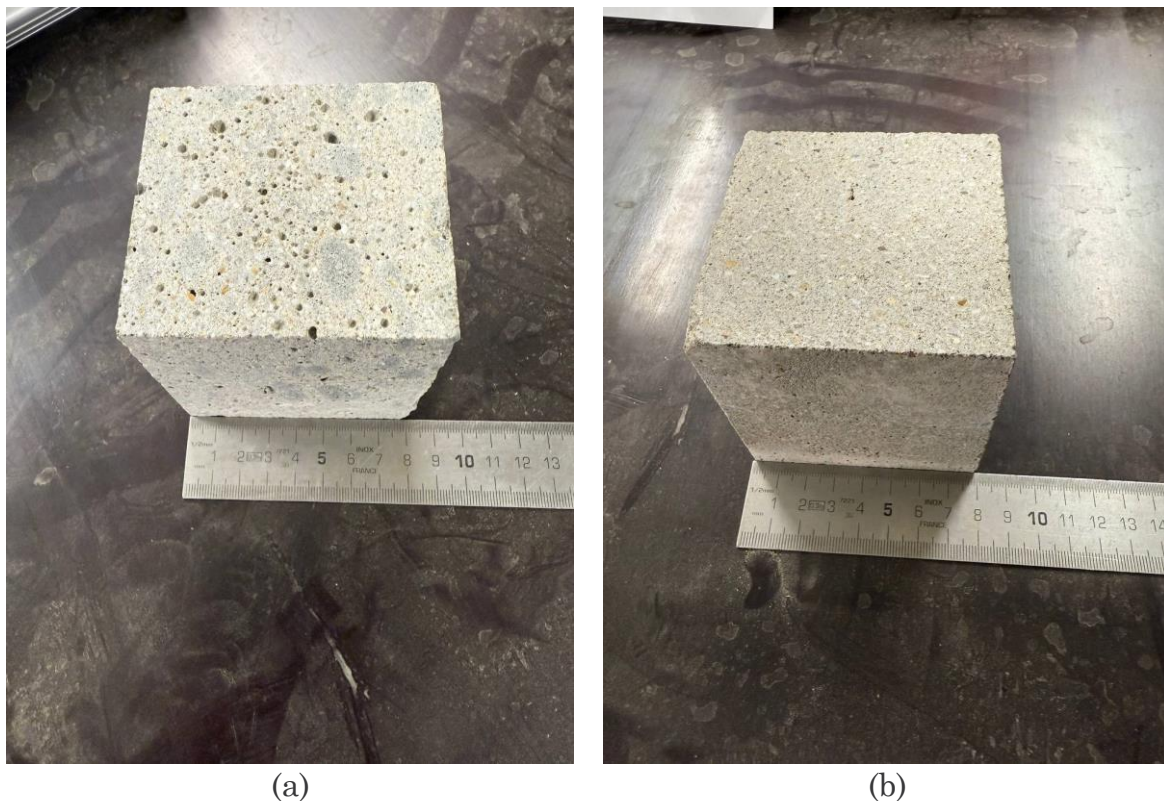


Figure 47: Cubic specimens representing (a) low w/c ratio and (b) high w/c ratio mix designs alongside measuring tools

In the direct transmission method, ultrasonic transducers are positioned on opposite faces of the concrete cube, allowing ultrasonic waves to travel directly through the specimen. Figure 48 illustrates the setup of the direct transmission method, where the transducers are applied to opposite sides of the cube. For this method, a distance of 8 cm (the thickness of the specimen) is used to determine the UPV by measuring the Time of Flight (TOF) of the wave from transmission to reception.



Figure 48: Setup of the direct transmission method applied to the specimen

Figure 49 shows the waveform obtained from a direct transmission measurement. The first wave arrival time, indicated on the graph, is 1.86928×10^{-5} seconds. The TOF is determined by identifying this initial arrival time, and this method is consistently applied across all direct measurements and further measurements performed using the indirect method.

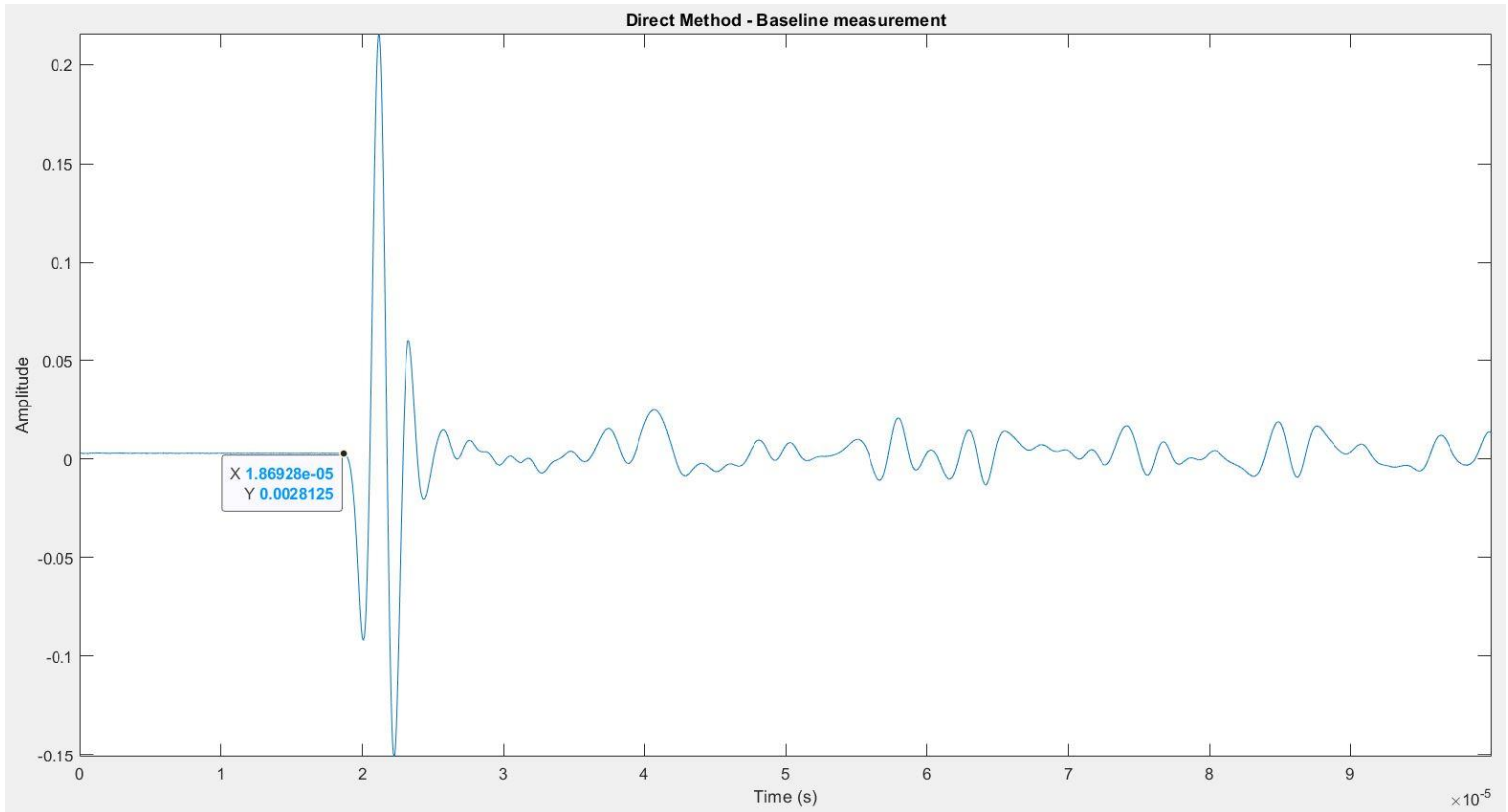


Figure 49: Waveform graph from the direct transmission method, showing the first wave arrival time (1.86928×10^{-5} seconds)

Each UPV measurement, was conducted a minimum of three times per specimen to ensure accuracy and reliability. The average of these three measurements was then taken as the representative UPV value for each mix design, providing a robust dataset for baseline comparison.

The results of the baseline measurements show that for the low W/C ratio mix design, the average UPV is 4608.36 m/s for the direct transmission method. For the high W/C ratio mix design, the average UPV is 4263.67 m/s. These values, summarized in Table 12, indicate that the low W/C ratio specimens consistently yield higher UPV values compared to the high W/C ratio specimens. This reflects the denser and stronger internal structure typically associated with lower W/C ratios.

Measurement Method	Direct Method	Average UPV Direct Method
Mix Design 1 (Low W/C ratio sample)	4587.16 m/s	4608.36 m/s
	4629.63 m/s	
	4608.29 m/s	
Mix Design 2 (High W/C ratio sample)	4280.36 m/s	4263.67 m/s
	4255.32 m/s	
	4255.32 m/s	

Table 12: Summary of baseline UPV measurements for both mix designs

The baseline UPV measurements correlate with the mechanical properties obtained from compression and flexural tests, shown in Figures 44 and 45. The low w/c ratio mix design (Mix Design 1) exhibits a compressive strength of 62.52 MPa (mean value) and a flexural strength of 10.84 MPa. Despite the higher UPV value of 4608.36 m/s (Direct Method), the compressive strength for the low w/c ratio sample is lower than expected. This discrepancy can be attributed to compaction issues which were earlier noticed in the low w/c ratio mixes.

In contrast, the high w/c ratio mix design (Mix Design 2) shows a higher compressive strength of 67.30 MPa (mean value) and a flexural strength of 10.38 MPa. Although the UPV values for this mix are lower (4263.67 m/s for the Direct Method), the higher water content enhances workability, allowing for better compaction and fewer air voids. This improved compaction results in higher compressive strength, even though the overall internal structure is more porous, as reflected by the lower UPV values.

The flexural strength results align more closely with the UPV measurements. The low w/c ratio mix design, with its higher UPV values, shows superior flexural strength (10.84 MPa) compared to the high w/c ratio mix (10.38 MPa). This indicates that while compressive strength is affected by compaction issues, the inherent density and lower porosity of the low w/c ratio concrete still contribute positively to flexural strength.

These findings highlight the importance of UPV measurements as a non-destructive indicator of concrete quality. The higher UPV values reflect a denser internal structure and generally correlate with better mechanical performance, particularly in flexural strength. However, for compressive strength, workability and compaction play a critical role, and low w/c ratio mixes can suffer from reduced compressive strength if compaction is inadequate.

4.3.2 Indirect Method 1 – Low W/C ratio

Figure 50 presents the contour plot of Ultrasonic Pulse Velocity (UPV) measurements for the low water-to-cement (w/c) ratio concrete sample, obtained using Indirect Method 1. The measured UPV values range from approximately 4320 m/s to about 4880 m/s, represented using a continuous colour scale. Warmer hues (reds and oranges) correspond to higher UPV values, while cooler hues (blues and greens) correspond to slightly lower values within this range.

In general, the contour plot suggests that the internal structure of the low w/c ratio concrete is dense and relatively uniform. The central portion of the measured area exhibits higher UPV readings (about 4800–4880 m/s), indicating that the ultrasonic waves travel through this region with limited resistance. This result implies that there are fewer internal voids, cracks, or other imperfections at the centre, and that the concrete there is well-consolidated and homogeneous.

When compared to the baseline measurements shown in Table 12, the average UPV for the low w/c ratio sample is 4608.36 m/s using the Direct Method. The highest values observed in the contour plot (4800–4880 m/s) exceeds this baseline average, indicating regions of exceptionally dense concrete. This suggests that the central portion of the specimen might have benefited from optimal curing conditions and aggregate distribution, enhancing wave propagation.

As the measurement points progress toward the edges of the analysed area, there is a gradual decrease in UPV values, down to around 4320–4380 m/s. All six pulse-echo measurements for Indirect Method 1 were performed at the edges of the specimen. This technique, which relies on wave reflections, may also influence the results, as waves reflecting off boundaries are more prone to attenuation and scattering. The differences observed at the edges could also be due to the inherent limitations of the pulse-echo technique when measuring near boundaries, compared to the direct measurements which were only conducted for baseline assessments.

The other method employed in this research is indirect wave transmission, where the transducers are placed on the same surface of the specimen, and the ultrasonic waves travel parallel to the surface. This approach, while useful for assessing surface and near-surface properties, typically results in lower UPV values compared to direct wave transmission due to the longer and more complex wave path. These lower values align with the measured UPV values at the edges of the specimen, further highlighting the differences between pulse-echo and indirect transmission techniques.

The mechanical properties of the low w/c ratio concrete support these findings. The flexural strength for this mix design is 10.84 MPa (Figure 45), reflecting the specimen's ability to resist bending stress. This high flexural strength is consistent with the dense internal structure indicated by the elevated UPV values. However, the compressive strength of 62.52 MPa (Figure 44) is lower than might be expected for such a dense specimen, likely due to compaction issues associated with the low workability of low w/c ratio mixes. These compaction issues can lead to trapped air voids, which reduce compressive strength despite the overall density observed in the UPV measurements.

It is important to emphasize that, despite having introduced controlled damage at the opposite face of the specimen, these localized defects are not clearly visible in the UPV

contour plot. The variations in UPV values appear smooth and continuous, without distinct signatures that would pinpoint the presence or severity of the induced damage. This observation is consistent with the baseline measurements and the observed mechanical properties, which indicate a generally dense internal structure. The inability to detect subtle defects using this approach highlights the limitations of indirect and pulse-echo UPV methods for identifying damage in concrete.

In summary, the results for the low w/c ratio concrete show a generally uniform and well-consolidated internal structure, with only minor variations in UPV from the centre to the edges. The measured UPV values align closely with or slightly exceed the baseline values, supporting the conclusion that this specimen exhibits dense concrete properties. The mechanical properties, particularly the high flexural strength of 10.84 MPa, further reinforce this conclusion. However, the lower compressive strength of 62.52 MPa shows the impact of compaction issues. The inability to detect induced damage through this approach suggests that additional measurement strategies, higher-resolution data collection, or complementary non-destructive testing methods may be necessary to identify and characterize localized defects within such dense concrete materials.

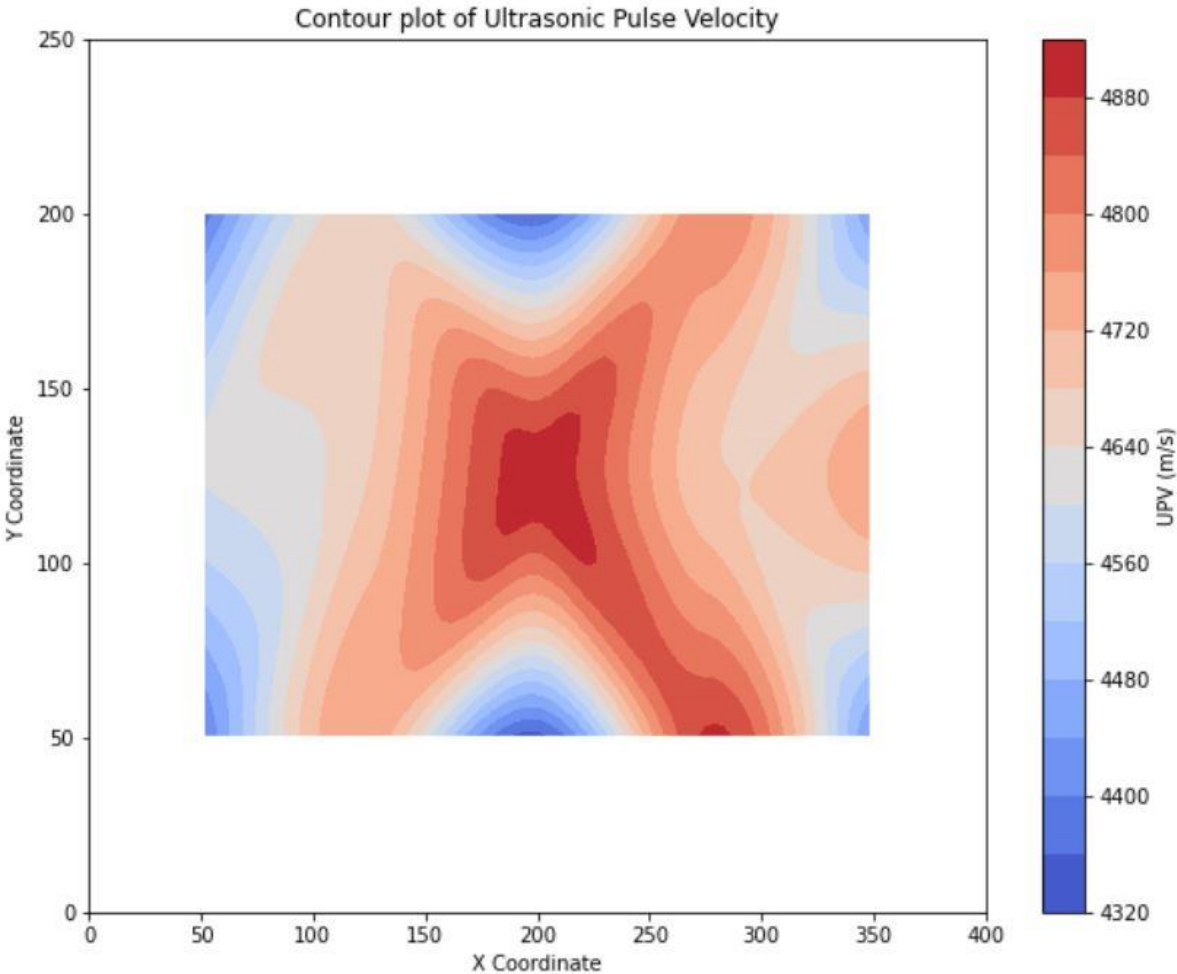


Figure 50: Contour plot of Indirect Method 1 (Low W/C ratio)

4.3.3 Indirect Method 1 – High W/C ratio

Figure 51 presents the contour plot of Ultrasonic Pulse Velocity (UPV) measurements for the high water-to-cement (w/c) ratio concrete sample, obtained using Indirect Method 1. In comparison to the previously discussed low w/c ratio specimen, the UPV values recorded here are noticeably lower and distributed in a more irregular pattern. Specifically, the UPV readings range from approximately 4180 m/s to about 4460 m/s, which represents a clear reduction compared to the values observed in the low w/c ratio sample. This decrease in wave speed reflects the expected influence of a higher w/c ratio. When more water is present in the mix, the resulting concrete has a more porous structure with an increased number of small cracks and voids that slow down the passage of ultrasonic waves.

Unlike the low w/c ratio sample, where a distinct gradient of UPV values was observed, the distribution in the high w/c ratio sample appears scattered and uneven. Within the contour plot, small areas showing relatively higher UPV readings of about 4380–4460 m/s are located near regions with lower values of approximately 4180–4260 m/s. Zones with higher velocities likely represent sections of the concrete that are still somewhat dense with fewer internal defects. In contrast, areas with lower velocities suggest the presence of internal imperfections such as tiny voids, microcracks, or weaker bonding between aggregates and the surrounding cement paste.

When compared to the baseline measurements shown in Table 12, the average UPV for the high w/c ratio sample is 4263.67 m/s. The values in the contour plot generally align with this baseline measurement, confirming the more porous and less dense nature of the high w/c ratio concrete. The pulse-echo measurements, which were performed at the edges of the specimen, may also contribute to the observed variability due to wave attenuation and scattering effects near boundaries.

The mechanical properties further support these findings. The compressive strength for the high w/c ratio mix design is 67.30 MPa (Figure 44), which, while higher than the low w/c ratio sample, reflects the better compaction achieved due to the improved workability of the mix. However, the flexural strength is 10.38 MPa (Figure 45), slightly lower than that of the low w/c ratio sample. This indicates that while the concrete may achieve reasonable compressive strength due to compaction, the higher porosity still affects its ability to resist bending stresses.

This irregular pattern implies that the internal quality of the high w/c ratio concrete is less uniform than that observed in the low w/c ratio sample. The greater porosity and variability within the structure make it more challenging to identify the intentionally introduced damage on the opposite face of the specimen. Instead of revealing clear signs of localized defects, the plot reflects a general background of uneven density and internal discontinuities that obscure the subtle differences created by the induced damage. As a result, it is difficult to determine the exact locations or severity of these defects based solely on the current UPV measurements.

While Indirect Method 1 successfully shows that the high w/c ratio sample exhibits lower overall quality, it is not sensitive enough in its present form to distinguish the induced damage from the natural variability present in the material. To improve the detection and mapping of such defects, it may be necessary to refine the testing approach. Possible

improvements include increasing the number of measurement points, using more advanced signal processing techniques, or combining UPV with other non-destructive testing methods. Without such enhancements, these subtle, localized defects will remain challenging to detect in high w/c ratio concretes.

In summary, the contour plot for the high w/c ratio sample presents a more irregular distribution of UPV values than that seen in the low w/c ratio sample. Although the overall reduction in quality is evident, the plot does not clearly reveal the induced internal or near-surface defects. The comparison with baseline measurements and mechanical properties highlights the limitations of the current testing configuration and suggests that further refinements may be needed to more accurately identify damage in concrete with higher porosity.

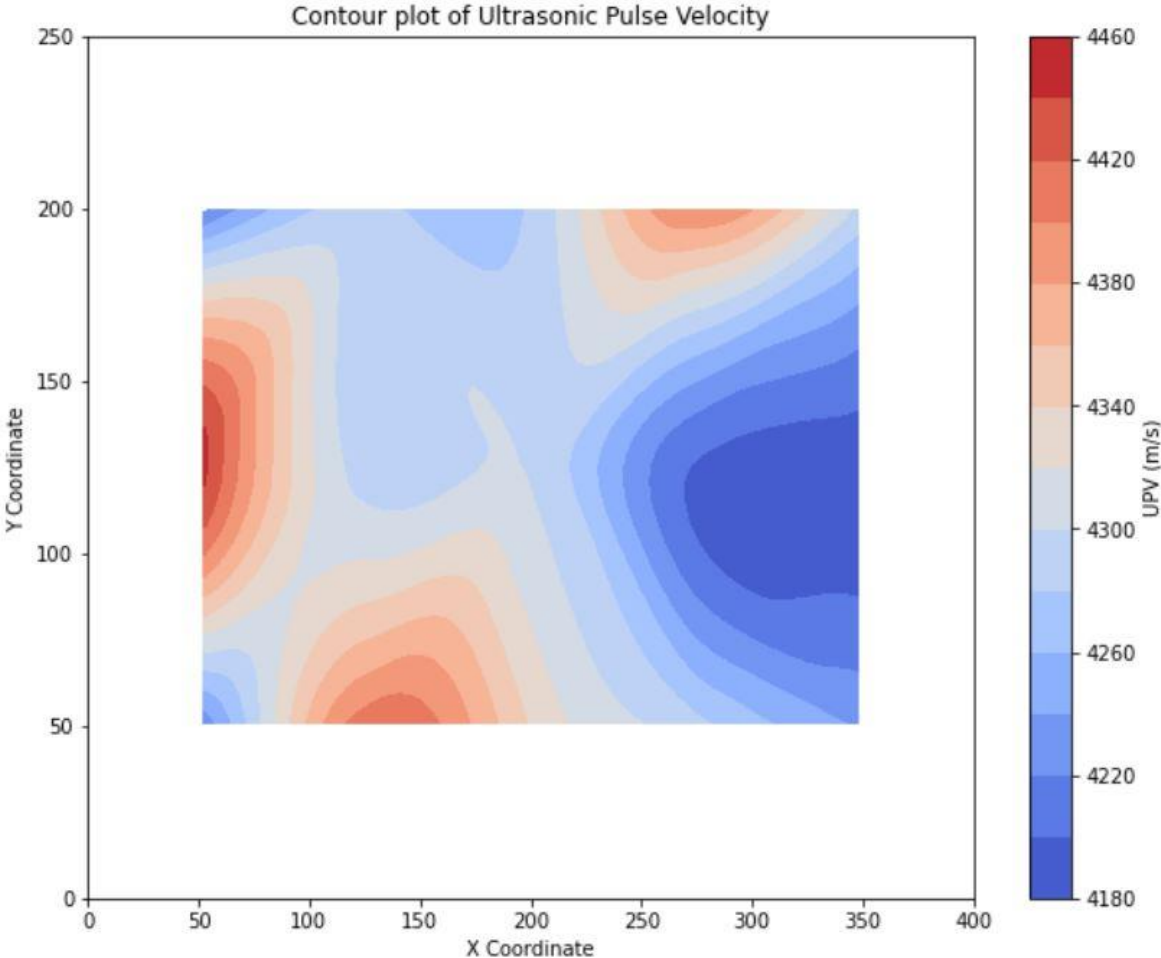


Figure 51: Contour plot of Indirect Method 1 (High W/C ratio)

4.3.4 Indirect Method 2 – Low W/C ratio

Following the inconclusive outcomes of Indirect Method 1, which did not clearly identify or map the introduced damage zones within the concrete sample, Indirect Method 2 was performed as a more targeted approach. This method involves selecting specific areas where damage was introduced and placing the ultrasonic transducers so that the region of interest lies directly between them. By narrowing the focus onto one damage level at a time, the intention is to determine if the sensors can at least detect a difference in the material's response when a known defect is centred between the transmitter and receiver.

Figure 52 illustrates the results obtained using Indirect Method 2 on the low w/c ratio concrete sample. Four separate measurements were recorded, each corresponding to a different damage zone, which are shown directly after the results in Figure 53. The Ultrasonic Pulse Velocity (UPV) values vary from about 4600 m/s at approximately 50 mm to nearly 4950 m/s at about 150 mm. Beyond this peak, the UPV settles around 4850 m/s at roughly 250 mm and then drops to about 4800 m/s at 350 mm.

When compared to the baseline measurements (Table 12), where the average UPV for the low w/c ratio sample is 4608.36 m/s (Direct Method), these results show that UPV values in Indirect Method 2 reach higher velocities (close to 4950 m/s) in certain regions. This suggests that some areas within the specimen remain densely consolidated despite the induced damage. The peaks in UPV may correspond to regions where the ultrasonic waves travel through more intact material or where damage is less severe.

If a straightforward relationship had been expected, such as deeper or more severe damage producing a simple and predictable change in wave travel time, the data might have shown a more linear trend. For example, if it were assumed that increasing damage would act as a nearer “reflection” point, effectively shortening the wave's travel path and thus increasing velocity, one might anticipate a clear progression in UPV values linked to the damage severity.

However, the actual measurements tell a more complex story. Rather than revealing a neat increase or decrease in UPV values that could be directly associated with the damage levels, the data show an irregular pattern. This suggests that the damage does not behave like a clean, flat interface that neatly reflects the ultrasonic waves back to the receiver. Instead, the internal defects likely introduce scattering, energy loss, and mode conversions. Ultrasonic waves encountering microcracks, voids, and rough, uneven interfaces may slow down, weaken, or take longer paths before reaching the receiver. As a result, the measured velocities do not form a simple pattern and do not steadily climb or fall as the damage depth or severity changes.

The mechanical properties further support these observations. The compressive strength of the low w/c ratio sample is 62.52 MPa (Figure 44), which is lower than expected due to compaction issues. These compaction issues likely result in trapped air voids, contributing to the irregular UPV readings. Conversely, the flexural strength of 10.84 MPa (Figure 45) indicates that the specimen still possesses good resistance to bending stress, which aligns with regions showing higher UPV values.

It is also important to consider that the concrete itself is not perfectly homogeneous. Even in a low w/c ratio sample, local variations in aggregate distribution, small

differences in moisture content, and subtle inconsistencies in microstructure can influence the readings. These natural irregularities add another layer of complexity, making it challenging to isolate the effect of the introduced damage from the background variability inherent in the material.

In essence, while Indirect Method 2 applies a more focused testing strategy than Indirect Method 1, it still does not yield a clear, linear relationship between damage severity and measured UPV. The transducers do not produce a simple signal that would confirm or deny the presence of damage in a straightforward manner. Instead, the results highlight the complexity of ultrasonic wave propagation in a heterogeneous medium and show the need for further refinement. Techniques such as increasing the number of measurement points, applying advanced signal processing methods, or combining UPV testing with other non-destructive evaluation tools may be necessary to gain a clearer understanding of how internal defects influence ultrasonic measurements and to reliably detect and map damage within concrete structures.

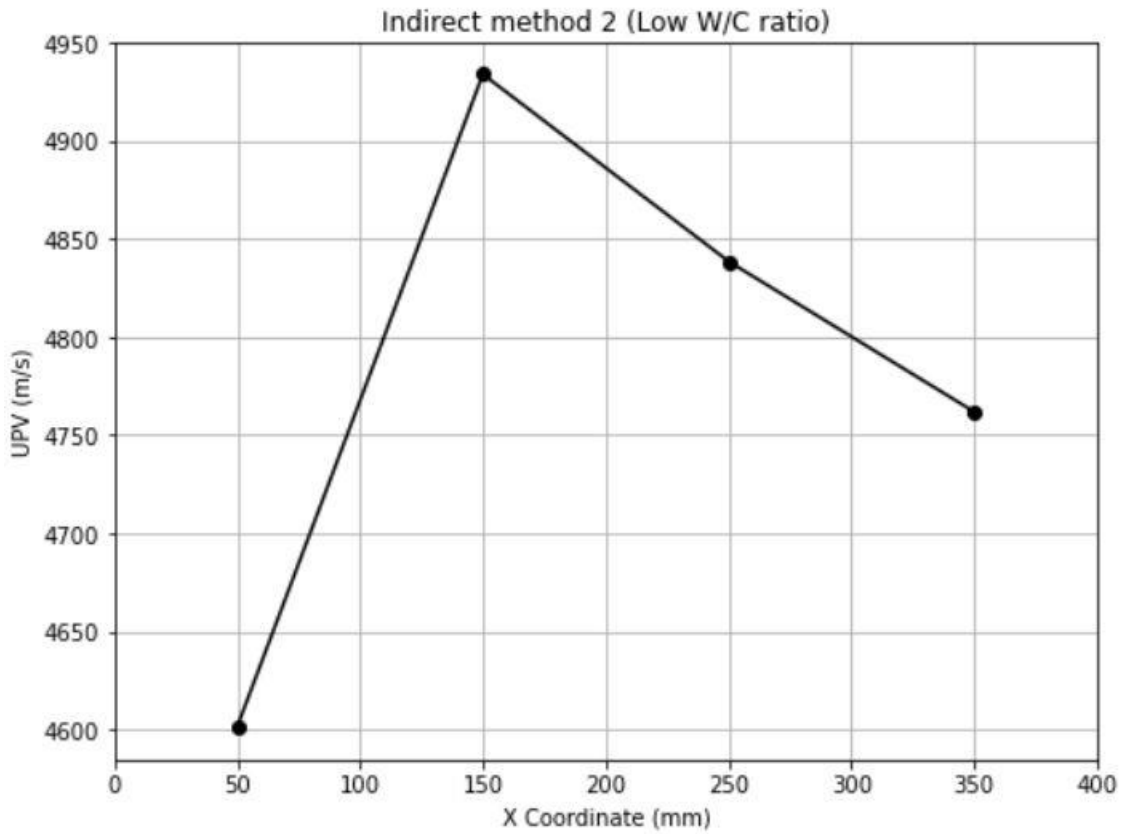


Figure 52: Ultrasonic Pulse Velocity (UPV) Values for Indirect Method 2 (Low W/C ratio Concrete)

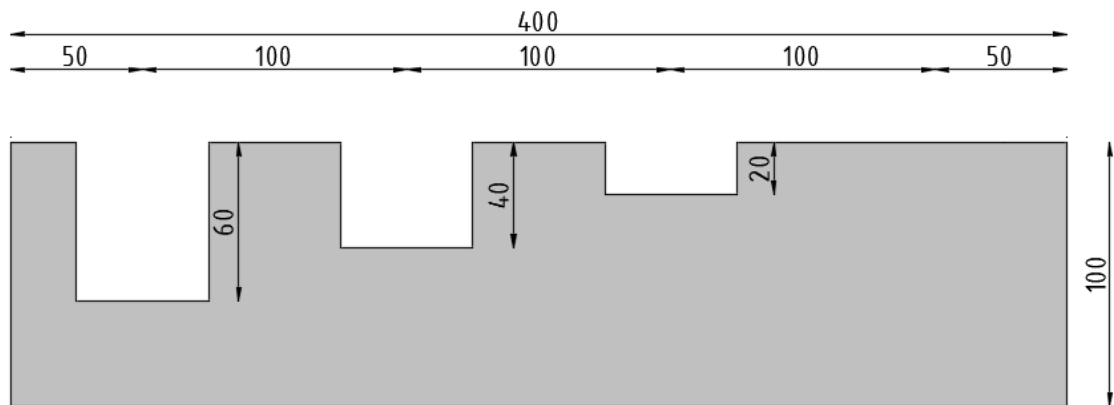


Figure 53: Cross-Section of the Concrete Sample showing the damage levels rising from right-to-left

4.3.5 Indirect Method 2 – High W/C ratio

Figure 54 displays the Ultrasonic Pulse Velocity (UPV) measurements for Indirect Method 2 applied to the high W/C ratio concrete sample. As with the low W/C ratio sample, this approach arranges each measurement so that the induced damage zone lies directly between the transducers. However, the higher W/C ratio creates a more porous and heterogeneous internal structure, influencing the way the ultrasonic waves travel through the material.

In this case, the recorded UPV values range from around 4200 m/s at the lower end to approximately 4500 m/s at the peak, reached near 150 mm. After this peak, the velocities decline steadily, dropping back down to about 4200 m/s by the time the measurement reaches the far end of the tested region. When compared to the baseline measurements (Table 12), the average UPV for the high W/C ratio sample is 4263.67 m/s (Direct Method). The measured values in Indirect Method 2 are consistent with this baseline average, confirming the porous nature of the high W/C ratio concrete.

If one expected a simple pattern, such as a linear increase or decrease in UPV with increasing damage severity, the results do not confirm such a relationship. Instead, the data follow a non-linear trend, showing an initial rise to a peak and then a steady decline. This irregular pattern suggests that the defects introduced from the opposite surface do not act as simple reflecting boundaries that shorten the travel path and thus increase UPV in a predictable manner. Instead, these internal flaws create complex conditions that scatter, absorb, or deflect the ultrasonic waves.

Rather than highlighting the location or severity of the damage through a clear and direct change in UPV, the waves may be slowed down or weakened due to energy losses and multiple interactions with internal features of the concrete. The greater porosity and variability inherent in the high W/C ratio mixture further complicates these measurements. Even slight changes in aggregate arrangement, the presence of microcracks, or inconsistencies in moisture distribution can influence the recorded UPV values.

The mechanical properties of the high W/C ratio concrete support these observations. The compressive strength of 67.30 MPa (Figure 44) reflects better compaction due to the higher workability of the mix, while the flexural strength of 10.38 MPa (Figure 45) is slightly lower than the low W/C ratio sample. This lower flexural strength indicates that while the concrete may have sufficient compressive capacity, its ability to resist bending is reduced due to increased porosity and the presence of internal microcracks. These structural characteristics contribute to the scattered and inconsistent UPV readings observed in the contour plot.

Furthermore, the damage does not stand out clearly against the background variations, making it difficult to draw straightforward conclusions about the defects based on the measured velocities alone. The pulse-echo measurements conducted at the edges may have further contributed to the variability due to wave attenuation and boundary reflections.

In summary, while Indirect Method 2 provides a more focused approach to assessing damage than Indirect Method 1, the results from the high W/C ratio concrete sample remain complex and do not yield a simple, linear correlation between the severity of

defects and the recorded UPV. The comparison to baseline measurements and mechanical properties reinforces this complexity. Additional testing strategies, more refined data collection methods, or complementary non-destructive techniques may be required to reliably identify and map the induced damage under such challenging conditions.

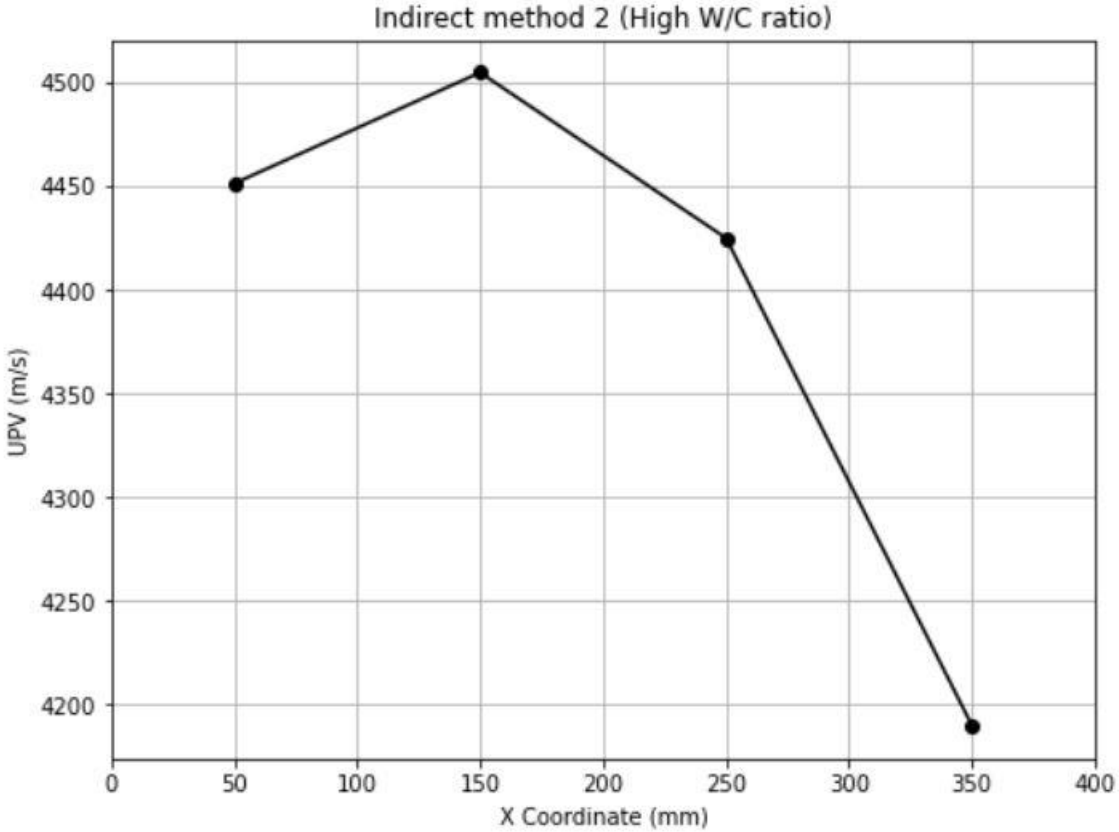


Figure 54: Ultrasonic Pulse Velocity (UPV) Values for Indirect Method 2 (High W/C ratio Concrete)

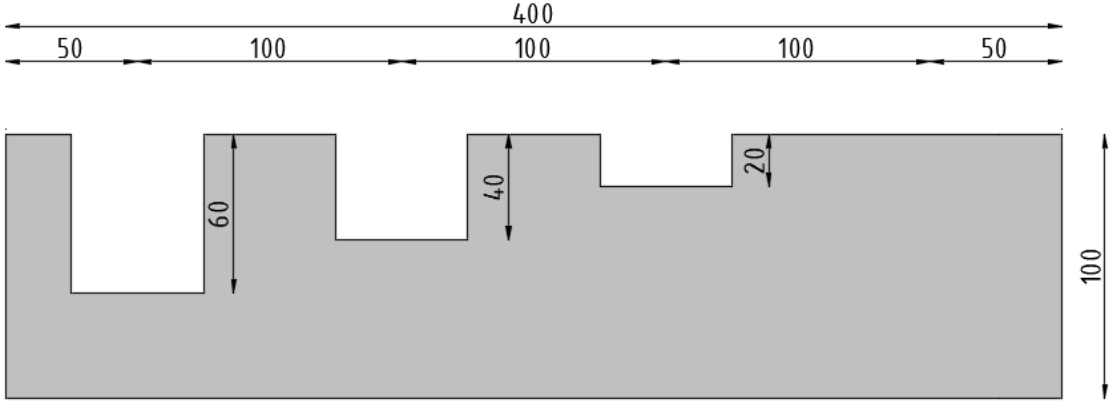


Figure 55: Cross-Section of Damage Levels in High W/C ratio Concrete Sample

4.3.6 Pulse-Echo Method – Low W/C ratio

After the Indirect Method 1 and Indirect Method 2 were conducted, the Pulse-Echo Method was applied to the low water-cement (W/C) ratio concrete sample to gain further insights into the internal structure and damage localization. This method demonstrated promising results, particularly for identifying and mapping thickness variations. The decision to present the local thickness distribution was driven by the clear variations observed in the Time of Flight (TOF) contour plot, which showed potential for accurately detecting the pre-intended damage levels.

The TOF contour plot, shown in Figure 56, displays values ranging from 2.4×10^{-5} seconds to 4.6×10^{-5} seconds. The edges of the sample exhibit the highest TOF values, ranging from 4.2×10^{-5} seconds to 4.6×10^{-5} seconds, corresponding to the undamaged regions where the sample maintains its original thickness of 10 cm. In the middle region, where the measurements were strategically positioned over the pre-intended damage levels, the TOF values decrease significantly. The central TOF values range between 3.0×10^{-5} seconds and 3.6×10^{-5} seconds, indicating regions with reduced thickness. The leftmost part of the plot shows the lowest TOF values, between 2.4×10^{-5} seconds and 2.7×10^{-5} seconds, which corresponds to the areas with the most severe damage.

Using the baseline UPV of 4608.36 m/s obtained from the Direct Method, the corresponding TOF for an undamaged sample thickness of 8 cm is 3.472×10^{-5} seconds (using twice the thickness as a path length). This baseline value serves as a reference for interpreting the TOF results. The undamaged regions in Figure 56 show TOF values above this baseline, while the damaged regions show TOF values below it, reflecting the reduced thickness due to the induced damage.

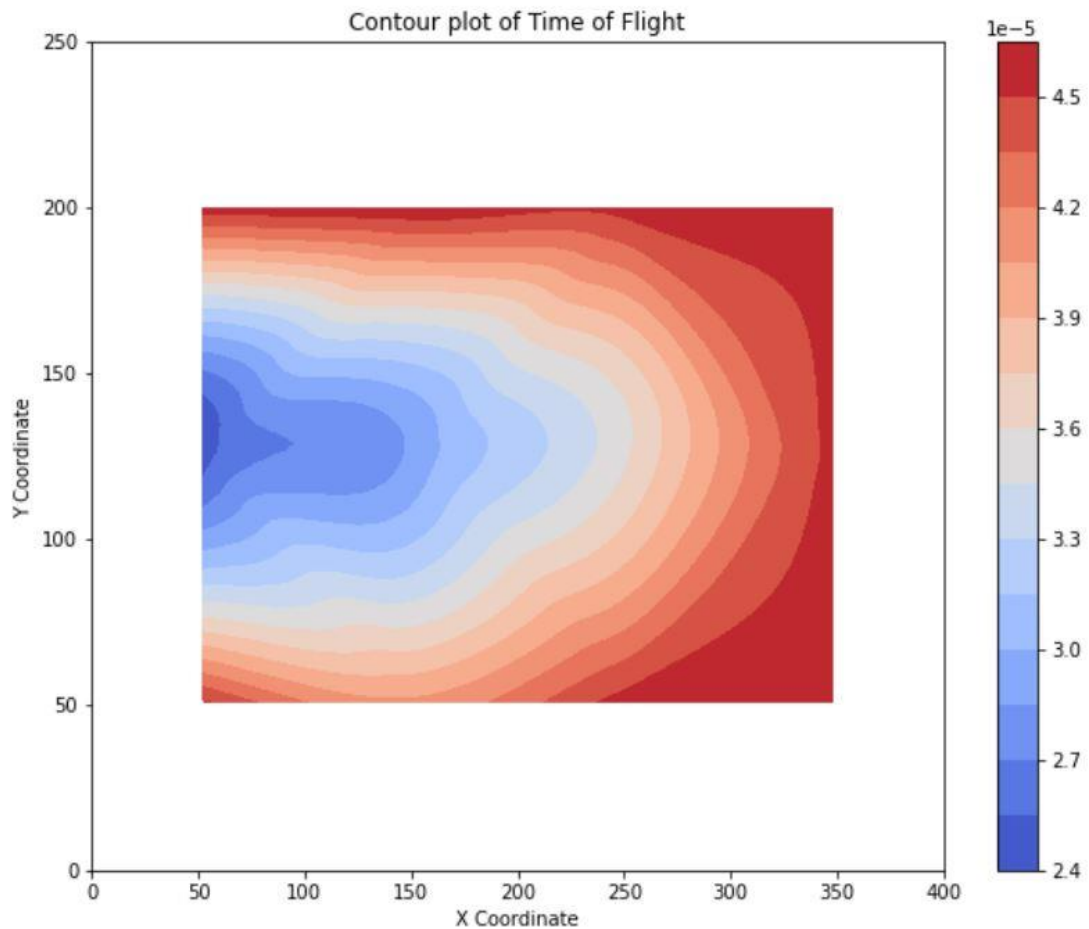


Figure 56: Contour plot of Pulse-Echo Method (Low W/C ratio)

The local thickness distribution derived from the TOF data using the baseline measurement is shown in Figure 57. The thickness values range from approximately 6 cm to 10 cm. The edges of the sample display thickness values near 10 cm, shown by the red regions, indicating that these areas remain undamaged. Moving toward the centre, the thickness decreases gradually, aligning with the pre-intended damage levels. The orange and yellow regions represent a thickness of about 8 cm, corresponding to damage level 1 (2 cm reduction). Further toward the left, the light blue regions indicate a thickness of approximately 7 cm, corresponding to damage level 2 (4 cm reduction). The dark blue regions on the far-left side show the lowest thickness values, around 6 cm, indicating the most severe damage (6 cm reduction).

When comparing the measured thickness values with the actual pre-intended damage reductions (shown in Figure 58), a few discrepancies become apparent. While the measurements for damage level 1 (2 cm reduction) and damage level 2 (4 cm reduction) align reasonably well with the pre-intended reductions, the largest deviation is observed for damage level 3 (6 cm reduction). In this case, the measured thickness is approximately 6 cm, which deviates from the expected thickness of 4 cm. This difference suggests that the Pulse-Echo Method may have limitations in detecting the most severe damage levels accurately, potentially due to factors such as wave scattering, signal attenuation, or interference caused by the extensive internal damage. The complexity of

the wave reflections in these severely damaged regions may result in an overestimation of the thickness.

The mechanical test results further support these observations. The compression and flexural tests indicated that the low W/C ratio concrete exhibited high strength and density. However, potential compaction issues may have introduced localized voids or imperfections that influenced the ultrasonic wave propagation. These imperfections may have contributed to the inaccuracies in the thickness measurements for damage level 3, as the ultrasonic waves encounter increased scattering and energy loss in these highly damaged regions.

The Pulse-Echo Method provided significantly better results compared to Indirect Method 1 and Indirect Method 2 in terms of damage localization and thickness determination. The baseline UPV of 4608.36 m/s and the corresponding TOF value of 3.472×10^{-5} seconds for an undamaged thickness of 8 cm were consistent with the measurements observed in the undamaged regions. In contrast, the lower TOF values in the damaged areas aligned well with the expected thickness reductions for damage levels 1 and 2, while damage level 3 showed the greatest deviation.

In conclusion, the local thickness contour plot derived from the Pulse-Echo Method accurately reflects the pre-intended damage levels, with thickness values ranging from 6 cm to 10 cm. However, the deviation observed for damage level 3 highlights the method's limitations in detecting the most severe damage accurately. The alignment between the schematic damage layout, TOF measurements, baseline UPV values, and mechanical test results validates the overall accuracy of these findings, while also pointing out areas where further refinement may be necessary. The Pulse-Echo Method offers a reliable approach for non-destructive evaluation, effectively identifying and mapping internal defects in the low W/C ratio concrete sample.

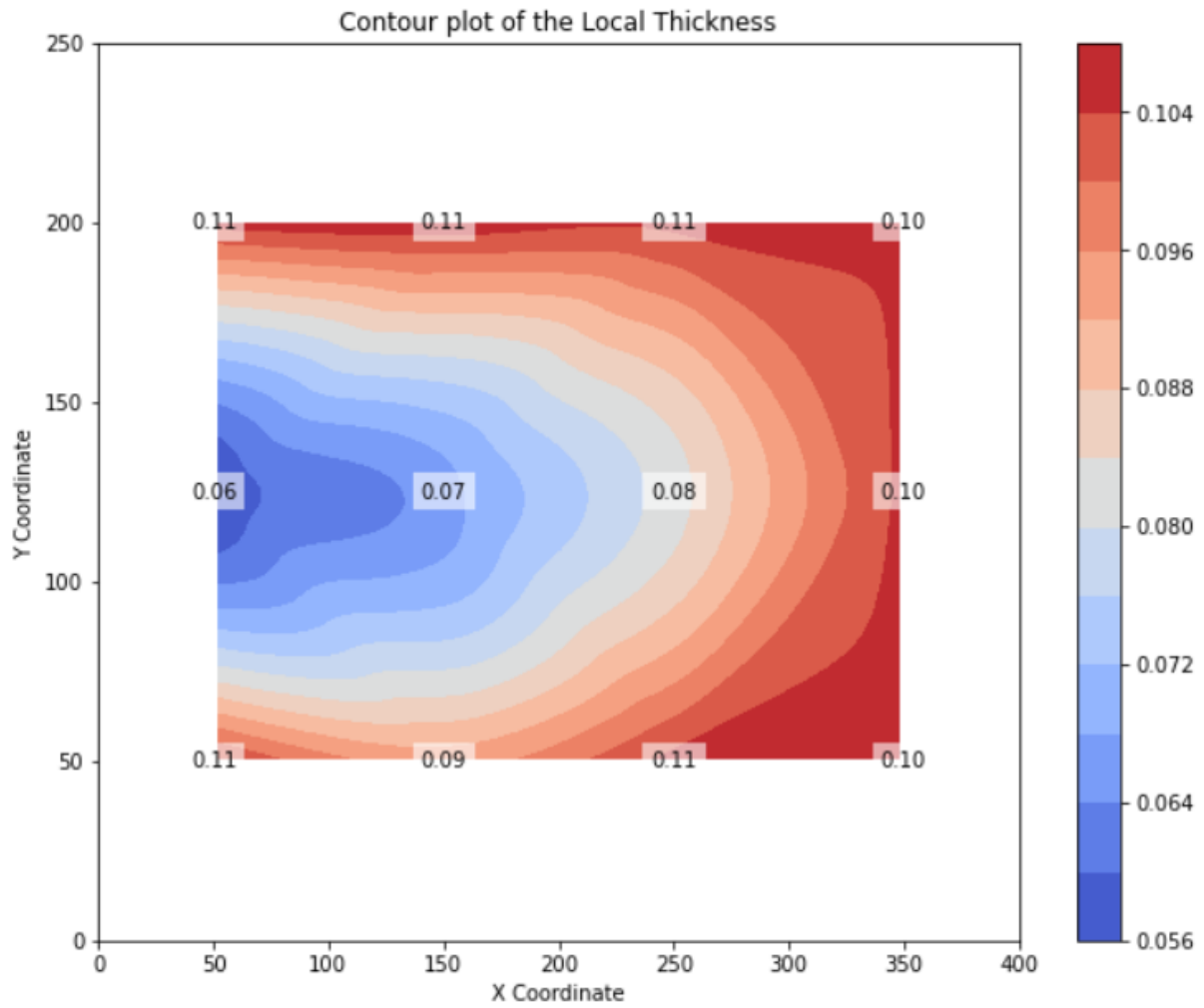


Figure 57: Contour plot of the local thickness (Low W/C ratio)

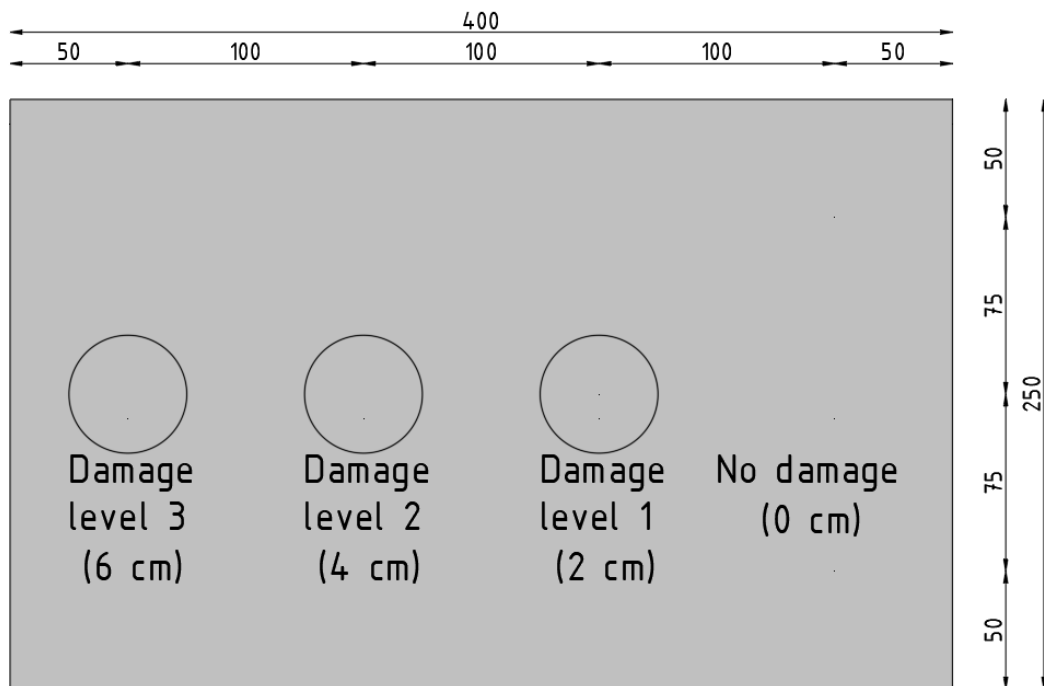


Figure 58: The four damage levels of the sample shown on top of the surface

4.3.7 Pulse-Echo Method – High W/C ratio

After completing the Pulse-Echo measurements for the low W/C ratio sample, the same methodology was applied to the high W/C ratio sample. Figure 59 shows the contour plot of the Time of Flight (TOF) values, ranging between 1.8×10^{-5} seconds and 4.6×10^{-5} seconds. The TOF values are distributed across the sample, reflecting the material's porosity and internal structure due to the higher water-cement ratio. The highest TOF values, between 4.2×10^{-5} and 4.6×10^{-5} seconds, are observed along the right edge of the plot, corresponding to the undamaged regions of the sample. These higher TOF values indicate greater material thickness, consistent with the baseline undamaged regions.

Toward the centre and left side of the plot, the TOF values decrease, indicating reduced thickness caused by the pre-intended damage levels. The lowest TOF values, between 1.8×10^{-5} and 2.6×10^{-5} seconds, are concentrated in the leftmost region, corresponding to the most severe damage. This distribution of TOF values clearly reflects a gradual reduction in thickness across the damaged regions. The measurements obtained from the high W/C ratio sample are generally consistent with the pre-intended damage levels, indicating that the Pulse-Echo method effectively captured the damage distribution.

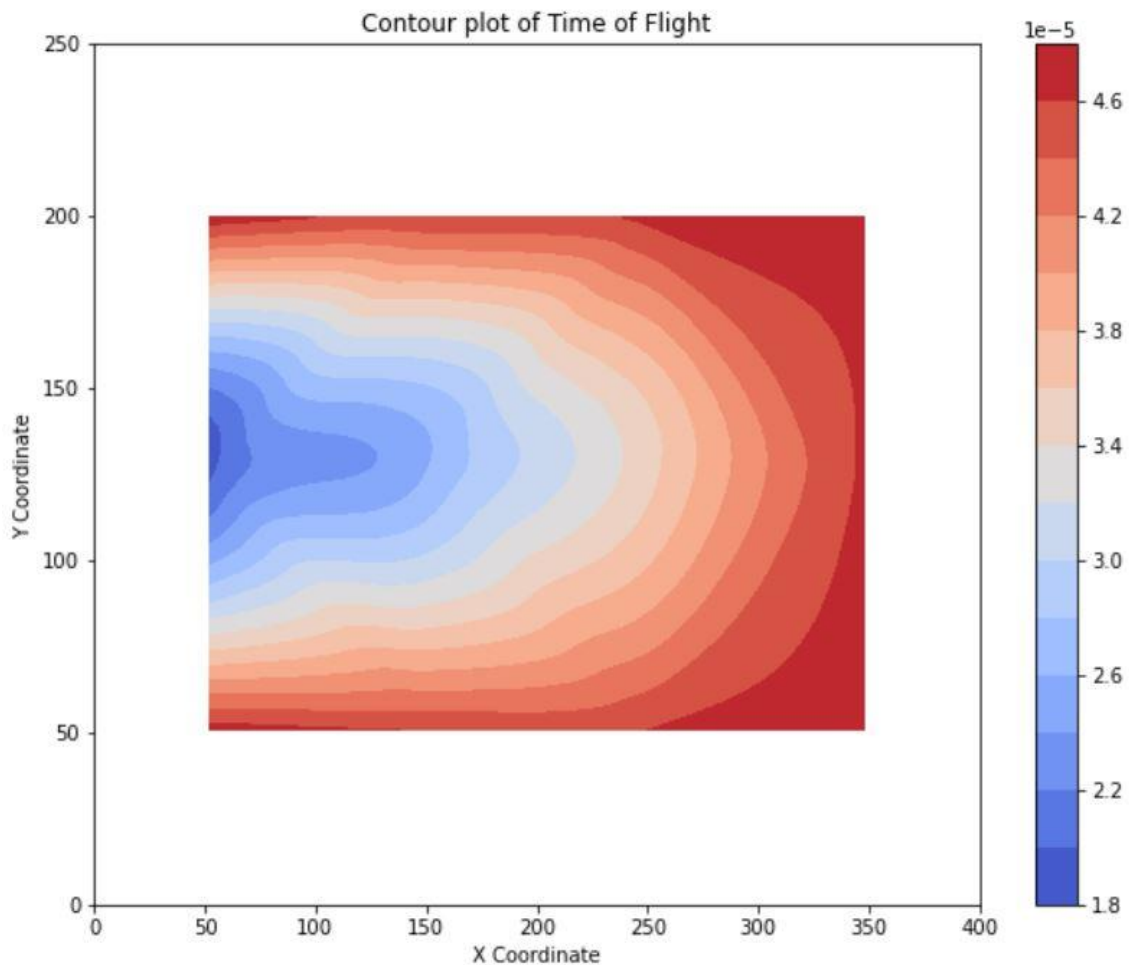


Figure 59: Contour plot of Pulse-Echo Method (High W/C ratio)

Figure 60 presents the contour plot of the local thickness distribution derived from the TOF data using the average baseline UPV of 4263.67 m/s for the high W/C ratio sample. The thickness values range between 4 cm and 10 cm. The undamaged edges of the sample consistently show thickness values equal to 10 cm, while the middle and left sections reflect reductions in thickness corresponding to the pre-intended damage levels shown in Figure 61. Specifically, the blue regions in the plot represent thickness values of approximately 8 cm (2 cm reduction), 6 cm (4 cm reduction), and 4 cm (6 cm reduction). As can be seen, these results perfectly align with the pre-intended damage levels, demonstrating that the Pulse-Echo method provides an accurate representation of the local thickness.

When comparing the high W/C ratio results to those of the low W/C ratio sample, the Pulse-Echo measurements for both samples accurately captured the general trend of thickness reduction. The low W/C ratio sample exhibited slightly higher UPV values, as seen in the baseline measurements, where the average UPV for the low W/C ratio sample is 4608.36 m/s, compared to 4263.67 m/s for the high W/C ratio sample. This difference reflects the denser internal structure of the low W/C ratio concrete, which allows for faster ultrasonic wave propagation.

The mechanical testing results further support these findings. The compressive strength of the high W/C ratio sample has a mean of 67.30 MPa, which is slightly lower than that of the low W/C ratio sample's mean of 63.52 MPa. For the flexural strength, the high W/C ratio sample has a slightly lower strength of 10.38 MPa compared to a strength of 10.84 MPa for the low W/C ratio sample. This difference suggests that while the compressive strength remains high, the higher water content in the high W/C ratio sample may have slightly reduced its tensile capacity, potentially influencing the Pulse-Echo measurements in regions with moderate damage.

In conclusion, the Pulse-Echo measurements for the high W/C ratio sample successfully captured the thickness reductions corresponding to the pre-intended damage levels. The results are consistent with the actual damage. When compared to the low W/C ratio sample, the high W/C ratio sample shows more accuracy in damage detection, although the lower UPV values reflect the higher porosity of the material. The Pulse-Echo method proved to be a reliable technique for identifying and mapping damage in both concrete types.

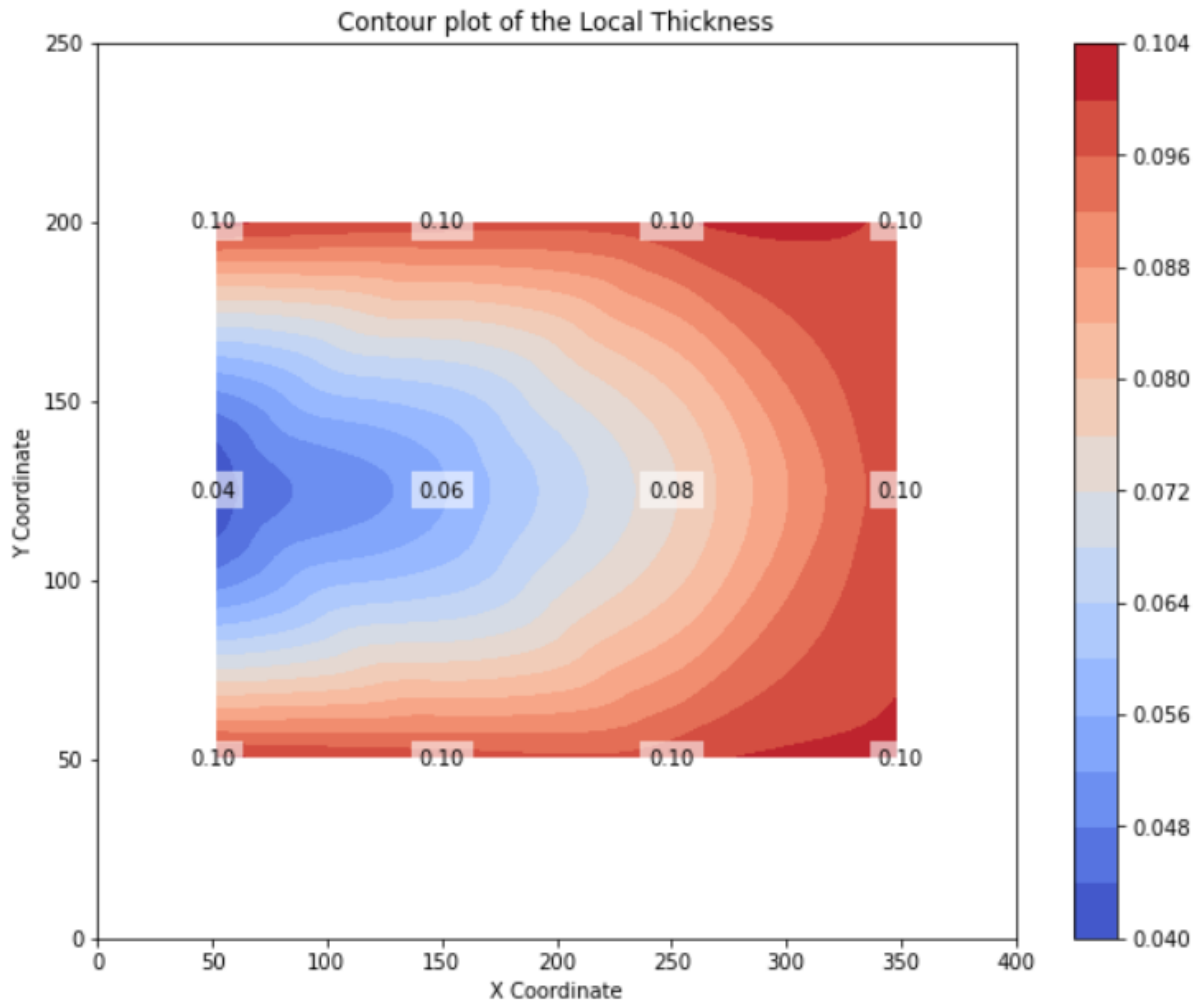


Figure 60: Contour plot of the local thickness (High W/C ratio)

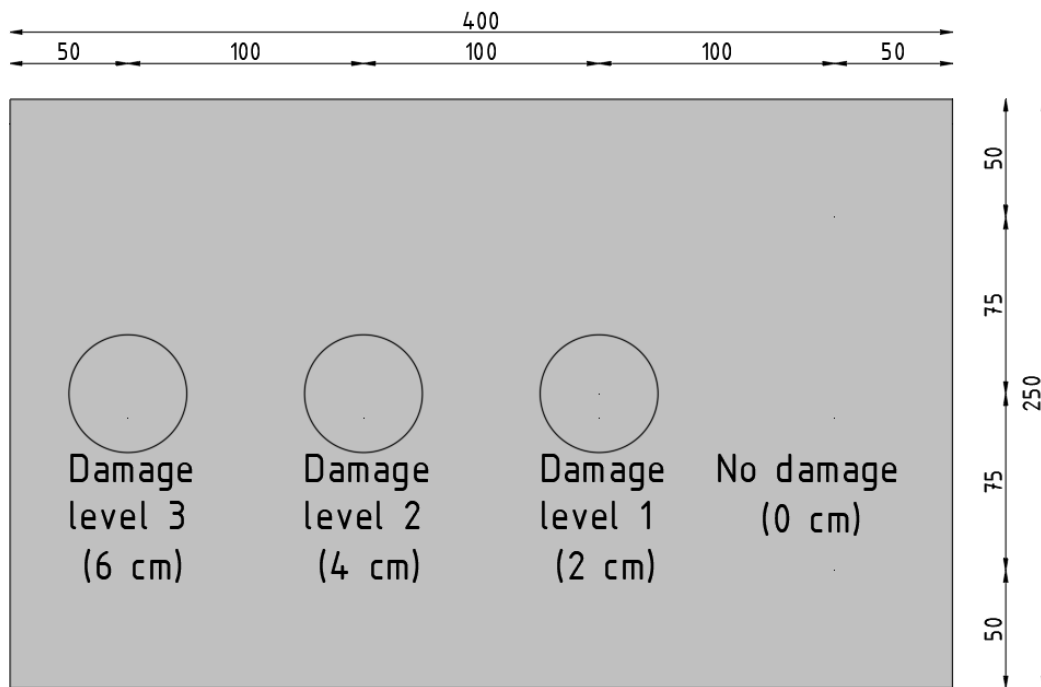


Figure 61: The four damage levels of the sample shown on top of the surface

4.4 Comparison of the UPV testing results

The results of Indirect Method 1 for Ultrasonic Pulse Velocity (UPV) testing, presented in Figure 62 and Table 13, along with the findings from the contour plots (Figure 50 and Figure 51), provide a detailed comparison of the Low and High Water-Cement (W/C) ratio concrete samples. These results illustrate significant differences in internal structure, consistency, and defect distribution between the two mix designs.

The Low W/C ratio sample consistently exhibits higher UPV values across all transducer positions, ranging between 4365.54 m/s and 4895.56 m/s. Notably, positions like 1-2 and 1-7 show particularly high values of 4895.56 m/s and 4891.30 m/s, respectively. This consistency in UPV measurements reflects a dense and well-consolidated internal structure with fewer voids and defects. The minimal fluctuation in UPV values suggests a uniform distribution of material properties, reinforcing the quality and structural integrity of the Low W/C ratio concrete. The contour plot of the Low W/C ratio sample shows a central region with higher UPV values (4800 m/s to 4880 m/s) that gradually decrease towards the edges, suggesting a homogeneous microstructure. Despite the pre-intended damage on the opposite surface, this damage is not distinctly visible in the UPV results, highlighting the limitations of Indirect Method 1 in detecting deeper or opposite-side defects in denser materials.

In contrast, the High W/C ratio sample shows lower and more variable UPV values, ranging between 4123.44 m/s and 4453.68 m/s. In Figure 62, positions such as 1-3 and 1-10 display values as low as 4188.38 m/s and 4123.44 m/s, respectively. These fluctuations indicate a more porous and inconsistent microstructure, likely caused by higher water content leading to weaker bonding and the formation of voids. The trend in Figure 62 reveals frequent drops in UPV values, suggesting the presence of micro-cracks and localized defects. The contour plot of the High W/C ratio sample reflects this inconsistency, showing a scattered and irregular distribution of UPV values. Areas with lower UPV values (4180 m/s to 4260 m/s) indicate regions of higher porosity and internal imperfections, which hinder wave propagation. This irregular pattern shows the challenges in maintaining compaction and structural integrity in the High W/C ratio mix.

The differences in UPV values between the two samples are significant, with discrepancies exceeding 500 m/s at several positions. For example, at position 1-2, the UPV difference is 598.39 m/s (4895.56 m/s for Low W/C vs. 4297.17 m/s for High W/C). Similarly, at position 1-7, the difference is 600.68 m/s (4891.30 m/s for Low W/C vs. 4290.62 m/s for High W/C). These variations highlight the superior density and structural consistency of the Low W/C ratio sample compared to the High W/C ratio sample, which is prone to internal defects and inconsistencies.

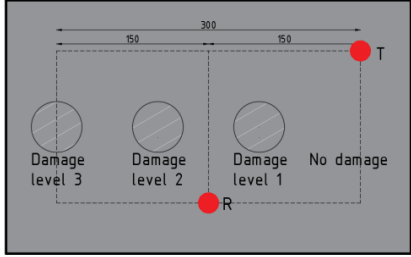
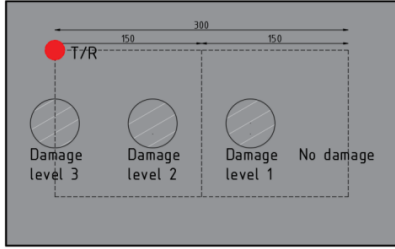
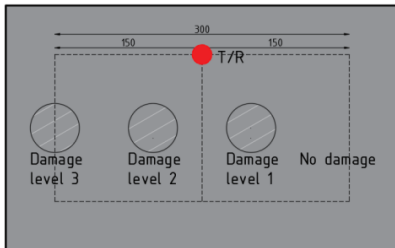
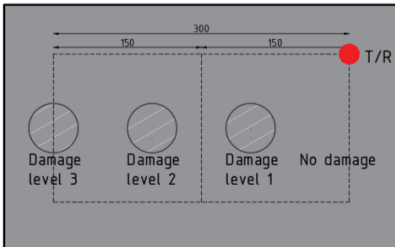
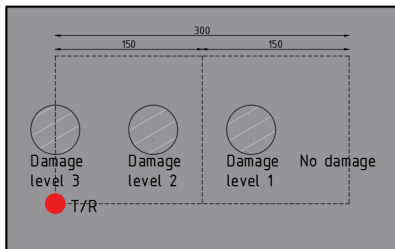
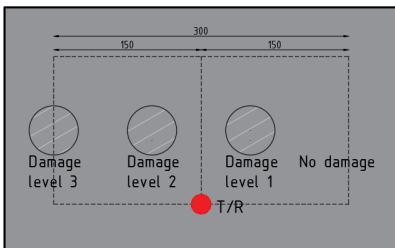
The findings from Indirect Method 1 are consistent with the mechanical testing results, where the Low W/C ratio sample demonstrated higher and more consistent flexural strength compared to the High W/C ratio sample. However, it is important to note that the mean compressive strength of the Low W/C ratio sample (62.52 MPa) was lower than that of the High W/C ratio sample (67.30 MPa) due to compaction issues. Despite this, the UPV results suggest that the Low W/C ratio sample maintains a denser and more uniform microstructure, which contributes to its overall structural reliability. Conversely, the High W/C ratio sample's higher compressive strength may reflect

localized regions of improved compaction, but its lower flexural strength and variable UPV results indicate greater overall porosity and inconsistency.

The contour plots further illustrate these structural differences, with the Low W/C ratio sample displaying a smooth and continuous gradient, while the High W/C ratio sample shows a fragmented and uneven distribution. These findings emphasize that controlling the water-cement ratio is critical for achieving superior concrete performance and reveal the challenges of detecting defects in denser materials using Indirect Method 1.

Position	Transducer placement	UPV Low W/C ratio	UPV High W/C ratio
1-1		4603.11 m/s	4453.68 m/s
1-2		4895.56 m/s	4297.17 m/s
1-3		4766.95 m/s	4188.38 m/s
1-4		4664.18 m/s	4284.08 m/s

<p>1-5</p>		<p>4799.49 m/s</p>	<p>4397.97 m/s</p>
<p>1-6</p>		<p>4750.84 m/s</p>	<p>4408.31 m/s</p>
<p>1-7</p>		<p>4891.3 m/s</p>	<p>4290.62 m/s</p>
<p>1-8</p>		<p>4598.03 m/s</p>	<p>4304.28 m/s</p>
<p>1-9</p>		<p>4757.63 m/s</p>	<p>4274.19 m/s</p>
<p>1-10</p>		<p>4668.23 m/s</p>	<p>4123.44 m/s</p>

<p>1-11</p>		<p>4715.3 m/s</p>	<p>4278.79 m/s</p>
<p>1-12</p>		<p>4365.54 m/s</p>	<p>4209.94 m/s</p>
<p>1-13</p>		<p>4355.4 m/s</p>	<p>4278.38 m/s</p>
<p>1-14</p>		<p>4433.93 m/s</p>	<p>4295.53 m/s</p>
<p>1-15</p>		<p>4387.25 m/s</p>	<p>4221.78 m/s</p>
<p>1-16</p>		<p>4341.53 m/s</p>	<p>4334.01 m/s</p>

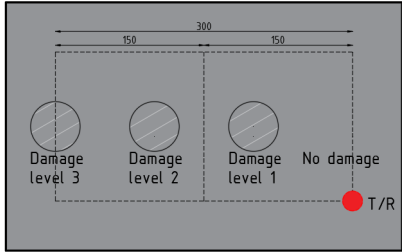
1-17		4413.06 m/s	4237.29 m/s
------	-----------------------------------------------------------------------------------	-------------	-------------

Table 13: Transducer Positioning and UPV Measurements for Indirect Method 1 (Low and High W/C ratios)

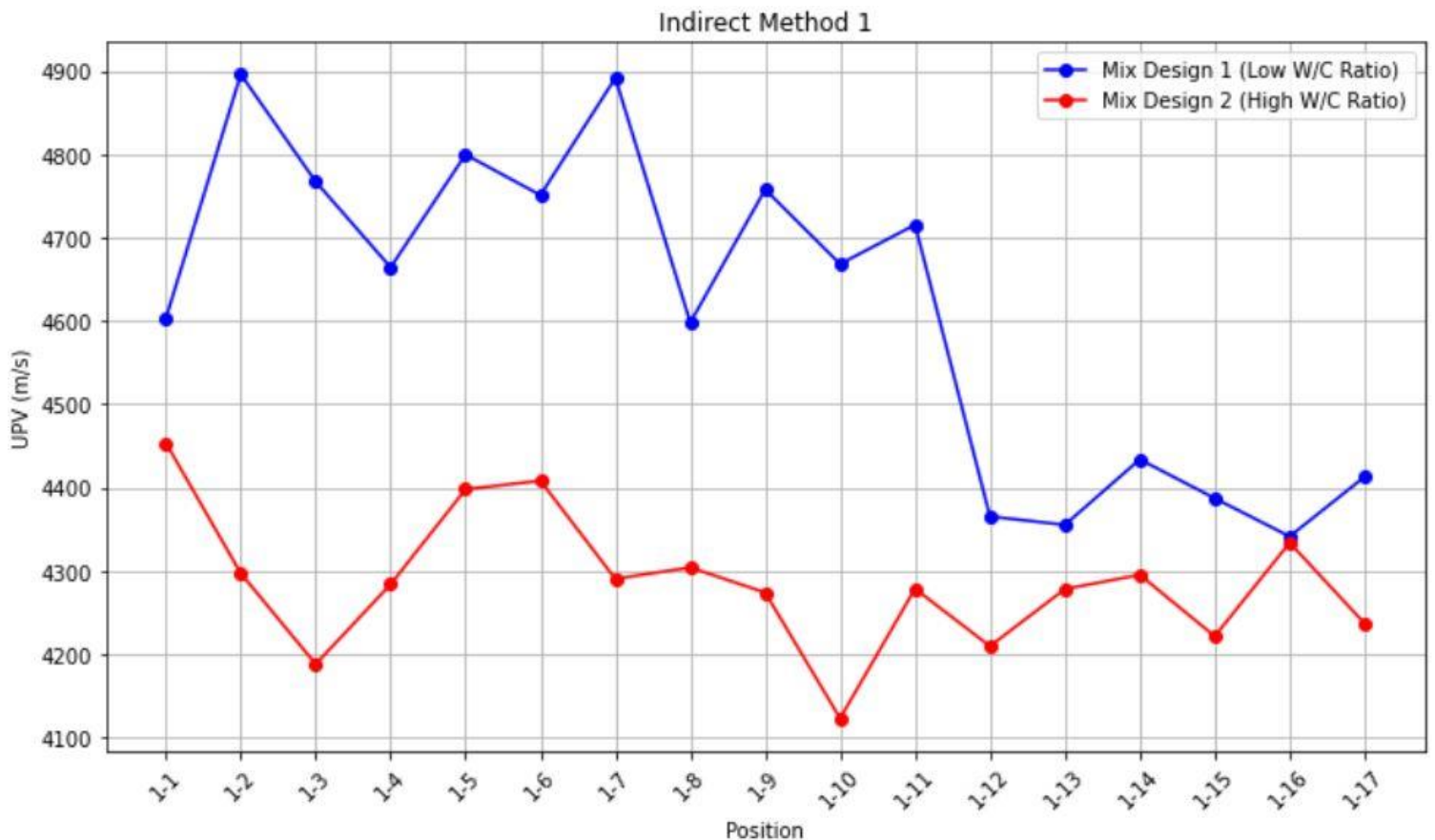


Figure 62: UPV Comparison for Low and High W/C ratio Samples Using Indirect Method 1

Building on the findings from Indirect Method 1, Indirect Method 2 provides a more focused evaluation by positioning the transducers around specific damage zones. The results, presented in Table 14 and Figure 63, allow for a targeted analysis of the internal structure of the Low and High Water-Cement (W/C) ratio samples. The primary goal of this study was to determine whether Ultrasonic Pulse Velocity (UPV) testing could detect the pre-intended damage on the opposite surface of the concrete samples. However, the findings reveal that while Indirect Method 2 highlights key differences in internal structure and consistency between the two mix designs, no clear signals were observed that could be directly linked to the induced internal damage.

For the Low W/C ratio sample, the UPV values range between 4603.11 m/s and 4929.89 m/s across the measured positions. The highest value, recorded at Position 2-3, is 4929.89 m/s, indicating a region of dense, well-consolidated material. Positions 2-1 and 2-2 also demonstrate high values of 4766.95 m/s and 4836.63 m/s, respectively. In Figure 63, the trend line for the Low W/C ratio sample (blue line) shows a steady increase in UPV values from Position 2-1 to Position 2-3, followed by a slight decline at Position 2-4. This consistent pattern reflects a dense and uniform microstructure with good aggregate distribution and minimal defects. The contour plot for Indirect Method 1 (Figure 50) supports these findings by showing a smooth and continuous gradient of UPV values, indicating well-consolidated regions. Despite this, the dense nature of the Low W/C ratio sample masked the pre-intended damage, making it difficult to detect using Indirect Method 2.

In contrast, the High W/C ratio sample exhibits lower and more variable UPV values, ranging between 4188.38 m/s and 4500 m/s. The highest value of 4500 m/s is recorded at Position 2-3, while positions 2-1 and 2-2 show values of 4188.38 m/s and 4425.65 m/s, respectively. In Figure 63, the trend line for the High W/C ratio sample (red line) shows an initial rise in UPV values from Position 2-1 to Position 2-3, followed by a decline at Position 2-4. The variability in these values reflects a more porous and inconsistent microstructure, with voids and micro-cracks impeding wave propagation. The contour plot for Indirect Method 1 (Figure 51), also in this case reinforces this conclusion, by showing an irregular distribution of UPV values with noticeable drops in areas of higher porosity and weaker bonding.

The differences between the two samples are evident in the magnitude of the UPV values. For example, at Position 2-1, the Low W/C ratio sample shows a UPV of 4766.95 m/s, while the High W/C ratio sample records only 4188.38 m/s, a difference of 578.57 m/s. Similarly, at Position 2-3, the UPV difference is 429.89 m/s (4929.89 m/s for Low W/C vs. 4500 m/s for High W/C). These discrepancies highlight the superior density and structural consistency of the Low W/C ratio sample compared to the High W/C ratio sample, which is more prone to defects and inconsistencies.

The findings from Indirect Method 2 correlate with the mechanical test results discussed earlier. The Low W/C ratio sample exhibits higher and more consistent flexural strength (10.84 MPa) compared to the High W/C ratio sample (10.38 MPa), reflecting better structural integrity. However, the compressive strength of the Low W/C ratio sample (62.52 MPa) was lower than that of the High W/C ratio sample (67.30 MPa), likely due to compaction issues. These compaction problems could explain why UPV results did not show greater differences between the two mix designs and why detecting the pre-intended damage remained challenging.

Despite the focused approach of Indirect Method 2, no clear UPV signals were observed that could be directly linked to the induced internal damage in either sample. In the Low W/C ratio sample, the dense microstructure likely masked the damage, preventing its detection. In the High W/C ratio sample, while structural inconsistencies were evident, the variability in UPV values made it difficult to distinguish induced damage from inherent defects. This limitation highlights the challenges of using UPV to identify subtle damage in concrete, particularly when the defects are located on the opposite surface or when the material structure is dense.

In conclusion, the results of Indirect Method 2 reinforce the findings from Indirect Method 1, showing that while UPV testing can reveal differences in material quality and structural consistency, it was not successful in detecting the pre-intended damage in either the Low or High W/C ratio samples. The Low W/C ratio sample consistently demonstrated higher UPV values, reflecting a dense and uniform microstructure, while the High W/C ratio sample showed lower and more variable UPV values, indicating a porous and inconsistent structure. These findings emphasize the need for complementary non-destructive techniques or refined testing strategies to accurately identify and map defects within concrete.

Position	Transducer placement	UPV Low W/C ratio	UPV High W/C ratio
2-1		4766.95 m/s	4188.38 m/s
2-2		4836.63 m/s	4425.65 m/s
2-3		4929.89 m/s	4500 m/s
2-4		4603.11 m/s	4453.68 m/s

Table 14: Transducer Positioning and UPV Measurements for Indirect Method 2 (Low and High W/C ratios)

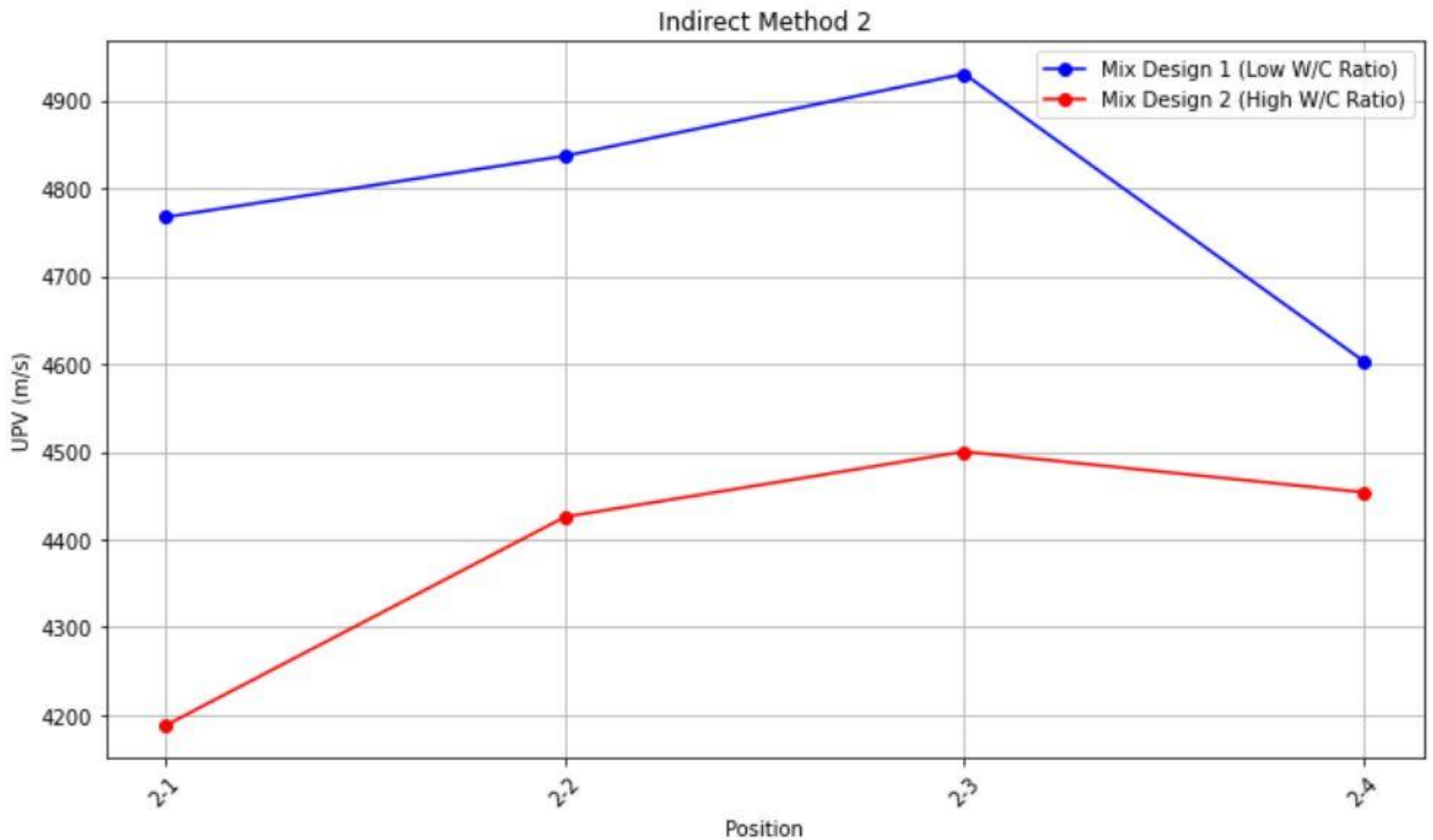


Figure 63: UPV Comparison for Low and High W/C ratio Samples Using Indirect Method 2

The results of the Pulse-Echo Method for Ultrasonic Pulse Velocity (UPV) testing, presented in Table 15 and Figure 64, provide a comparison of the Low and High Water-Cement (W/C) ratio concrete samples. This method measures the Time of Flight (TOF) of ultrasonic waves to assess thickness variations and internal defects within the samples. The main goal was to determine if UPV could detect pre-intended damage in the concrete. The results accurately captured the locations of severe damage, with distinct reductions in TOF values corresponding to areas of maximum thickness reduction.

For the Low W/C ratio sample, the TOF values range between 2.45×10^{-5} seconds and 4.63×10^{-5} seconds (Table 15). The average baseline TOF value using the direct method is 3.472×10^{-5} seconds, specifically for a sample with 8 cm thickness. The TOF values at Positions 3-1 to 3-4 and 3-8 to 3-12 remain between 4.51×10^{-5} and 4.63×10^{-5} seconds, reflecting regions with little to no damage where the sample thickness remains close to 10 cm. At Position 3-5, a sharp drop to 2.45×10^{-5} seconds corresponds to the most severe damage, indicating a 6 cm thickness reduction. This reduction aligns with the baseline UPV measurement of 4608.36 m/s (Table 12).

The TOF values recorded at Positions 3-6 and 3-7, which are placed directly over 4 cm and 2 cm damage, are 2.88×10^{-5} seconds and 3.57×10^{-5} seconds, respectively. These moderate damage levels produce TOF reductions that are less pronounced than the severe damage at Position 3-5. This is consistent with the expectation that smaller damage results in less reduction in thickness, and the longer wave path due to the greater remaining thickness leads to higher TOF values. The contour plot of TOF values

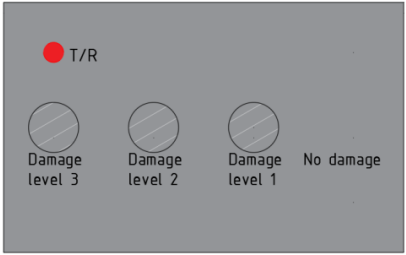
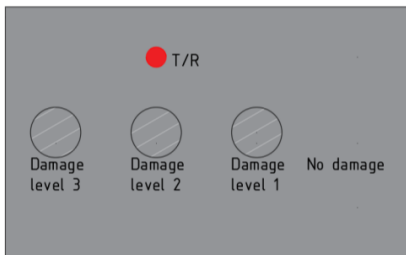
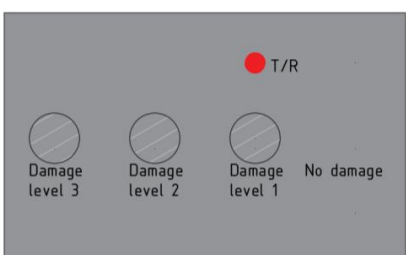
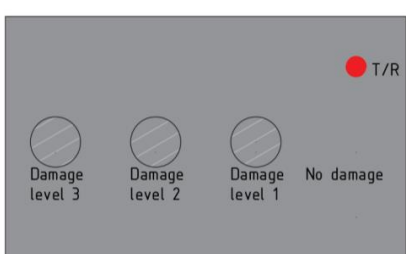
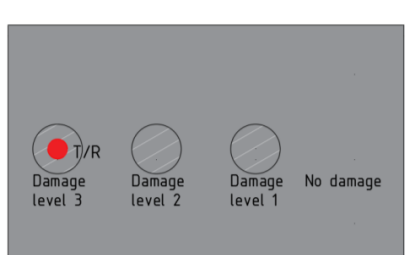
for the Low W/C ratio sample shows a relatively smooth distribution with localized deviations where severe damage was introduced.

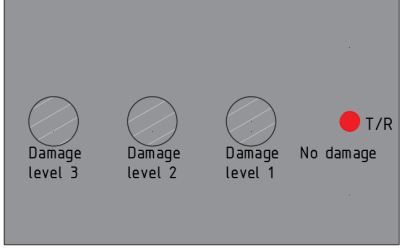
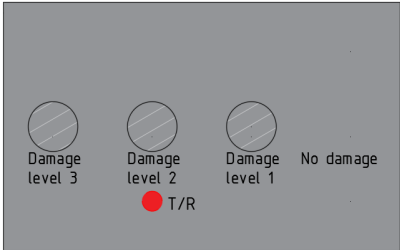
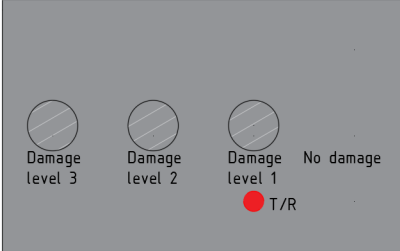
In the High W/C ratio sample, the TOF values range between 1.91×10^{-5} seconds and 4.75×10^{-5} seconds (Table 15). The average baseline TOF value using the Direct method is 3.753×10^{-5} seconds. The TOF values at Positions 3-1 to 3-4 and 3-8 to 3-12 are between 4.60×10^{-5} and 4.75×10^{-5} seconds, indicating regions with minimal damage where the sample thickness remains close to 10 cm. At Position 3-5, the TOF drops sharply to 1.91×10^{-5} seconds, indicating a 6 cm thickness reduction. The TOF values at Positions 3-6 and 3-7, directly placed over 4 cm and 2 cm damage, are 2.60×10^{-5} seconds and 3.53×10^{-5} seconds, respectively. As with the Low W/C ratio sample, the less pronounced TOF reductions for moderate damage are due to the smaller reduction in thickness and the longer wave path caused by the greater remaining thickness.

The variability in TOF values across positions reflects the porous and inconsistent microstructure of the High W/C ratio sample, characterized by voids, micro-cracks, and weaker aggregate bonding. The contour plot for the High W/C ratio sample shows an irregular distribution of TOF values, with noticeable variations across the damaged regions.

In general, greater results (higher TOF values) were obtained for the Low W/C ratio sample, reflecting its denser structure. However, at the locations of the induced damage (Positions 3-5, 3-6, and 3-7), the opposite trend was observed, with the High W/C ratio sample showing lower TOF values. This may be due to the influence of compaction issues in the Low W/C ratio sample, where the effect of these issues became more pronounced as the wave travel path shortened due to the induced damage levels. The reduced travel path amplified the impact of these compaction flaws, resulting in lower TOF values compared to the High W/C ratio sample at these specific positions.

The Pulse-Echo Method detects severe damage effectively in both mix designs, with clear TOF reductions at locations corresponding to 6 cm thickness reductions (Position 3-5). Moderate damage at 4 cm (Position 3-6) and 2 cm (Position 3-7) is also captured, though the TOF reductions are less pronounced. This is logical because smaller damage results in less thickness reduction, increasing the wave path length, which subsequently leads to higher TOF values. The ability to localize damage in these positions demonstrates the method's potential for identifying significant internal defects within concrete samples.

Position	Transducer placement	TOF Low W/C ratio	TOF High W/C ratio
3-1		4.58e-5 seconds	4.75e-5 seconds
3-2		4.63e-5 seconds	4.60e-5 seconds
3-3		4.56e-5 seconds	4.66e-5 seconds
3-4		4.51e-5 seconds	4.66e-5 seconds
3-5		2.45e-5 seconds	1.91e-5 seconds

<p>3-6</p>		<p>2.88e-5 seconds</p>	<p>2.60e-5 seconds</p>
<p>3-7</p>		<p>3.57e-5 seconds</p>	<p>3.53e-5 seconds</p>
<p>3-8</p>		<p>4.55e-5 seconds</p>	<p>4.64e-5 seconds</p>
<p>3-9</p>		<p>4.56e-5 seconds</p>	<p>4.74e-5 seconds</p>
<p>3-10</p>		<p>4.09e-5 seconds</p>	<p>4.61e-5 seconds</p>
<p>3-11</p>		<p>4.53e-5 seconds</p>	<p>4.61e-5 seconds</p>

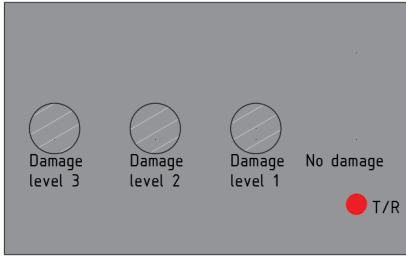
3-12		4.53e-5 seconds	4.72e-5 seconds
------	-----------------------------------------------------------------------------------	--------------------	--------------------

Table 15: Transducer Positioning and UPV Measurements for the Pulse-Echo Method (Low and High W/C ratios)

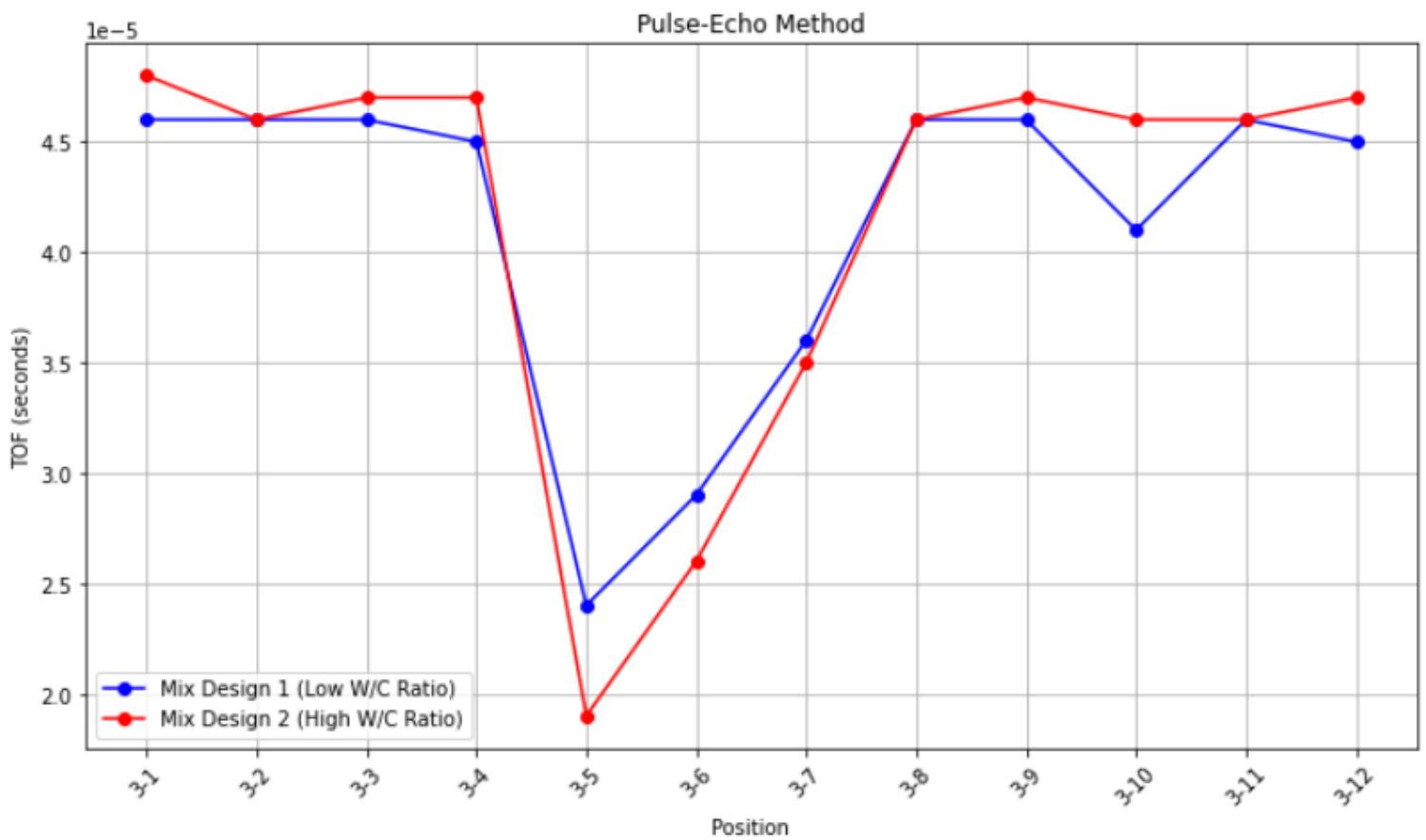


Figure 64: TOF Comparison for Low and High W/C ratio Samples Using the Pulse-Echo Method

The results from Indirect Method 1, Indirect Method 2, and the Pulse-Echo Method for Ultrasonic Pulse Velocity (UPV) testing provide a comprehensive assessment of the Low and High Water-Cement (W/C) ratio concrete samples. Each method offers unique insights into the internal structure, consistency, and defect distribution of these samples.

Indirect Method 1 demonstrated that the Low W/C ratio sample consistently exhibited higher UPV values, indicating a denser and more uniform microstructure compared to the High W/C ratio sample, which showed more variability and lower UPV values due to

its porous and inconsistent structure. However, this method was limited in detecting pre-intended damage, especially in denser materials.

Indirect Method 2 offered a more focused analysis by positioning transducers around specific damage zones. While the method highlighted structural differences between the Low and High W/C ratio samples, no clear UPV signals directly correlated to the induced damage. The dense microstructure of the Low W/C ratio sample masked subtle defects, while the High W/C ratio sample's variability made it difficult to distinguish induced damage from inherent imperfections.

The Pulse-Echo Method measured Time of Flight (TOF) values and successfully identified severe damage where thickness reductions were significant. When compared with the average baseline TOF values of 3.472×10^{-5} seconds (Low W/C ratio) and 3.753×10^{-5} seconds (High W/C ratio) for an 8 cm thick undamaged sample, the Pulse-Echo measurements revealed clear TOF reductions corresponding to damage zones. The Low W/C ratio sample's TOF values remained relatively consistent, reflecting its dense structure, while the High W/C ratio sample exhibited greater variability due to its more porous nature. The Pulse-Echo Method effectively localized severe damage but showed less sensitivity to moderate damage.

5 Conclusions and Recommendations

In this chapter, the key findings of the research are summarized, highlighting the effectiveness of the Ultrasonic Pulse Velocity (UPV) methods in detecting and measuring surface damage in concrete structures. The limitations of the techniques are discussed, and recommendations are made for future studies and practical improvements in concrete testing methods.

5.1 Conclusion

This study evaluated the effectiveness of Ultrasonic Pulse Velocity (UPV) methods in detecting and measuring near-surface damage in concrete structures. To achieve this, small concrete samples were utilized, which were produced with pre-intended damage designed to simulate delamination in an exaggerated way. This approach allowed to assess whether UPV had the potential to detect such damage effectively. Each sample had four damage levels: No Damage, Damage Level 1, Damage Level 2, and Damage Level 3, representing damage depths of 0 cm, 2 cm, 4 cm, and 6 cm, respectively. Three UPV techniques were assessed: Indirect Method 1, Indirect Method 2, and the Pulse-Echo Method. Complementary mechanical tests, including compressive and flexural strength assessments, provided additional insights into the concrete's structural properties. The evaluation was conducted on concrete samples with different water-cement (W/C) ratios under varying conditions, providing a thorough evaluation of how each method performed under different conditions. It is important to note that the conclusions drawn from this study are based solely on the controlled experiments performed on these small-scale concrete samples. These findings should not be directly extrapolated to real-world scenarios, particularly in assessing actual structural damage, as real-world conditions introduce complexities not accounted for in this experimental setup.

Indirect Methods 1 and 2 provided valuable insights for surface-level assessments, showing sensitivity to variations in the concrete surface, which probably relate to material uniformity. However, these methods struggled to detect the pre-intended damage levels, likely due to sensor configuration, material consistency, and sample heterogeneity. Refining sensor placement, improving sensor quality, and optimizing sensor angles are necessary to enhance wave propagation and improve detection accuracy.

In contrast, the Pulse-Echo Method showed significant advantages in assessing damage depth and internal structure in this study. Along the surface of the sample, multiple measurements were performed using the Pulse-Echo technique, during which the Time-of-Flight (TOF) was measured. These TOF measurements and the resulting contour plots, produced with this data, offered detailed insights into damage zones and thickness variations. By approximating local thickness, the Pulse-Echo Method effectively estimated near-surface damage, providing a clearer picture of internal structural integrity. However, the accuracy was limited by the sparse grid of measurement points, restricting the comprehensive mapping of damage shape and distribution. Increasing the measurement density and refining TOF interpretation algorithms and sensor sensitivity would enhance this method's reliability.

Mechanical testing results supported the UPV findings, highlighting differences between Low and High W/C ratio mixes. Although clear signs of compaction issues were present, the Low W/C ratio samples generally exhibited higher UPV values, indicating a denser microstructure. In areas with induced damage, these samples showed reduced UPV speeds in the Pulse-Echo Method due to flaws affecting wave propagation. In contrast, High W/C ratio samples displayed more uniform compaction, resulting in higher compressive strength and consistent UPV measurements. These findings show the complex interplay between material consistency, mechanical performance, and UPV results.

Consistency in sample preparation is critical for reliable UPV measurements. Issues encountered during production, such as variability in material consistency, air voids, and curing inconsistencies, significantly influenced UPV accuracy; while these issues were not due to a lack of standards, they highlight the importance of maintaining quality control throughout the production process. The study's findings also suggest that combining mechanical testing with UPV methods provides a more comprehensive understanding of concrete integrity.

However, it is equally important to acknowledge that absolute consistency is rarely achievable in practical settings. Even with rigorous procedures, small discrepancies in material properties or environmental conditions can introduce unavoidable variability, this shows the importance of quality checks, documentation, and cross-validation methods to ensure that such variations do not compromise the reliability of UPV measurements.

The insights gained from this study have important implications for structural health monitoring and maintenance. The Pulse-Echo Method, showed within the dimensions of this study that it might be a valuable tool in detecting damage. By identifying near-surface damage and internal flaws early, these techniques, when further investigated, can enhance infrastructure safety, reliability, and maintenance efficiency by performing quality controls either during initial construction or throughout the service life of structures. Additionally, their potential to detect defects such as delamination and other flaws allows for timely intervention, potentially reducing long-term costs.

Despite promising results, the study also showed some limitations. The sparse grid of measurement points in the Pulse-Echo Method restricted detailed damage mapping, and laboratory-prepared samples as told earlier may not fully represent real-world conditions. The experimental setup should be matched to the dimensions of the structure being tested, including sensor frequency and configuration. Since the methods are not generically applicable, adjustments are necessary to optimize performance based on specific use cases. These factors should be considered when applying the findings in practice.

In summary, UPV methods in general offer significant potential for assessing near-surface damage in concrete structures. The Pulse-Echo Method excelled at measuring damage thickness and identifying internal flaws, while the Indirect Methods did not. Addressing limitations in sensor configuration, measurement density, and data interpretation might help to enhance the accuracy and reliability of these methods. By refining UPV techniques, researchers and engineers can develop more effective tools for monitoring and maintaining concrete structures, contributing to safer and more durable environments.

5.2 Recommendations

Based on the findings of this research, several recommendations can be made for both future studies and practical applications in concrete design and testing:

1. Further Investigations into Compaction and Curing Techniques

The compaction problems this study found highlight how crucial it is to perform comprehensive quality checks on materials and equipment prior to starting any tests or investigations. Such checks can help identify and address potential sources of incomplete or inconsistent consolidation, reducing the likelihood of voids that compromise concrete performance. The larger and more frequent pores observed in Mix Design 1 (low W/C ratio) highlight the importance of standardized compaction and curing practices to control porosity. By ensuring that procedures are strictly followed and verified, future studies can more accurately assess the overall impact of different production parameters on mechanical performance and optimize concrete performance across a range of mix designs.

2. Improvement of Sensor Suitability for Indirect Methods

Indirect Method 1 and Indirect Method 2 were less effective in detecting deeper damage or damage on the opposite surface, suggesting that the sensors or configurations employed may not be optimal. Future investigations should test different types of sensor frequencies and designs beforehand to determine which combination yields the most accurate results, then base the final testing configuration on the outcomes of these preliminary evaluations. Refining data processing algorithms to reduce noise and improve interpretation could also help broaden the practical utility of indirect methods in diverse field conditions.

3. Exploration of Multiple Frequencies

In this study, a consistent frequency of 500 kHz was used due to its suitability for the 10-cm sample dimensions and availability of sensors. However, future studies should explore the effects of using multiple frequencies on wave penetration and resolution. A parametric study comparing transducers at 250 kHz, 500 kHz, and 1 MHz could provide insights into the optimal frequency for detecting various damage types and depths. This approach would help determine the most effective configurations for different applications.

4. Improvement of Measurement Density for Near-Surface or Inner Damage Mapping

The Pulse Echo Method proved capable of detecting near-surface or inner damage and measuring its thickness through point measurements. However, the relatively sparse distribution of measurement points limited the ability to fully map the extent and shape

of this damage. Future research should use denser grid patterns or scanning methods to capture detailed damage patterns, as well as integrate automated or semi automated data collection techniques for improved efficiency. A more comprehensive mapping can provide greater insight into damage progression and potential failure mechanisms.

5. Refining Non-destructive Testing (NDT) Approaches

The Pulse Echo Method demonstrated its effectiveness for identifying internal defects, yet improvements can still be made to enhance both accuracy and range. Future research should focus on developing more advanced algorithms for time of flight (TOF) data interpretation, increasing sensor sensitivity to detect defects at greater depths, and addressing wave reflection and signal attenuation challenges, particularly in large or complex structures. Exploring hybrid techniques such as combining ultrasound with tomography or ground penetrating radar could yield more comprehensive assessments of subsurface damage. These refinements would facilitate broader, more reliable applications in both laboratory and field contexts.

6. Field Applications of NDT Methods

The scope of this research was restricted by the laboratory samples used, which may not fully represent real scale structures. Consequently, some of the techniques and findings may need modifications, such as adjusting sensor layouts, data processing algorithms, or testing parameters, when applied to larger, more complex structures. To validate the reliability of the NDT techniques under realistic conditions, field testing in different climates and on larger scale structures is essential. Environmental factors such as temperature, humidity, and structural dimensions can significantly affect test outcomes. Field trials would help pinpoint the practical limitations of each method, inform procedure modifications, and ultimately support more robust and reliable applications in real-scale concrete structures.

7. Future Research and Simulation Studies

Future research could explore using a steel plate with a Teflon layer inserted and subsequently removed after the concrete hardens to simulate a crack, thereby assessing how different damage types affect signal propagation in UPV measurements. This method would simulate a different kind of subsurface damage and provide valuable data for refining NDT approaches.

Final Thought

In conclusion, the Pulse Echo Method proved to be the most reliable for detecting and measuring near-surface or inner damage. Although the other methods did not successfully detect the intended damage or produce the desired outcomes, they still have potential for further development. By upgrading sensor technology, improving data processing, and refining field testing procedures, these methods could become more accurate and broadly applicable. Ongoing research into better testing procedures, innovative production techniques, and advanced damage simulations will help us create more reliable, efficient, and comprehensive NDT solutions for both laboratory and full-scale scenarios.

Appendices

Appendix A.1: Python code for Indirect Method 1

```
import pandas as pd
import numpy as np
import matplotlib.pyplot as plt
from scipy.interpolate import griddata

# Load the data file
file_path = 'Indirect Method 1.txt'
with open(file_path) as file:
    lines = file.readlines()

# Process the file line by line to correct format issues
processed_lines = []
for line in lines:
    processed_line = line.replace(',', '.').replace(' ', '').strip()
    if processed_line:
        processed_lines.append(processed_line.split())

# Convert processed data to DataFrame
column_names = ['Position', 'Time_of_flight', 'Distance', 'X', 'Y']
data = pd.DataFrame(processed_lines[1:], columns=column_names)

# Convert columns to appropriate data types
data['Time_of_flight'] = data['Time_of_flight'].astype(float)
data['Distance'] = data['Distance'].astype(float)
data['X'] = data['X'].astype(int)
data['Y'] = data['Y'].astype(int)

# Calculate Ultrasonic Pulse Velocity (UPV)
data['UPV'] = data['Distance'] / data['Time_of_flight']

# Prepare data for contour plot
X = data['X']
Y = data['Y']
Z = data['UPV']

# Create grid values first
xi = np.linspace(0, 400, 100)
yi = np.linspace(0, 250, 100)
zi = griddata((X, Y), Z, (xi[None, :], yi[:, None]), method='cubic')

# Create contour plot
plt.figure(figsize=(10, 8))
contour = plt.contourf(xi, yi, zi, levels=15, cmap="coolwarm")
colorbar = plt.colorbar(contour)
colorbar.set_label('UPV (m/s)')

# Plot the data
plt.xlim(0, 400)
plt.ylim(0, 250)
plt.title('Contour plot of Ultrasonic Pulse Velocity')
plt.xlabel('X Coordinate')
plt.ylabel('Y Coordinate')
plt.show()
```

Appendix A.2: Python code for Indirect Method 2

```
import matplotlib.pyplot as plt
import pandas as pd

# File path
file_path = 'Indirect Method 2.txt'

# Reading the data
data = pd.read_csv(file_path, sep='\t')
data['average time of flight'] = data['average time of flight'].str.replace
data['Distance'] = data['Distance'].str.replace(',', '.').astype(float)

# Calculating UPV
data['UPV'] = data['Distance'] / data['average time of flight']

# Reversing the order of x-coordinates and UPV values to plot right to left
x_coordinates = data['X'][::-1]
upv_values = data['UPV'][::-1]

# Plotting the Line graph for UPV
plt.figure(figsize=(8, 6))
plt.plot(x_coordinates, upv_values, marker='o', linestyle='-', color='black')
plt.title('Indirect method 2 (Low W/C ratio)')
plt.xlabel('X Coordinate')
plt.ylabel('UPV (m/s)')
plt.grid(True)
plt.xlim(0, 400)
plt.show()
```

Appendix A.3: Python code for the Pulse-Echo Method

```
import pandas as pd
import numpy as np
import matplotlib.pyplot as plt
from scipy.interpolate import griddata

# Load the data file
file_path = 'Pulse-Echo method.txt'
with open(file_path) as file:
    lines = file.readlines()

# Process the file line by line to correct the format
processed_lines = []
for line in lines:
    processed_line = line.replace(',', '.').replace(' ', '').strip()
    if processed_line:
        processed_lines.append(processed_line.split())

# Convert processed data to DataFrame
column_names = ['Position', 'Time_of_flight', 'Distance', 'X', 'Y']
data = pd.DataFrame(processed_lines[1:], columns=column_names)

# Convert columns to appropriate data types
data['Time_of_flight'] = data['Time_of_flight'].astype(float)
data['Distance'] = data['Distance'].astype(float)
data['X'] = data['X'].astype(int)
data['Y'] = data['Y'].astype(int)

# Prepare data for contour plot
X = data['X']
Y = data['Y']
Z = data['Time_of_flight'] # Use Time_of_flight for the Z values

# Create grid values first
xi = np.linspace(0, 400, 100)
yi = np.linspace(0, 250, 100)
zi = griddata((X, Y), Z, (xi[None, :], yi[:, None]), method='cubic')

# Create contour plot
plt.figure(figsize=(10, 8))
contour = plt.contourf(xi, yi, zi, levels=15, cmap="coolwarm")
plt.colorbar(contour)

# Plot the data
plt.xlim(0, 400)
plt.ylim(0, 250)
plt.title('Contour plot of Time of Flight')
plt.xlabel('X Coordinate')
plt.ylabel('Y Coordinate')
plt.show()
```

Appendix A.4: Python code for the Pulse-Echo Method (Thickness)

```
import pandas as pd
import numpy as np
import matplotlib.pyplot as plt
from scipy.interpolate import griddata

# Load the data file
file_path = 'Pulse-Echo method (Thickness).txt'
with open(file_path) as file:
    lines = file.readlines()

# Process the file line by line to correct the format
processed_lines = []
for line in lines:
    processed_line = line.replace(',', '.').replace(' ', '').strip()
    if processed_line:
        processed_lines.append(processed_line.split())

# Convert processed data to DataFrame
column_names = ['Position', 'Time_of_flight', 'Distance', 'X', 'Y']
data = pd.DataFrame(processed_lines[1:], columns=column_names)

# Convert columns to appropriate data types
data['Time_of_flight'] = data['Time_of_flight'].astype(float)
data['Distance'] = data['Distance'].astype(float)
data['X'] = data['X'].astype(int)
data['Y'] = data['Y'].astype(int)

# Apply the formula to compute Local thickness by dividing by the Average Baseline TOF value
data['Thickness'] = (data['Time_of_flight'] / Average Baseline TOF) * 0.16 / 2

# Prepare data for contour plot
X = data['X']
Y = data['Y']
Z = data['Thickness'] # Use Thickness for the Z values (Local thickness of the sample)

# Create grid values first
xi = np.linspace(0, 400, 100)
yi = np.linspace(0, 250, 100)
zi = griddata(X, Y, Z, (xi[None, :], yi[:, None]), method='cubic')

# Create contour plot
plt.figure(figsize=(10, 8))
contour = plt.contourf(xi, yi, zi, levels=15, cmap="coolwarm")
plt.colorbar(contour)

# Add labels to each point
for i in range(len(X)):
    plt.text(X.iloc[i], Y.iloc[i], f'{Z.iloc[i]:.2f}',
             color='black', fontsize=10, ha='center', va='center',
             bbox=dict(facecolor='white', edgecolor='none', alpha=0.6))

# Plot the data
plt.xlim(0, 400)
plt.ylim(0, 250)
plt.title('Contour plot of the Local Thickness')
plt.xlabel('X Coordinate')
plt.ylabel('Y Coordinate')
```

Appendix A.5: Python code for Mechanical testing - Compression test

```
import matplotlib.pyplot as plt
import numpy as np

# Sample data: Compression test results for two mix designs
mix1_measurements = [64.25, 65.553, 62.532, 56.188, 59.982, 66.641]
mix2_measurements = [79.941, 66.519, 73.661, 74.201, 54.137, 55.326]

# Combine data into a List of Lists for boxplot
data = [mix1_measurements, mix2_measurements]

# Calculate mean values
means = [np.mean(mix1_measurements), np.mean(mix2_measurements)]

# Create boxplot
plt.figure(figsize=(10, 6))
box = plt.boxplot(data, patch_artist=True, labels=['Mix Design 1', 'Mix Design 2'], showmeans=True)

# Add Labels and title
plt.xlabel('Mix Designs', labelpad=20)
plt.ylabel('Compressive Strength (MPa)')
plt.title('Compression Test Results of Concrete Samples')

# Customize boxplot appearance
colors = ['lightblue', 'lightgreen']
for patch, color in zip(box['boxes'], colors):
    patch.set_facecolor(color)

# Customize mean point appearance
for mean, line in zip(means, box['means']):
    line.set_marker('o')
    line.set_markerfacecolor('red')
    line.set_markeredgecolor('red')

# Annotate mean values
for i, mean in enumerate(means):
    plt.text(i + 1, mean + 0.5, f'{mean:.2f}', horizontalalignment='center', color='red')

# Customize other parts of the boxplot
plt.setp(box['medians'], color='blue')
plt.setp(box['whiskers'], linestyle='-', color='black')
plt.setp(box['caps'], color='black')
plt.grid(axis='y', linestyle='--', alpha=0.7)
plt.tight_layout()
plt.show()
```

Appendix A.6: Python code for Mechanical testing – Flexural bending test

```
import matplotlib.pyplot as plt
import numpy as np

# Sample data: Three point bending test results for two mix designs
mix1_measurements = [11.8, 9.2, 11.51]
mix2_measurements = [10.96, 11.47, 8.71]

# Combine data into a list of lists for boxplot
data = [mix1_measurements, mix2_measurements]

# Calculate mean values
means = [np.mean(mix1_measurements), np.mean(mix2_measurements)]

# Create boxplot
plt.figure(figsize=(10, 6))
box = plt.boxplot(data, patch_artist=True, labels=['Mix Design 1', 'Mix Design 2'], showmeans=True)

# Add Labels and title
plt.xlabel('Mix Designs', labelpad=20)
plt.ylabel('Flexural Strength (MPa)')
plt.title('Three point bending Test Results of Concrete Samples')

# Customize boxplot appearance
colors = ['lightblue', 'lightgreen']
for patch, color in zip(box['boxes'], colors):
    patch.set_facecolor(color)

# Customize mean point appearance
for mean, line in zip(means, box['means']):
    line.set_marker('o')
    line.set_markerfacecolor('red')
    line.set_marteredgcolor('red')

# Annotate mean values
for i, mean in enumerate(means):
    plt.text(i + 1, mean + 0.5, f'{mean:.2f}', horizontalalignment='center', color='red')

# Customize other parts of the boxplot
plt.setp(box['medians'], color='blue')
plt.setp(box['whiskers'], linestyle='-', color='black')
plt.setp(box['caps'], color='black')
plt.grid(axis='y', linestyle='--', alpha=0.7)
plt.tight_layout()
plt.show()
```

Appendix A.7: Python code for the comparison of Indirect Method 1

```
import matplotlib.pyplot as plt
import pandas as pd

# Create a DataFrame from the provided data
data = {'Position'      : ['1-1', '1-2', '1-3', '1-4', '1-5', '1-6', '1-7', '1-8', '1-9', '1-10',
                          '1-11', '1-12', '1-13', '1-14', '1-15', '1-16', '1-17'],
        'UPV Low W/C Ratio' : [4603.1, 4895.6, 4767, 4664.2, 4799.5, 4750.8, 4891.30, 4598, 4757.6,
                              4668.2, 4715.3, 4365.5, 4355.4, 4433.9, 4387.3, 4341.5, 4413],
        'UPV High W/C Ratio': [4453.7, 4297.2, 4188.4, 4284.1, 4398, 4408.3, 4290.6, 4304.3, 4274.2,
                              4123.4, 4278.8, 4209.9, 4278.4, 4295.5, 4221.8, 4334, 4237.3]}

data = pd.DataFrame(data)

# Plot UPV for Low and High W/C ratios
plt.figure(figsize=(10, 6))

# Plot data for Low W/C ratio
plt.plot(data['Position'], data['UPV Low W/C Ratio'], marker='o', linestyle='-', color='blue',
         label='Mix Design 1 (Low W/C Ratio)')

# Plot data for High W/C ratio
plt.plot(data['Position'], data['UPV High W/C Ratio'], marker='o', linestyle='-', color='red',
         label='Mix Design 2 (High W/C Ratio)')

# Adding titles and labels
plt.title('Indirect Method 1')
plt.xlabel('Position')
plt.ylabel('UPV (m/s)')
plt.grid(True)
plt.xticks(rotation=45)
plt.legend()

# Show the plot
plt.tight_layout()
plt.show()
```

Appendix A.8: Python code for the comparison of Indirect Method 2

```
import matplotlib.pyplot as plt
import pandas as pd

# Create a DataFrame from the provided data
data = {'Position'      : ['2-1', '2-2', '2-3', '2-4'],
        'UPV Low W/C Ratio' : [4767, 4836.6, 4929.9, 4603.1],
        'UPV High W/C Ratio': [4188.4, 4425.7, 4500, 4453.7]}

data = pd.DataFrame(data)

# Plot UPV for Low and High W/C ratios
plt.figure(figsize=(10, 6))

# Plot data for Low W/C ratio
plt.plot(data['Position'], data['UPV Low W/C Ratio'], marker='o', linestyle='-', color='blue',
         label='Mix Design 1 (Low W/C Ratio)')

# Plot data for High W/C ratio
plt.plot(data['Position'], data['UPV High W/C Ratio'], marker='o', linestyle='-', color='red',
         label='Mix Design 2 (High W/C Ratio)')

# Adding titles and labels
plt.title('Indirect Method 2')
plt.xlabel('Position')
plt.ylabel('UPV (m/s)')
plt.grid(True)
plt.xticks(rotation=45)
plt.legend()

# Show the plot
plt.tight_layout()
plt.show()
```

Appendix A.9: Python code for the comparison of the Pulse-Echo Method

```
import matplotlib.pyplot as plt
import pandas as pd

# Create a DataFrame from the provided data
data = {'Position'      : ['3-1', '3-2', '3-3', '3-4', '3-5', '3-6', '3-7',
                          '3-8', '3-9', '3-10', '3-11', '3-12'],
        'TOF Low W/C Ratio (s)' : [4.6e-5, 4.6e-5, 4.6e-5, 4.5e-5, 2.4e-5, 2.9e-5,
                                    3.6e-5, 4.6e-5, 4.6e-5, 4.1e-5, 4.6e-5, 4.5e-5],
        'TOF High W/C Ratio (s)': [4.8e-5, 4.6e-5, 4.7e-5, 4.7e-5, 1.9e-5, 2.6e-5,
                                    3.5e-5, 4.6e-5, 4.7e-5, 4.6e-5, 4.6e-5, 4.7e-5]}

data = pd.DataFrame(data)

# Plot UPV for Low and High W/C ratios
plt.figure(figsize=(10, 6))

# Plot data for Low W/C ratio
plt.plot(data['Position'], data['TOF Low W/C Ratio (s)'], marker='o', linestyle='-', color='blue',
         label='Mix Design 1 (Low W/C Ratio)')

# Plot data for High W/C ratio
plt.plot(data['Position'], data['TOF High W/C Ratio (s)'], marker='o', linestyle='-', color='red',
         label='Mix Design 2 (High W/C Ratio)')

# Adding titles and labels
plt.title('Pulse-Echo Method')
plt.xlabel('Position')
plt.ylabel('TOF (seconds)')
plt.grid(True)
plt.xticks(rotation=45)
plt.legend()

# Show the plot
plt.tight_layout()
plt.show()
```

Bibliography

- [1] C. R. Gagg, "Cement and concrete as an engineering material: An historic appraisal and case study analysis," *Elsevier*, 2014.
- [2] D. A. S. B. V. Anitha Selvasofia S.D, "Investigation of waste marble powder in the development of sustainable," *Elsevier*, 2020.
- [3] M. M. ., M. P. Giada Frappa, "Destructive and non-destructive tests on columns and cube specimens made with the same concrete mix," *Elsevier*, 2022.
- [4] UNI EN 12504-2:2021, "Testing concrete in structures - Part 2: Non-destructive - Determination of rebound number.," 2021.
- [5] UNI EN 12504-4:2021, "Testing concrete in structures - Part 4: Determination of ultrasonic pulse velocity," 2021.
- [6] RILEM NDT 4, "Recommendation for in Situ Concrete Strength Determination by Combined Non-destructive Methods," E&FN Spon, U.K., London, 1993.
- [7] M. S. S. Ashok Kumar, "Detection of Concrete Damage Using Ultrasonic Pulse Velocity Method," Department of Civil Engineering, IIT Madras, Chennai, 2006.
- [8] S. C. G. R. Luigi Biolzi, "Evaluating residual properties of thermally damaged concrete," *Elsevier*, 12 September 2008.
- [9] G. K. G. C. M. Y. N. G. J. N. Euichul Hwang, "Evaluation of concrete degradation depending on heating conditions by ultrasonic pulse velocity," *Elsevier*, 21 March 2018.
- [10] M. N. K. B. K. A. B. P. Kuruppu, "Study on Honeycombs in Structural Concrete Elements," in *2022 Moratuwa Engineering Research Conference (MERCon)*, Moratuwa, Sri Lanka, 2022.
- [11] S. K. F. Dethof, "Design of Concrete Mock-Ups with Complex Defect Scenarios Using Numerical Simulations," *Journal of Nondestructive Evaluation*, 6 May 2024.
- [12] Z. Li, "A study on ultrasonic echo tomography for non-destructive evaluation of hardened cementitious concrete," *Journal of Building Pathology and Rehabilitation*, 3 April 2020.
- [13] M. N. S. P. J. van Leeuwen, "Study of Pulsed Phase Thermography for the Detection of Honeycombing Defects in Concrete Structures," *e-Journal of Nondestructive Testing Vol. 16(5) - Online Workshop: NDT&E of Composite Materials*, May 2011.
- [14] P. O. A. D.-H. L. L. B. R. O.E. Babalola, "A review of residual strength properties of normal and high strength concrete exposed to elevated temperatures: Impact of materials modification on behaviour of concrete composite," 2021.

- [15] d. G. Ye, *CIE5110 - Concrete Science and Technology*, Delft: TU Delft, 2020.
- [16] T. A. J.C. Agunwamba, "A COMPARATIVE ANALYSIS OF THE REBOUND HAMMER AND ULTRASONIC PULSE VELOCITY IN TESTING CONCRETE," Department of Civil Engineering, University of Nigeria, Nsukka, 2012.
- [17] G. L. Golewski, "The Phenomenon of Cracking in Cement Concretes and Reinforced Concrete Structures: The Mechanism of Cracks Formation, Causes of Their Initiation, Types and Places of Occurrence, and Methods of Detection - A Review," Lublin University of Technology, Lublin, Poland, 2023.
- [18] H. W. M. Z. Y. L. a. C. C. Rui Wang, "The classification and Mechanism of Microcrack Homogenization Research in Cement Concrete Based on X-ray CT," *Buildings*, 14 July 2022.
- [19] T. C. Powers, "A Working Hypothesis for Further Studies of Frost Resistance of Concrete," *Journal of the American Concrete Institute*, 1945.
- [20] A. C666/C666M, "Standard Test Method for Resistance of Concrete to Rapid Freezing and Thawing".
- [21] Y. M. M. A. B. B. Fournier, "Understanding Alkali-Aggregate Reaction and its Mitigation in Concrete Structures," *Canadian Journal of Civil Engineering*, 2000.
- [22] B. K. & W. C. P. S. H. Kosmatka, "Design and Control of Concrete Mixtures," Portland Cement Association, 2002.
- [23] T. C. Powers, *The air Requirement of Frost-Resistant Concrete*, Portland Cement Association.
- [24] V. M. a. N. Carino, *Handbook on Nondestructive Testing of Concrete*, Florida: CRC Press, 2004.
- [25] .. Z. Z. Y. K. Zhang, "Experimental Study on Mechanical Properties and Pore Structure Deterioration of Concrete under Freeze–Thaw Cycles," *Materials* 14, no. 21: 6568, 2021.
- [26] J. L. Y. Lin, "Ultrasonic Testing for Concrete Delamination Detection," *NDT&E International*, 2005.
- [27] H. W. M. Schickert, "Applications of Ultrasonic Testing in Concrete Structures," *NDT&E International*, 2003.
- [28] THE CONSTRUCTOR, "Alkali Aggregate Reaction in Concrete - Types, Causes, and Effects," [Online]. Available: <https://theconstructor.org/concrete/alkali-aggregate-reaction-concrete/67/>.
- [29] A. C1293, "Standard Test Method for Determination of Length Change Due to Alkali-Silica Reaction."
- [30] A. 201.2R, "Guide to Durable Concrete".

- [31] Federal Highway Administration (FHWA), “Reports on infrastructure maintenance and repair costs related to freeze-thaw damage”.
- [32] V. H. M. Q. H. T. K.-Y. L. J.-I. L. C. K. J. Huh, “Detectability of Delamination in Concrete Structure Using Active Infrared Thermography in Terms of Signal-to-Noise Ratio,” *Applied Sciences* 8, no. 10: 1986, 2018.
- [33] K. K. M. Schneider, “Chemical Reactions and their Impacts on Concrete Durability,” *Cement and Concrete Research*, 2001.
- [34] Scandinavian Road Association, “Effects of Freeze-Thaw Cycles on Highway Pavements in Northern Europe,” 2008.
- [35] C. M. o. Transportation, “Survey of Parking Structures: Delamination Prevalence and Costs,” 2020.
- [36] European Concrete Repair Standards Committee, “Best Practices for Mitigating Delamination in Commercial Structures,” 2015.
- [37] A. Neville, *Properties of Concrete*, Pearson Education Limited, 2011.
- [38] “Honeycombing in Concrete: Causes, Types and How to Fix it,” [Online]. Available: <https://www.ultratechcement.com/for-homebuilders/home-building-explained-single/descriptive-articles/honeycombing-in-concrete>.
- [39] A. C. 309, *Guide for Consolidation of Concrete (ACI 309R-05)*, American Concrete Institute.
- [40] P. M. P.K. Mehta, *Concrete: Microstructure, properties, and Materials*, McGraw-Hill Education, 2014.
- [41] M. Shetty, *Concrete Technology: Theory and Practice*, S. Chand & Company Ltd., 2005.
- [42] M. L. Gambhir, *Concrete Technology: Theory and Practice (5th ed.)*, McGraw-Hill Education, 2013.
- [43] ALMISNED READYMIX, “CAUSES OF CONCRETE HONEYCOMBING,” [Online]. Available: <https://almisnedrm.com/blog/almisned-readymix-5/causes-of-concrete-honeycombing-13>.
- [44] J. Y. a. D. D. S. Mindess, *Concrete*, 2003.
- [45] A. C. 222, “Protection of Metals in Concrete Against Corrosion,” American Concrete Institute.
- [46] A. International, “ASTM - C 597, Standard Test Method for Pulse Velocity Through Concrete,” 2016.

- [47] H.-W. R. G. D. C. Maierhofer, "Non-Destructive Evaluation of Reinforced Concrete Structures: Deterioration Processes and Standard Test Methods," Woodhead Publishing, 2010.
- [48] W. B. S. M. Sansalone, *Impact-Echo: Nondestructive Evaluation of Concrete and Masonry*, Bulbrier Press, 1997.
- [49] D. J. Daniels, *Ground Penetrating Radar*, The Institution of Engineering and Technology, 2004.
- [50] S. M. a. M. G. J. Bungey, *Testing of Concrete in Structures*, Abingdon: Taylor & Francis, 2006.
- [51] A. R. M. G. P. N N Kencanawati, "Study on robustness of rebound hammer and ultrasonic pulse velocity measurement in several concrete damage levels," *IOP Conference Series: Earth and Environmental Science*, 2021.
- [52] E. Whitehurst, *Evaluation of Concrete Properties from Sonic Tests*, Detroit: American Concrete Institute, 1966.
- [53] N. H. R.-S. M. M. A. K. H. S. H. S. Mahdi Shariati, "Assessing the strength of reinforced concrete structures through Ultrasonic Pulse Velocity and Schmidt Rebound Hammer tests," Department of Civil Engineering, University of Malaya, Kuala Lumpur, Malaysia, 2010.
- [54] E. G. G. Bradfield, "Determining the Thickness of Concrete Pavements by Mechanical Waves: Directed Beam Method," *Magazine of Concrete Research V. 16, No. 46*, pp. 49-53, March 1964.
- [55] S. D. Howkins, "Measurement of Pavement Thickness by Rapid and Nondestructive Methods," NCHRP Report 52, Washington, D.C., 1968.
- [56] H. Mailer, "Pavement Thickness Measurement Using Ultrasonic Techniques," pp. 20-28, 1972.
- [57] H. T. J. T. A. M. Alexander, "Ultrasonic Pich-Catch and Pulse-Echo Measurements in Concrete," *Nondestructive Testing of Concrete, H. S. Lew*, pp. 21-40, March 1989.
- [58] American Concrete Institute, "Nondestructive Test Methods for Evaluation of Concrete in Structures".
- [59] W. Hillger, "Imaging of Defects in Concrete by Ultrasonic Pulse-Echo Technique," *Engineering Technics press*, pp. 59-65, 1 July 1993.
- [60] BS EN 12504-4, "Testing concrete - Part 4: Determination of ultrasonic pulse velocity," European Comittee for Standardization, Brussels, 2004.
- [61] F. C. E. F. F. F. O. P. Daniel Melo Zárata, "Strength of Concrete through Ultrasonic Pulse Velocity and Uniaxial Compressive Strength," *International Journal of Technology*, pp. 103-114, September 2021.

- [62] R. O. R. E. N. Ramón Mata, "Correlation between compressive strength of concrete and ultrasonic pulse: A case of study and a new correlation method," *Elsevier*, 10 March 2023.
- [63] Z. M. R. A. Rasoul, "Correlation between the Compressive Strength of Concrete and Ultrasonic Pulse Velocity; Investigation and Interpretation," *Journal of Kerbala University*, August 2018.
- [64] S. K. V. Ashutosh Chouhan, "Condition Evaluation of Concrete Through Ultrasonic Pulse Velocity," 2023.
- [65] A. D. D. G. A. D. V. H. G. Karaiskos, "Monitoring of concrete structures using the ultrasonic pulse velocity method," *Smart MAterials and Structures*, 15 October 2015.
- [66] A. P. B. G. P. R. François Saint-Pierre, "Concrete Quality Designation based on Ultrasonic Pulse Velocity," *Elsevier*, 6 September 2016.
- [67] H. C. K. M. Izabela Hager, "Damage Assessment Of Concrete Subjected To High Temperature By Means of The Ultrasonic Pulse Velocity - UPV Method," 2013.
- [68] S. M. D. W. A. W. A. S. Dermawan, "Development Of Concrete Damage Classification in Beam-Column Joint based on Ultrasonic Pulse Velocity," IOP Conference Series: Materials Science and Engineering, 2022.
- [69] Y. C. J. L. Y. K. Jeongnam Kim, "Defect Detection and Characterization in Concrete Based on FEM and Ultrasonic Techniques," *Materials*, 17 November 2022.
- [70] M. V. André Valente Monteiro, "Effect of elevated temperatures on the residual durability related performance of concrete," *Materials and Structures*, 26 November 2021.
- [71] Z. Guo, *Principles of Reinforced Concrete*, Oxford, Waltham: Elsevier Inc., 2014.
- [72] C. L. Luoshu Gong, "Durability, Protection and Reparation of Concrete," Construction Industry Press of China, Beijing, 1990.
- [73] K.-M. L. J.-W. B. a. S.-J. K. Yun-Yong Kim, "Effect of W/C Ratio on Durability and Porosity in Cement Mortar with Constant Cement Amount," 15 April 2014.
- [74] F. M. M. S. N. a. H. M. S. Widodo, "Correlation of Ultrasonic Pulse Velocity with Porosity and Compressive Strength of Mortar with Limestone for Building Quality Assessment," *U Karst*, pp. 190-202, 15 November 2022.
- [75] National Standard of People's Republic of China,, "Standard for test method of mechanical properties on ordinary concrete GB/T 50081-2002," Construction Industry Press of China, Beijing, 2003.
- [76] G. P. C. B. P. Hughes, "The complete Stress-Strain Curve for Curve for Concrete in Direct Tension," *Rilem Bulletin*, Paris, 1966.

- [77] X. Q. Z. Z. H. Guo, "Investigation of Complete Stress-Deformation Curves for Concrete in Tension," *ACI Materials Journal*, pp. 278-285, 1987.
- [78] A. C. 318, "Building Code Requirement for Structural Concrete (ACI 318-95) and Comment (ACI 318R-95)," American Concrete Institute, 1995.
- [79] Z. Teng, *Basic Member of Reinforced Concrete*, Beijing: Tsinghua University Press, 1987.
- [80] C. E.-I. d. Beton, NO. 213/214 CEB-FIP Model Code 1990 (Concrete Structures), Lausanne, 1993.
- [81] X. Z. Zhenhai Guo, "Experimental investigation on complete stress-strain curve of concrete under monotonically loading," *Symposium No. 3 A seismic Behaviors of Reinforced Concrete Structures*, pp. 1-18, 1981.
- [82] Z. T. Chuanzhi Wang, *Theory of Reinforced Concrete Structure*, Beijing: Construction Industry Press of China, 1985.
- [83] Z. G. Qi Zhang, "Experimental research on shear strength and deformation of concrete," *Journal of Building Structures*, pp. 17-24, 1992.
- [84] C. B. S. D. A. G. D.-D. B.-N. V. V. Bogdan Bolborea, "Concrete Compressive Strength by Means of Ultrasonic Pulse Velocity and Moduli of Elasticity," *Materials*, 19 November 2021.
- [85] M. C. A. A. Narmane Fodil, "The influence of steel reinforcement on ultrasonic pulse velocity measurements in concrete of different strength ranges," *Materials Science and Engineering*, 2019.
- [86] C.-P. L. T. Y. Yiching Lin, "Prediction of ultrasonic pulse velocity (UPV) in concrete," *ACI Materials Journal*, pp. 21-28, January 2003.
- [87] R. L. N. O. C. C. E. P. E. P. R. A. M.-J. Sandro E. S. Mendes, "Mixture Design of Concrete Using Ultrasonic Pulse Velocity," *International Journal of Civil Engineering*, pp. 113-122, 10 October 2019.
- [88] I. M. Fayez Moutassem, "Mathematical model for predicting the ultrasonic pulse velocity of concrete," *Cogent Engineering*, April 2023.
- [89] V. R.-C. M. S. F. F. V. O.-L. Ana B. Espinosa, "Utility of Ultrasonic Pulse Velocity for Estimating the Overall Mechanical Behavior of Recycled Aggregate Self-Compacting Concrete," in *Applied sciences*, 2023.
- [90] C. Sansalone, 1991.
- [91] Carino, 1994.
- [92] A. D4788, "Standard Test Method for Detecting Delaminations in Bridge Decks Using Infrared Thermography," 2022.

- [93] Schlessinger, 1995.
- [94] T. Jayakumar, "NDT Techniques: Acoustic Emission," *Elsevier*, pp. 6001-6004, 2001.
- [95] British Standard, "Methods of testing cement - Part 1: Determination of strength," 2002.
- [96] "Normensand.de," [Online]. Available: <https://www.normensand.de/en/products/cen-standard-sand-en-196-1/>.
- [97] L. F. C. J. A. C. a. L. C. P. d. S. F. Alexandre Lorenzi, "Investigation of the Potential for Evaluation of Concrete Flaws Using Nondestructive Testing Methods," *Hindawi*, 11 May 2014.
- [98] A. 224, "Causes, Evaluation, and Repair of Cracks in Concrete Structures," American Concrete Institute, 2001.
- [99] S. K. Ghosh, "Advanced Concrete Technology," CRC Press.
- [100] D. M. O. Dr. Henk jonkers, *CIE4100 - Materials and Ecological Engineering*, Delft: TU Delft, 2020.
- [101] I. F. R. JONES, "Recommendations for testing concrete by the ultrasonic pulse method," *Materiaux et constructions*, 1969.
- [102] M. R. K. Armin Ziari, "Investigation of direct tension cracking and leakage in RC elements," *Elsevier*, February 2009.
- [103] M. R. K. M. M. M. L. H. S. E. B. Alireza Ahmadi, "Investigation on repair of tension cracks in reinforced concrete panels," *Elsevier*, 15 October 2021.
- [104] G. L. B. A. Borosnyói, in *Models for flexural cracking in concrete: the state of the art*, Structural Concrete, 2005, pp. 53-62.
- [105] S. M. R. L. R. N. F. d. C. Adelino V. Lopes, in *Stiffness of reinforced concrete slabs subjected to torsion*, 2014, pp. 227-238.
- [106] G. L. Golewski, "A novel specific requirements for materials used in reinforced concrete composites subjected to dynamic loads," *Elsevier*, 1 September 2019.
- [107] T. G. C. R. G. Charan Behera, "Torsional Capacity of High Strength Concrete Beams Jacketed with Ferrocement U-Wraps," *Asian Journal of Civil Engineering*, pp. 411-422, 2008.
- [108] J. W. H. W. S. S. F. A. G. E. Mahmoud A. El-Mandouh, "Torsional Improvement of RC Beams Using Various Strengthening Systems," *Buildings*, 24 October 2022.
- [109] P. C. P. Z. P. Bazant, "Measurement of Mode III Fracture Energy of Concrete," *Elsevier*, pp. 1-8, 16 July 1987.

- [110] P. C. P. M. R. T. Z. P. Bazant, "Antiplane Shear Fracture Tests (Mode III)," *ACI Materials Journal*, pp. 12-19, 1990.
- [111] H. L. J. W. F. H. Z. W. Z. Y. Y. X. H. D. Zhiqiang Yang, "The microstructure evolution of ballastless track high-strength concrete exposed to compressive and flexural fatigue loads," *Elsevier*, January 2023.
- [112] H. N.-H. A. Vaziri, "The effect of crack surface interaction on the stress intensity factor in Mode III crack growth in round shafts," *Elsevier*, March 2005.
- [113] D. Q. A. C. Reardon, "Fracture surface interference effects in mode III," *Elsevier*, pp. 213-226, January 1995.
- [114] M. F. R. A. M. Francesco Moccia, "Spalling of concrete cover induced by reinforcement," *Elsevier*, 2021.
- [115] Z. B. a. M. Kaplan, "Concrete at High Temperatures: Material Properties and Mathematical Models," *Elsevier*, 2021.
- [116] M.-A. B. Benoit Fournier, "Alkali-aggregate reaction in concrete: a review of basic concepts and engineering implications," *Canadian Journal of Civil Engineering*, February 2011.
- [117] American Concrete Institute, "Guide to Concrete Floor and Slab Construction," 2015.
- [118] N. Hong, "Considerations of reinforcement rusting resulted by chlorate and durability during design," Tsinghua University, Beijing, 2002.
- [119] X. Q. Z. Z. H. Guo, "Investigation of Complete Stress-Deformation Curves for Concrete in Tension," pp. 278-285, 1987.
- [120] Research Group, "Several indices for basic mechanical behavior of concrete.," in *Symposium of Experimental Investigation of Reinforced Concrete Structure*, Beijing, 1977.
- [121] C. E.-I. d. Beton, "Bulletin D'information No. 213/214 CEB-FIP Model Code 1990 (Concrete Structures)," Lausanne, 1993.
- [122] V. Malhotra, "Testing Hardened Concrete: Nondestructive Methods," American Concrete Institute, Detroit, 1976.
- [123] J. Kolek, "An Appreciation of the Schmidt Rebound Hammer," *Magazine of Concrete Research*, pp. 27-36, 1958.
- [124] N. Carino, "Non Destructive Testing of Concrete: History and Challenges," *ACI SP-144, Concrete Technology - Past, Present and Future*, P.K. Mehta, pp. 623-678, 1994.
- [125] M. F. D.M. McCann, "Review of NDT methods in the assessment of concrete and masonry structures," *Elsevier*, 2001.

- [126] O. R. DeBaun, "Portable linear accelerators for X-ray and electron beam applications in civil engineering Proceedings of the Seventh International Conference on Structural Faults & Repair-97," *vol. 2. Engineering Technics Press*, pp. 395-405, 8-10 July 1997.
- [127] A. V. Mishin, "Portable linear electron accelerators for electron beam curing of composites, non-destructive testing and other applications," *Proceedings of the seventh International Conference on Structural Faults & Repair-97*, pp. 367-373, 8-10 July 1997.
- [128] A. 304, "Guide for Measuring, Mixing, Transporting, and Placing Concrete," American Concrete Institute, 2000.
- [129] A. 315, "Guide to Presenting Reinforcing Steel Design Details," American Concrete Institute, 2014.